BABAR Analysis Document #2288, Version 6

Search for hadronic decays of a light Higgs produced in radiative decays of the $\Upsilon(2S)$ and the $\Upsilon(3S)$

C. Hearty and R. So

July 18, 2011

Abstract

We search for a light Higgs produced in the radiative decay of the $\Upsilon(2S)$ and the $\Upsilon(3S)$. The Higgs boson is reconstructed using fully inclusive hadronic final states in the mass range 0.29 to 7.1 GeV/c^2.

Contents

0 Changes from previous versions

0.1 Changes from version 1 to version 2

- Sec. 1: unchanged
- Sec. 2: minor edits
- Sec. 3: unchanged
- Sec. 4: minor edits
- Sec. 5: minor edits
- Sec. 6: Largely rewritten. Add fits to Run 7 on peak narrow resonances. Add additional cross checks. Add table summarizing numbers of events. Remove cross check using off peak data.
- Sec. 7: minor edits
- Sec. 8: unchanged
- Sec. 9: Add discussion of fit quality. Add subsection on optimizing the number of mass hypotheses. Higher statistics on bias studies.
- Sec. 10: unchanged
- Sec. 11: unchanged
- Sec. 12: Add one line on combining $\Upsilon(2S)$ and $\Upsilon(3S)$ results.

0.2 Changes from version 2 to version 3

- Sec. 1: Unchanged
- Sec. 2: Results in journal article will be based on combined data set.
- Sec. 3: Final luminosities.
- Sec. 4: Unchanged
- Sec. 5: Remove cut on highest momentum track. Update plots on QED rejection.
- Sec. 6: Add plots and tables for combined data sets. Improve captions and descriptions as per Bryan's comments.

- Sec. 7: Unchanged
- Sec. 8: Minor edits.
- Sec. 9: Minor edits, as per Bryan. Add trials penalty studies using combined data set.
- Sec. 10: Unchanged.
- Sec. 11: Updated table and plots with new efficiencies resulting from removal of xp1 cut
- Sec. 12: Describe how upper limit is found on combined data set. Add corresponding plot of expected upper limit.

0.3 Changes for version 4

Add Section 13, Unblinding strategy.

0.4 Changes for version 5

Add residual plots from fits in the initial unblinding stage.

0.5 Changes for version 6

Unblinded results for Run 7 on peak data. Sections on the unblinding procedure and test fits to off peak data removed. Sections reordered to match the presentation in the journal article.

1 Introduction

A light CP-odd Higgs boson is expected in a number of extensions to the standard model, including non-minimal Supersymmetry (SUSY) [1]. Light, in this context, means a mass less than $2m_B$. Such a Higgs could be produced in radiative decays of the Υ [2], $\Upsilon \to \gamma A^0$. *BABAR* has previously searched for this process where the A^0 decays to muons [3], taus [4], or invisibly [5, 6]. CLEO has used $\Upsilon(1S)$ data to search in the muon pair and tau pair final state [7].

The quantum numbers of the A^0, $J^{PC} = 0^{-+}$, are the same as the η_b, and could therefore mix with it [8]. There would then be two amplitudes that would contribute to the decay of an Υ to a lepton pair: the direct decay $\Upsilon \to \ell^+\ell^-(\gamma)$, and the decay through the η_b and the A^0: $\Upsilon \to \gamma\eta_b$,

$\eta_b \to A^0 \to \ell^+\ell^-$. Given the different couplings of the A^0 to different lepton species, the result would be a violation of lepton universality in Υ decay. *BABAR* has set limits such a violation [9].

The coupling of the A^0 to an up-type fermion pair is $m_f X_d/\sqrt{2}\nu \tan^2\beta$, while for a down-type fermion pair it is $m_f X_d/\sqrt{2}\nu$. $X_d = \cos\theta_A \tan\beta$, where $\cos\theta_A$ gives the doublet component of the A^0, and $\tan\beta$ is a standard SUSY parameter. For large (or rather, not small) values of $\tan\beta$, the A^0 will primarily decay to the heaviest down-type fermion that is kinematically available. Figure 1, taken from Ref. [10], summarizes the A^0 branching fractions as a function of $\tan\beta$ and mass.

Fig. 2, from the same reference, summarizes the expected $\Upsilon \to \gamma A^0$ branching fraction for various SUSY model parameters, with the constraint that the model not require "fine tuning". (See Ref. [1] for discussion). The *BABAR* results rule out many, but not all, of the points shown in these plots. For example, at $\tan\beta = 3$, the $\mu^+\mu^-$ results rule out approximately 80% of the $m_{A^0} < 2m_\tau$ parameter points. [11] interprets the *BABAR* and CLEO results in terms of limits on X_d. For $\tan\beta = 5$, these results imply an approximate limit of $X_d < 0.5$ (Fig. 3).

Hadronic decays become increasingly important at low values of $\tan\beta$. For example, if $m_{A^0} = 2\,\mathrm{GeV}/c^2$, the branching ratio $B(A^0 \to gg)/B(A^0 \to \mu^+\mu^-) \sim 3$ for $\tan\beta = 3$ and ~ 20 for $\tan\beta = 1$, while $B(A^0 \to s\bar{s})/B(A^0 \to \mu^+\mu^-) \sim 9$ for both values of $\tan\beta$ (Fig. 1). At high masses and low $\tan\beta$, the decay to $c\bar{c}$ becomes dominant.

This analysis searches for the decay of the A^0 to hadronic final states for $m_{A^0} < 7\,\mathrm{GeV}/c^2$.

2 Overview of the analysis

This analysis looks for narrow resonances in the A^0 mass spectrum in fully reconstructed $\Upsilon \to \gamma A^0$ events. The Higgs decay final state must contain at least two charged tracks and must not contain any leptons. Otherwise, no restrictions are placed on the final state.

Kinematic and particle identification cuts eliminate an otherwise large background from radiative Bhabha and radiative muon pair events. Additional selection criteria ensure that the event is correctly reconstructed, and that the radiative photon candidate is not the daughter of a π^0 or an η. The analysis proceeds with two different hypotheses regarding the nature of the A^0: that it is CP odd, or else the CP nature is not specified ("CP all").

The remaining events are primarily initial state radiation (ISR) contin-

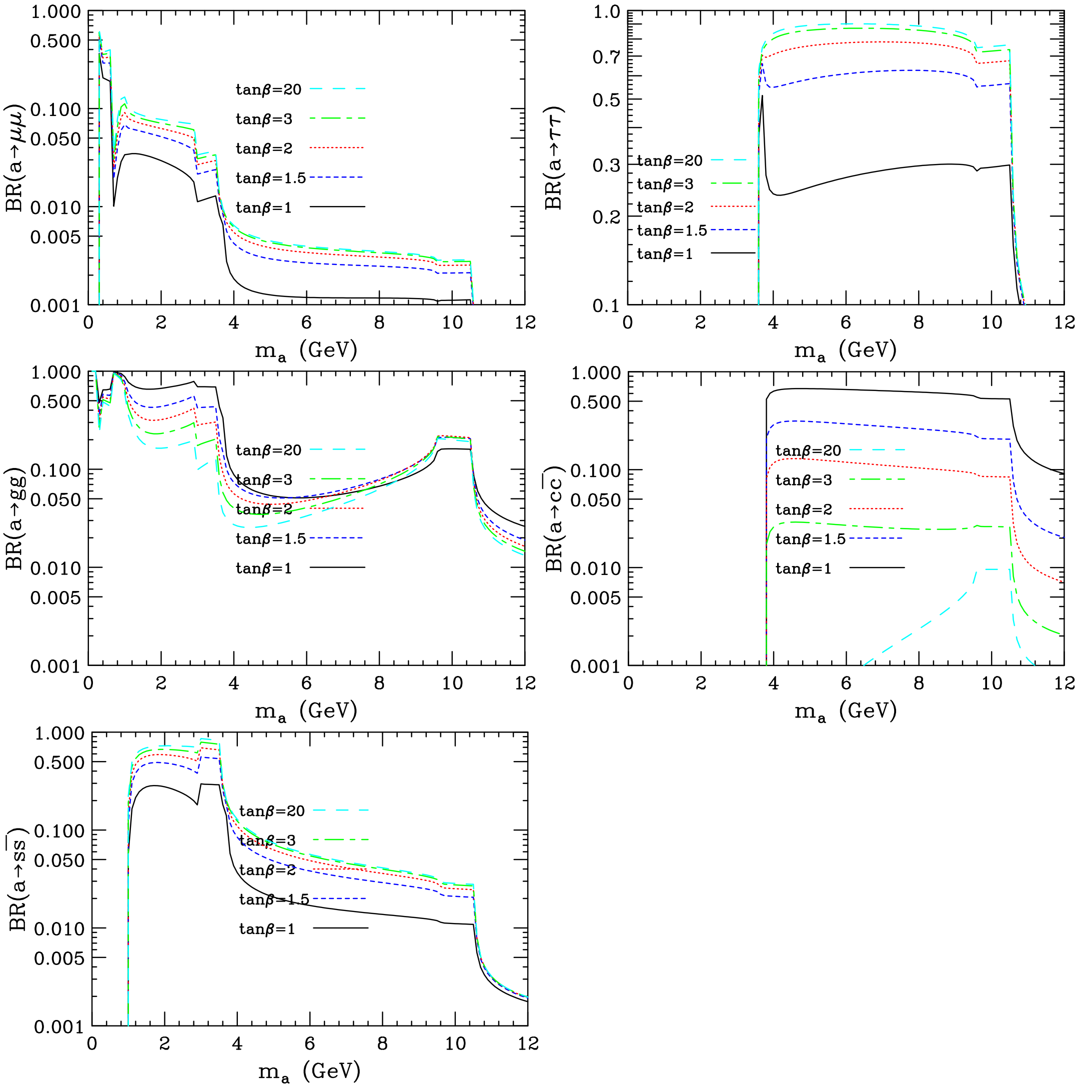

Figure 1: Branching fraction of the A^0 to different final states as a function of A^0 mass, for different values of $\tan\beta$. Figures taken from [10].

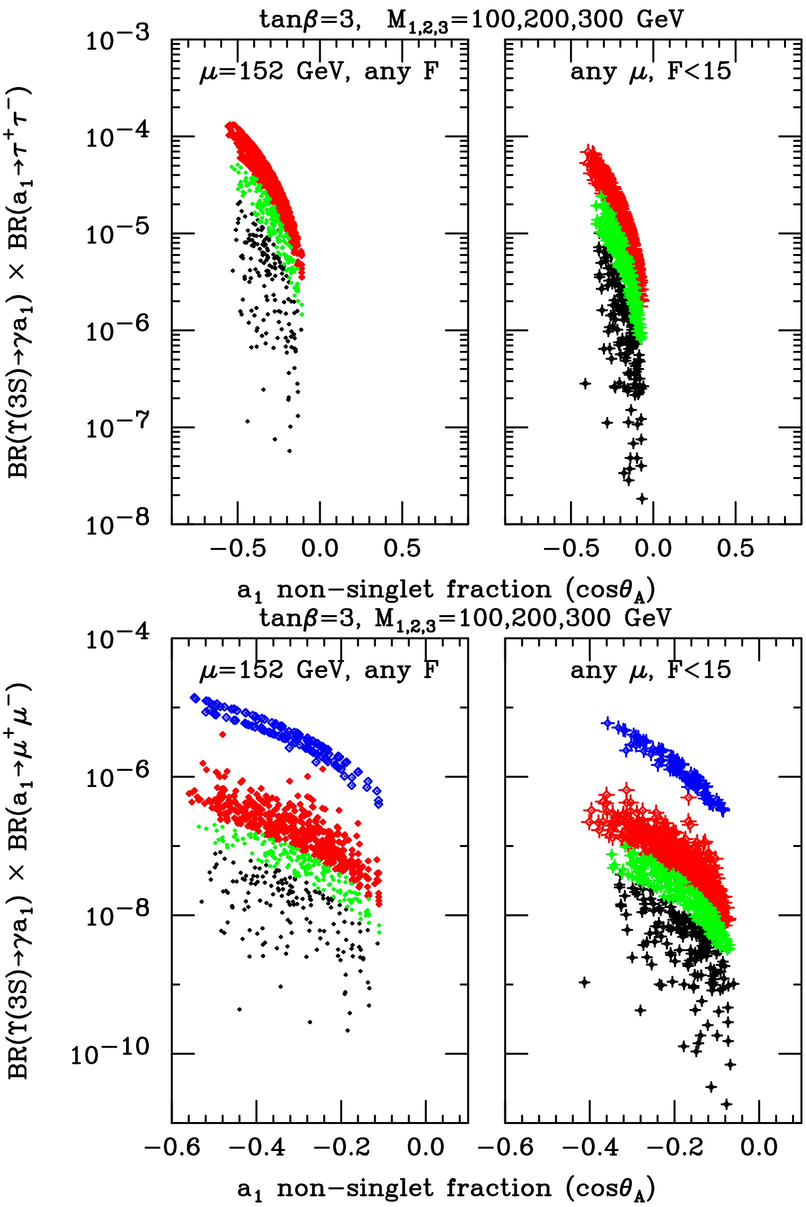

Figure 2: Predicted product branching fraction $\Upsilon(3S) \to \gamma A^0$, $A^0 \to \ell^+\ell^-$ for (top) $\tau^+\tau^-$ and (bottom) $\mu^+\mu^-$. These plots, taken from [10], are for $\tan\beta = 3$; plots for larger values are in the reference. Blue points are for $m_{A^0} < 2m_\tau$; red points are $2m_\tau < m_{A^0} < 7.5\,\mathrm{GeV}/c^2$; green points are $7.5 < m_{A^0} < 8.8\,\mathrm{GeV}/c^2$; and black points are $8.8 < m_{A^0} < 2m_B$. Different points correspond to different SUSY parameters, as do the left and right plots.

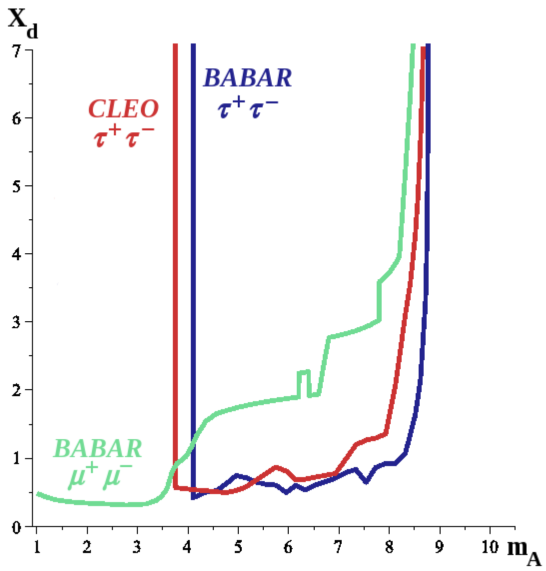

Figure 3: Upper limits on X_d from BABAR searches for $A^0 \to \mu^+\mu^-$ and $A^0 \to \tau^+\tau^-$, and the CLEO search for $A^0 \to \tau^+\tau^-$, derived assuming $\tan\beta = 5$. The BABAR lepton universality results also provide significant constraints at higher masses. Figure is copied from [11].

uum, plus some radiative Υ decays. Of particular note is the ISR production of the narrow resonances ω, ϕ, J/ψ and $\psi(2S)$, since the signature of a signal is a narrow resonance in the mass spectrum. The radiative Υ decays can be either non-resonant $\Upsilon \to \gamma gg$ or resonant $\Upsilon \to \gamma X$. The resonant spectrum is not well measured, but the known light mesons are distinguishable from a Higgs boson by their significantly greater widths.

The number of Higgs events at a particular mass is equal to the number of events observed within a mass window about that value, less the sum of the backgrounds (continuum, non-resonant Υ decays, and resonant Υ decays) in that window. 6701 mass hypotheses are considered for the CP odd case (1 MeV/c^2 steps from 0.3–7 GeV/c^2), and 6710 for CP all. The significance of an observed peak is degraded by a "trials penalty" of 3.5σ due to the number of hypotheses.

The backgrounds are determined by a fit to the candidate mass spectrum that includes three components, continuum, resonant Υ decay, and non-resonant Υ decay. The continuum component is a continuum data set (Run 6 plus Run 7 off peak), whose normalization is allowed to float in the fit. Various resonances are included for the resonant component, and a smooth curve is used to model the non-resonant component.

90% CL upper limits on the product branching fraction $B(\Upsilon \to \gamma A^0) \cdot B(A^0 \to \text{hadrons})$ are calculated from the combined $\Upsilon(2S)$ and $\Upsilon(3S)$ datasets assuming equal matrix elements for the $\Upsilon(2S) \to \gamma A^0$ and $\Upsilon(3S) \to \gamma A^0$ decays. The upper limits include the impact of systematic errors, the most important being uncertainties in the A^0 decay branching fractions, and uncertainty in the normalization of the continuum component in the fit.

The signal extraction methods have been studied using simulated experiments. The expected 90% CL upper limits range from 10^{-6} at $m_{A^0} = 0.3\,\mathrm{GeV}/c^2$ to 10^{-4} at $m_{A^0} = 7\,\mathrm{GeV}/c^2$.

Note that this analysis does not cover the Higgs mass range above 7 GeV/c^2. In this region, significantly better resolution and efficiency are obtained by studying the radiative photon energy spectrum instead of the hadronic system, as was done in the η_b analysis. An analysis using radiative events tagged with the presence of a D^0 or $D^\pm$ is in the early stages.

3 Data sets

The data used in the analysis are summarized in Table 1, signal MC is summarized in Table 2, and background MC in Table 3.

The continuum data sample used is the sum of Run 6 on peak and off

Table 1: Datasets used in the analysis. Runs 1–5 are used only in the generation of Toy experiments. Values are from BbkLumi after the final luminosity update [12].

		Collection	Lum. pb-1	±	N_Ups (M)	±
Run 1	On	AllEventsSkim-Run1-OnPeak-R24c	20373	92		
	Off	AllEventsSkim-Run1-OffPeak-R24c	2564	12		
Run2	On	AllEventsSkim-Run2-OnPeak-R24c	61322	258		
	Off	AllEventsSkim-Run2-OffPeak-R24c	6869	30		
Run 3	On	AllEventsSkim-Run3-OnPeak-R24c	32279	132		
	Off	AllEventsSkim-Run3-OffPeak-R24c	2444	11		
Run 4	On	AllEventsSkim-Run4-OnPeak-R24c	99606	418		
	Off	AllEventsSkim-Run4-OffPeak-R24c	10016	43		
Run 5	On	AllEventsSkim-Run5-OnPeak-R24c	132372	582		
	Off	AllEventsSkim-Run5-OffPeak-R24c	14277	67		
Run 6	On	AllEventsSkim-Run6-OnPeak-R24c	78308	352		
	Off	AllEventsSkim-Run6-OffPeak-R24c	7753	36		
Y3S	On	AllEventsSkim-Run7-Y3S_OnPeak-R24d-v05	27852	176	121.3	1.2
	Test	AllEvents-Run7-R24-Y3S-OnPeak-Low	1145	8	5.13	0.05
	Off	AllEventsSkim-Run7-Y3S_OffPeak-R24d	2602	24		
Y2S	On	AllEventsSkim-Run7-Y2S_OnPeak-R24d-v05	13561	90	98.3	0.9
	Off	AllEventsSkim-Run7-Y2S_OffPeak-R24d	1419	12		

peak, plus Run 7 off peak. Run 6 alone is used among the $\Upsilon(4S)$ data to ensure a consistent particle ID system. The luminosity of this continuum sample is twice that of the combined $\Upsilon(2S)$ plus $\Upsilon(3S)$ on-peak sample.

Signal MC uses a P-wave (VSP_PWAVE) for the decay of the Υ and phase space for the decay of the A^0. For each mass hypothesis, two different versions of the MC are produced. In the "CP-all" case, all decays are permitted. In the "CP-odd" case, the Higgs is assumed to have $J^{PC} = 0^{-+}$, and decays violating CP or P are explicitly forbidden. A sample decay file is shown in Fig. 4. The biggest difference is at low mass, where the CP-all case is 100% $\pi^+\pi^-$, while the CP-odd case is 100% $\pi^+\pi^-\pi^0$. In reality the CP-odd Higgs could decay to $\pi^+\pi^-\gamma$ (as do the η and η', which share the same quantum numbers), but existing signal MC does not reflect this.

SP background modes are all produced in R24. The generic Υ decay MC is not particularly useful, as it does not include radiative production of resonances $\Upsilon \to \gamma X$. It does include non-resonant $\Upsilon \to \gamma gg$, but only for cases where the invariant mass of the hadronic system is greater than $2\,\mathrm{GeV}/c^2$. The initial state radiation events are used in the study of the continuum normalization.

```
#####################################################
#                                                   #
# Ups(2S) --> Higgs gamma                           #
# Higgs --> hadrons                                 #
# m_Higgs = 1.5 GeV                                 #
# CP Odd Higgs                                      #
#                                                   #
# Contact: Christopher Hearty                       #
# hearty@physics.ubc.ca                             #
# Created 13-Feb-2008                               #
#                                                   #
#####################################################
ChangeMassMin Higgs0 1.49
ChangeMassMax Higgs0 1.51
Particle Higgs0 1.5 0.001

Decay  Upsilon(2S)
1.    Higgs0 gamma    VSP_PWAVE;
Enddecay

Decay  Higgs0
0.5   s anti-s  JETSET  32;
0.5   g g   JETSET  32;

#explicitly forbid decays violating P or CP
0.      pi+         pi-     PHSP;
0.      K+      K-      PHSP;
0.  pi(2S)+     pi-     PHSP;
0.  pi(2S)+     pi(2S)-     PHSP;
0.  K0      anti-K0     PHSP;
0.  pi0     pi0         PHSP;
0.  pi(2S)0     pi0     PHSP;
0.  eta     pi0     PHSP;
0.  eta(2S)     pi0     PHSP;
0.  eta(1405)   pi0     PHSP;
0.  eta(1475)   pi0     PHSP;
0.  eta'        pi0     PHSP;
0.  pi(2S)0     pi(2S)0     PHSP;
0.  eta     pi(2S)0     PHSP;
0.  eta(2S)     pi(2S)0     PHSP;
0.  eta(1405)   pi(2S)0     PHSP;
0.  eta(1475)   pi(2S)0     PHSP;
0.  eta'        pi(2S)0     PHSP;
0.  eta     eta     PHSP;
0.  eta(2S)     eta     PHSP;
0.  eta(1405)   eta     PHSP;
0.  eta(1475)   eta     PHSP;
0.  eta'        eta     PHSP;
0.  eta(2S)     eta(2S)     PHSP;
0.  eta(1405)   eta(2S)     PHSP;
0.  eta(1475)   eta(2S)     PHSP;
0.  eta'        eta(2S)     PHSP;
0.  eta(1405)   eta(1405)   PHSP;
0.  eta(1475)   eta(1405)   PHSP;
0.  eta'        eta(1405)   PHSP;
0.  eta(1475)   eta(1475)   PHSP;
0.  eta'        eta(1475)   PHSP;
0.  eta'        eta'        PHSP;
Enddecay

End
```

Figure 4: Decay file for SP-9024, $\Upsilon(2S) \to \gamma A^0$, with the A^0 decaying 50% to $s\bar{s}$ and 50% to gg, under the CP-odd hypothesis.

Table 2: Summary of signal MC modes used in the analysis. Top table lists the mode numbers; bottom table lists the number of generated events.

	50% gg + 50% s-sbar				gg				c-cbar			
	Y(2S)		Y(3S)		Y(2S)		Y(3S)		Y(2S)		Y(3S)	
Mass	CP odd	CP all	CP odd	CP all	CP odd	CP all	CP odd	CP all	CP odd	CP all	CP odd	CP all
0.35						10197		10196				
0.5					9017	9018	8744	8750				
1					9022	9023	8828	8751				
1.5	9024	9025	8829	8826	10135	10147	10107	10119				
2	9026	9027	8830	8752	10136	10148	10108	10120				
2.5	9028	9072	8831	8753	10137	10149	10109	10121				
3	9073	9030	8832	8754	10138	10150	10110	10122				
3.5	9817	9829	9793	9805	10139	10151	10111	10123				
4	9818	9830	9794	9806	10140	10152	10112	10124	10375	10389	10369	10382
4.5	9819	9831	9795	9807	10141	10153	10113	10125	10376	10390	10370	10383
5	9820	9832	9796	9808	10142	10154	10114	10126	10377	10391	10371	10384
5.5	9821	9833	9797	9809	10143	10155	10115	10127	10378	10392	10372	10385
6	9822	9834	9798	9810	10144	10156	10116	10128	10379	10393	10368	10386
6.5	9823	9835	9799	9811	10145	10157	10117	10129	10380	10394	10373	10387
7	9824	9836	9800	9812	10146	10158	10118	10130	10381	10395	10374	10388

	50% gg + 50% s-sbar				gg				c-cbar			
	Y(2S)		Y(3S)		Y(2S)		Y(3S)		Y(2S)		Y(3S)	
Mass	CP odd	CP all	CP odd	CP all	CP odd	CP all	CP odd	CP all	CP odd	CP all	CP odd	CP all
0.35						73,000		172,000				
0.5					145,000	282,000	153,000	200,000				
1					145,000	145,000	172,000	200,000				
1.5	145,000	74,000	172,000	172,000	73,000	73,000	172,000	172,000				
2	145,000	137,000	172,000	200,000	73,000	73,000	172,000	172,000				
2.5	145,000	145,000	172,000	200,000	73,000	73,000	172,000	172,000				
3	145,000	145,000	172,000	200,000	73,000	73,000	172,000	172,000				
3.5	73,000	49,000	124,000	172,000	73,000	73,000	172,000	172,000				
4	73,000	73,000	52,000	172,000	73,000	73,000	172,000	172,000	73,000	73,000	172,000	172,000
4.5	73,000	73,000	132,000	172,000	73,000	73,000	172,000	172,000	73,000	73,000	172,000	172,000
5	73,000	57,000	172,000	172,000	73,000	73,000	172,000	172,000	73,000	73,000	172,000	172,000
5.5	73,000	49,000	164,000	172,000	73,000	73,000	172,000	172,000	73,000	73,000	172,000	172,000
6	73,000	73,000	172,000	172,000	73,000	73,000	172,000	172,000	73,000	73,000	172,000	172,000
6.5	73,000	41,000	172,000	172,000	73,000	73,000	172,000	172,000	73,000	73,000	172,000	172,000
7	73,000	17,000	172,000	172,000	73,000	73,000	172,000	172,000	73,000	73,000	172,000	172,000

Table 3: Number of events used for each of the background SP modes. Collection names for the Upsilon datasets are of the form SP-8739-Run7-Y3S_OnPeak-R24. For Run6, they are SP-7957-Run6-R24 for on-peak and SP-7957-Run6-OffPeak-R24 for off peak.

Description	Mode	Run 6 On	Run 6 Off	Y3S On	Y3S Off	Y2S On	Y2S Off
Y3S generic	8739	-	-	198,189,000	-	-	-
Y2S generic	9016	-	-	-	-	115,664,000	-
e+e- -> gamma omega	7957	1,947,000	198,000	2,046,000	228,000	1,176,000	123,000
e+e- -> gamma phi, phi->K+K-	7900	1,552,000	158,000	2,038,000	228,000	957,000	99,000
ISR psi inclusive	8188	471,000	47,000	8,310,000	1,062,000	12,819,000	1,359,000

4 Reconstruction of final state and preliminary selection

The initial stage of the analysis is done in BetaMiniUser in analysis-51 (24.3.6). The following tags are used:

```
BetaMiniUser V00-04-05
BetaPid V00-15-04
workdir V00-04-21
```

The code fully reconstructs the decay $\Upsilon \rightarrow \gamma A^0$ assuming hadronic decays of the A^0. It applies minimal cuts, and stores the resulting information in ntuples. The Higgs candidate is created by sequentially adding BtaCandidates. A BtaCandidate is added to the list from which the Higgs is composed only if it does not overlap with the candidates already on the list. The order of the operations is therefore important.

The basic lists are GoodTracksLoose for charged tracks, and GammaForPi0 for photons (including those used in making π^0 candidates). The photon list requires center-of-mass energy greater than 90 MeV, $0 < \mathrm{LAT} < 0.8$, ≥ 4 crystals, and $Z42 < 0.11$.

The photon selection criteria are based on a study using simulated $e^+e^- \rightarrow \gamma\omega$, $\omega \rightarrow \pi^+\pi^-\pi^0$ events. Signal MC was not available at the time the study was performed. The selection maximizes the number of fully reconstructed events in which there are no additional photons. Figure 5 shows the energy spectrum of various categories of photons in such events.

The code starts by selecting the highest energy photon to be the radiative decay photon.

The composition of the Higgs candidate starts by adding K_s candidates from the KsTight list.

All entries on the GoodTracksLoose list (excluding those used to create K_s candidates) are then set to be either $\pi^\pm$, $K^\pm$, or $p^\pm$, and added to the Higgs. The order of decisions in assigning the particle type is:

1. proton: track is on pKMSuperLoose with $\theta_{lab} > 0.45$, and there are exactly 2 or 4 such protons with zero net charge.

2. pion: track is on piKMSuperTight.

3. kaon: track is on KBDTKaonTight.

4. pion: track is on piKMTight.

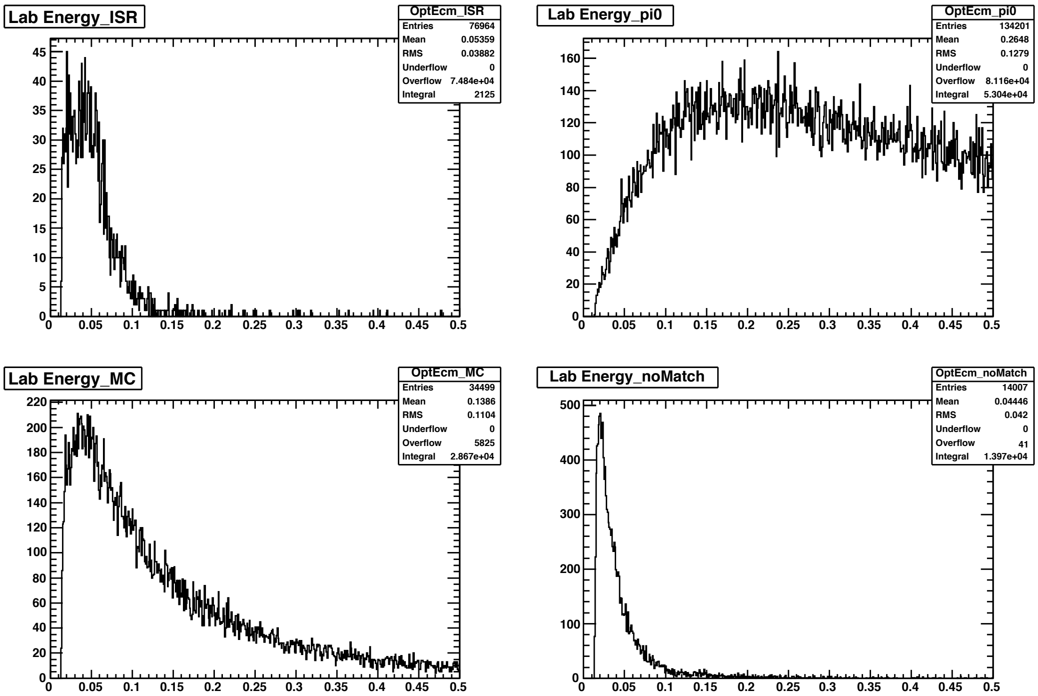

Figure 5: Center-of-mass energies of different categories of photons in simulated $e^+e^- \to \gamma\omega$, $\omega \to \pi^+\pi^-\pi^0$ events. (Histograms are incorrectly labeled as laboratory energies). Upper left: ISR photons (note overflows). Upper right: Photons from π^0 decays. Lower left: hadronic split offs. Lower right: beam backgrounds. Only photons with energy above 0.09 GeV are used in the analysis.

5. kaon: track is on KBDTKaonVeryLoose.

6. pion: otherwise.

Note that the code records electron and muon identification information for the purpose of rejecting QED events at a subsequent stage of the analysis.

π^0 candidates from the pi0Loose list that do not overlap with the radiative photon are then added to the Higgs.

Finally, any unused photons from the GammaForPi0 list are added.

The Υ candidate is formed from the radiative photon and the Higgs candidate, constrained to a common vertex, and with its energy constrained to $\sqrt{s}$. TreeFitter is used for the fit. The mass of the Higgs candidate resulting from this fit is used in the subsequent analysis.

The event is stored in the ntuple if there are at least two charged tracks with zero net charge (excluding those used to create K_s candidates), and at least one photon with a center-of-mass energy greater than 2.5 GeV ($\Upsilon(3S)$) or 2.2 GeV ($\Upsilon(2S)$). The corresponding upper limit on the Higgs mass, given that this is a two-body decay, ranges from 7.68 GeV/c^2 at $\sqrt{s}$ = 10.58 GeV/c^2 to 7.06 GeV/c^2 at $\sqrt{s} = 9.993$ GeV/c^2 ($\Upsilon(2S)$ off peak).

5 Final event selection

The final event selection is performed at the ntuple level in a stand-alone ROOT 5.26 installation, as are all subsequent stages of the analysis. The final selection includes trigger and filter, cuts to reject QED events, and criteria to select correctly reconstructed events.

5.1 Trigger and Filter

Events are required to satisfy either L3OutDch or L3OutEmc, and at least one physics BGFilter flag. The signal MC efficiency of this requirement is effectively 100% for most Higgs masses, and is above 99.5% for all. A significant fraction of Run 6 on peak events are Bhabhas that fail this requirement, although almost all are also rejected by the criteria outlined in the next section.

5.2 Rejection of QED events

The vast majority of the events written to ntuples are $e^+e^- \to e^+e^-\gamma$ or $e^+e^- \to \mu^+\mu^-\gamma$. To suppress this background, an event is rejected if it satisfies any of the following kinematic or particle identification criteria:

1. Angle between the second-highest momentum track and the radiative photon is less than 1 radian.
2. Either of the two highest momentum tracks satisfy eKMSuperLoose.
3. Either of the two highest momentum tracks satisfy muBDTVeryLoose.

Note that many Bhabhas are also eliminated by the requirement that the event satisfy a physics BGFilter flag. Together, these requirements reject 96% of the events in the Run 6 On-peak ntuples, at a cost of 10–20% of signal events (Fig. 6–7). The largest source of inefficiency is the muon veto. The angular cut costs approximately 8% of the signal at the highest Higgs masses, while rejecting 27% of continuum events that satisfy all other requirements.

An earlier version of the analysis also rejected events in which the center-of-mass momentum of the highest momentum track $> 0.45 \cdot \sqrt{s}$. However, more detailed examination of this cut revealed that it rejected approximately 20% of low-mass CP-all Higgs, while rejecting only 3% of continuum.

5.3 Selection of correctly reconstructed events

As part of the event reconstruction, the radiative photon and the Higgs candidate are fit to a common vertex and to $\sqrt{s}$. Events in which the probability of the χ^2 of this fit is low are rejected. The value of this cut is a function of mass, and is different for the CP odd and CP all hypotheses.

The values for this cut were optimized together with the π^0 and η vetoes. The optimization used $\Upsilon(3S)$ signal MC of various masses decaying 50% to two gluons and 50% to $s\bar{s}$, with an assumed branching fraction of 10^{-5} for $\Upsilon \to \gamma A^0$. Run 6 was the background sample. The figure of merit for the optimization was the significance of the Higgs signal, where the Higgs signal was the number of events in a mass window centered on the true Higgs mass after a continuum and a mass sideband subtraction. The width of this mass window was selected for each Higgs mass hypothesis as part of the optimization procedure. The Higgs mass window is used in the final analysis, although the sideband subtraction is not. Note that the optimized quantities are taken to be a function of the Higgs mass hypothesis, but not the center-of-mass energy of the sample.

The resulting cuts on the probability χ^2 are shown in Fig. 8, while the width of the Higgs mass window is shown in Fig. 9.

A π^0 veto is applied for Higgs hypothesis masses above 5 GeV/c^2, and an η veto is applied above 6 GeV/c^2. An event is rejected if the radiative photon, when combined with any other photon in the event, forms a π^0 or

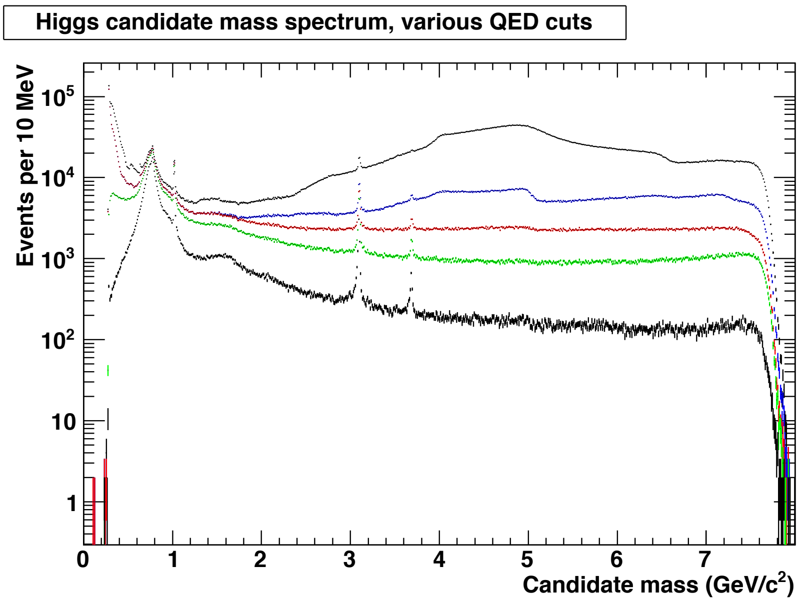

Figure 6: Mass spectrum of candidates in the Run 6 on-peak data, after various QED rejection criteria are applied. Events pass all other CP all cuts. The five lines from top to bottom are: no QED rejection and no BGFlag requirement; BGFlag requirement only; BGFlag plus kinematic cut only; BGFlag, kinematic cut, and electron ID; full selection criteria.

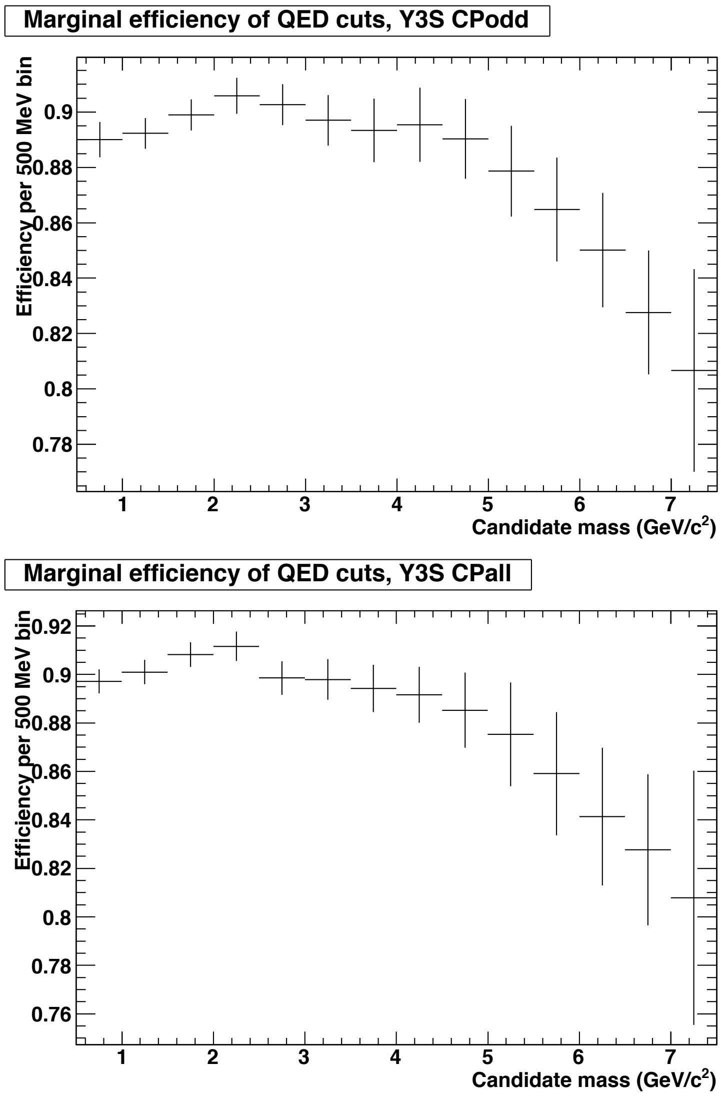

Figure 7: Efficiency vs Higgs mass for the QED suppression criteria for signal MC events that pass all other cuts. Top plot is for CP odd, bottom plot for CP all. Note the suppressed zero on the vertical axis.

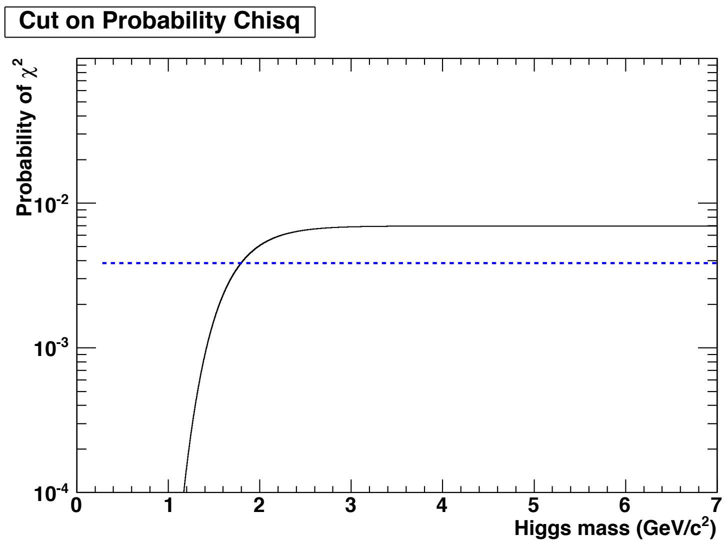

Figure 8: Minimum value required for the probability χ^2 of the fit of the Higgs candidate and the radiative photon to a common vertex and to $\sqrt{s}$. CP odd hypothesis is the black line; CP all is the dashed blue line. The requirement for the CP odd case at low masses is effectively probability $\chi^2 > 0$.

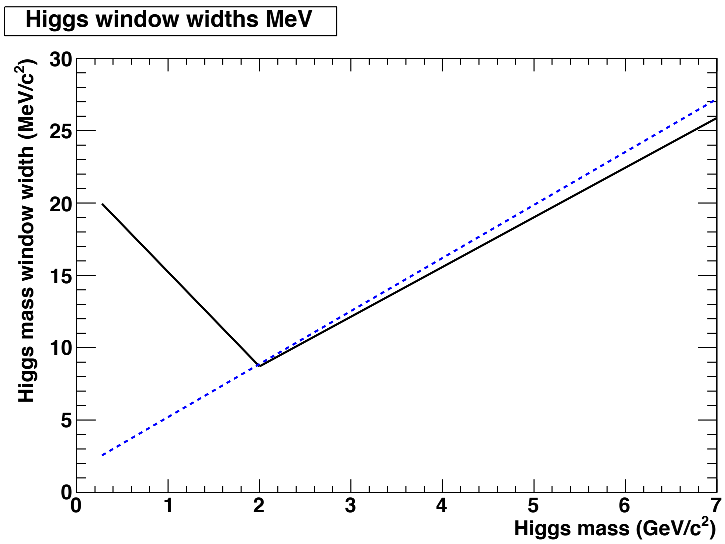

Figure 9: Higgs window width as a function of mass for the CP odd hypothesis (black line) and the CP all hypothesis (dashed blue line). The Higgs signal at a particular mass is the net number of events after background subtraction within the window centered on that mass.

η candidate with mass within 50 MeV/c^2 of the true value. These criteria were optimized at the same time as the probability χ^2 cut and the mass window. All photons must satisfy the selection criteria listed in Sec. 4. In approximately 5% of the remaining events in generic $\Upsilon(2S)$ MC the radiative photon is a daughter of π^0. Roughly a third of these are merged π^0, while the remainder are asymmetric decays.

Simulation indicates that no $B\overline{B}$ events satisfy the selection criteria, which allows us to include the Run 6 on-peak data in the continuum sample.

Under the CP odd hypothesis, events in which the Higgs decays to $\pi^+\pi^-$ or K^+K^- are rejected.

6 The Higgs signal

The number of Higgs events H_i at mass m_i is equal to the total number of events N_i observed in the Higgs mass window centered on that mass, less the total background expected in that window, B_i. B_i is the integral over that window of the fit to the candidate mass spectrum, described in Sec. 7.

The Higgs signal is found in 1 MeV/c^2 steps from the lower mass limit to 7 GeV/c^2. The lower limit is 0.290 GeV/c^2 plus one-half the width of the Higgs window, 0.300 GeV/c^2 for CP odd, and 0.291 GeV/c^2 for CP all, giving a total of 6701 CP odd mass hypotheses and 6710 CP all mass hypotheses.

The signal is also characterized by its nominal statistical significance, $\mathcal{S}_i = H_i/\delta_i$, where $\delta_i = \sqrt{N_i + f_L^2 \cdot C_i}$, C_i is the number of events in the continuum data set in that window, and f_L is the factor that normalizes the continuum data set to the on peak data. The actual significance of an observed signal is degraded by the trials penalty resulting from looking for a signal at many thousands of different masses: $\mathcal{S}'_i = \sqrt{\mathcal{S}_i^2 - t^2}$, where t is the trials penalty, which has been calculated using simulated experiments (Sec. 8.4).

A histogram of the 6701 or 6710 values of $\mathcal{S}_i$ is a useful way to illustrate the significance (or not) of an upwards fluctuation at a particular mass.

Sample signal plots from Toy studies are shown in Sec. 8.

6.1 Angular distributions

The underlying angular distributions of the radiative photon in signal events and in the ISR background are quite different (Fig. 10). However, the differences are rather small for events that satisfy all selection criteria, particularly

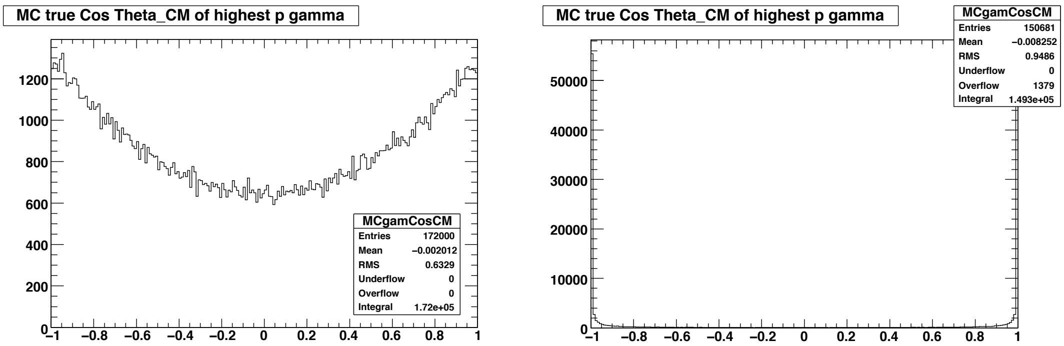

Figure 10: Generated MC truth generated distribution for $\cos\theta$ for the radiative photon in (left) $\Upsilon(3S) \rightarrow \gamma A^0$ ($m_{A^0} = 2\,\mathrm{GeV}/c^2$) and (right) $e^+e^- \rightarrow \gamma J/\psi$ ($\sqrt{s} = 10.355\,\mathrm{GeV}/c^2$).

the requirement that the event be fully contained (Fig. 11). If we do see a significant signal, it will be important to verify that the observed angular distribution is consistent with the expected $1 + \cos^2\theta$.

7 Fit to the candidate mass spectrum

The candidate mass spectra resulting from the above selection criteria are fit to obtain the the number of background events. The fit is a binned likelihood fit in 5 MeV/c^2 bins ranging from 0.29 to 7.1 GeV/c^2 (1362 bins). It is performed in ROOT.

The mass region from 0.28 to 0.29 GeV/c^2 is excluded from the fit because of an apparent different between Run 6 and Run 7 in the number of events at kinematic threshold, which are assumed to be due to conversions (Fig. 12). Cutting on helicity does not improve the agreement.

A fit has three components: continuum, Υ non-resonant, corresponding to $\Upsilon \rightarrow \gamma gg$, and Υ resonant, corresponding to radiative decay to a light resonance X, $\Upsilon \rightarrow \gamma X$.

The continuum component is the continuum data set scaled by a normalization factor f_L, which is a free parameter in the fit. The continuum sample contains a number of narrow initial-state-radiation (ISR) produced resonances (Fig. 13). We verify that the shapes of these resonances are consistent between continuum and on-peak data by looking at four samples, all of which are subsets of the normal CP all selection:

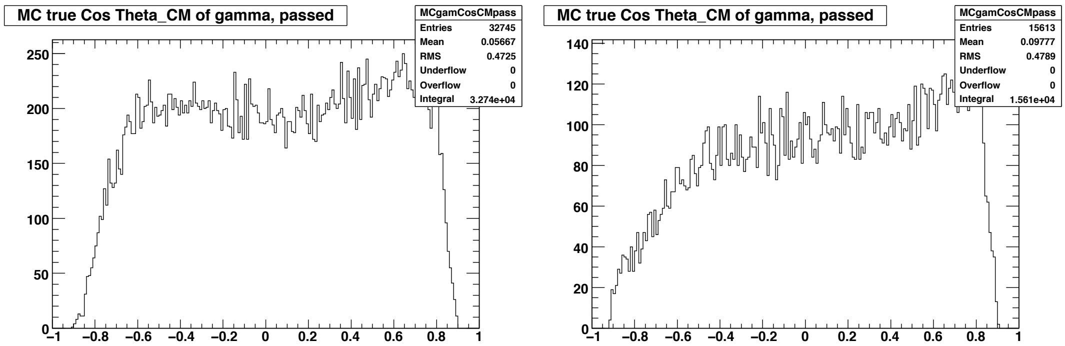

Figure 11: Reconstructed $\cos\theta$ for the radiative photon in events satisfying all selection criteria. (left) $\Upsilon(3S) \to \gamma A^0$ ($m_{A^0} = 2\,\mathrm{GeV}/c^2$); (right) $e^+e^- \to \gamma J/\psi$.

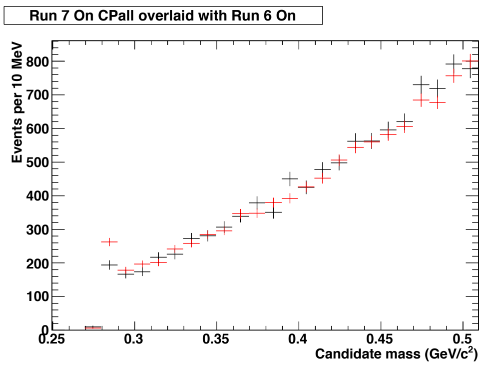

Figure 12: CP all candidate mass distribution for Run 7 on peak data (black) and Run 6 on peak data (red). The excess at threshold is also present in Run 6 off peak data, but not Run 7 off peak data.

- $\omega \to \pi^+\pi^-\pi^0$: zero protons, zero kaons, exactly two tracks, and at least one π^0. Fit range 0.70–0.9 GeV/c^2; 1 MeV/c^2 bins.

- $\phi \to K^+K^-$: exactly two tracks and exactly two kaons. Fit range 0.99–1.15 GeV/c^2; 1 MeV/c^2 bins.

- $J/\psi \to \geq 4$ tracks: at least four tracks and no π^0. Fit range 2.8–3.3 GeV/c^2; 2 MeV/c^2 bins.

- $J/\psi \to \geq 4$ tracks $1\pi^0$: at least four tracks and exactly 1 π^0. Fit range 2.8–3.3 GeV/c^2; 2 MeV/c^2 bins.

Figures 15–21 compare the four resonances in Run 7 on-peak and continuum data. In each case, a linear background is subtracted from the distribution, then the continuum is normalized to the same area as the on peak data. The plots show good agreement in the shapes of the narrow resonances. Note, however, that there is a systematic error due to the overall normalization of the continuum (Sec. 11.1).

The non-resonant pdf is a 16-knot cubic spline—i.e., the magnitude of the spline is specified at 16 different masses: 0.2895, 0.4141, 0.5, 1.0, ..., 4.5, 5.1, 5.7, 6.3, 6.8, 7.1 GeV/c^2. The first two are the lower edge of the fit ($\approx 2m_{\pi^\pm}$) and $3m_\pi$ respectively. The magnitude at the first knot is fixed to be 0, and the magnitude of the last is fixed to be 1. The magnitudes at the other 14 knots are free parameters in the fit. There is also an overall normalization parameter, giving 15 free parameters for the non-resonant component. The locations of the last few knots were adjusted after unblinding to better match a background in data that rises with mass at high masses. This background is presumably due to hadronic Υ decays in which the radiative photon is from π^0 decay.

Because the spacing of the knots, typically 0.5 GeV/c^2, is large compared to the width of a Higgs, the presence of a signal will not significantly distort the fit to the underlying non-resonant component (Sec. 8).

Light meson resonances in the Υ mass spectrum are fit with relativistic Breit-Wigners:

$$f(m) \propto \frac{m^2}{(m^2 - M^2) + m^4 \cdot \Gamma^2/M^2}, \tag{1}$$

where M and Γ are the mass and full width of the resonance respectively.

The fit nominally includes five resonances for which CLEO has seen some evidence [13] (Table 4). This study looked at two-body radiative decays of the $\Upsilon(1S)$ in a sample of $21.2 \pm 0.2 \times 10^6$ $\Upsilon(1S)$. Note that the fit does not

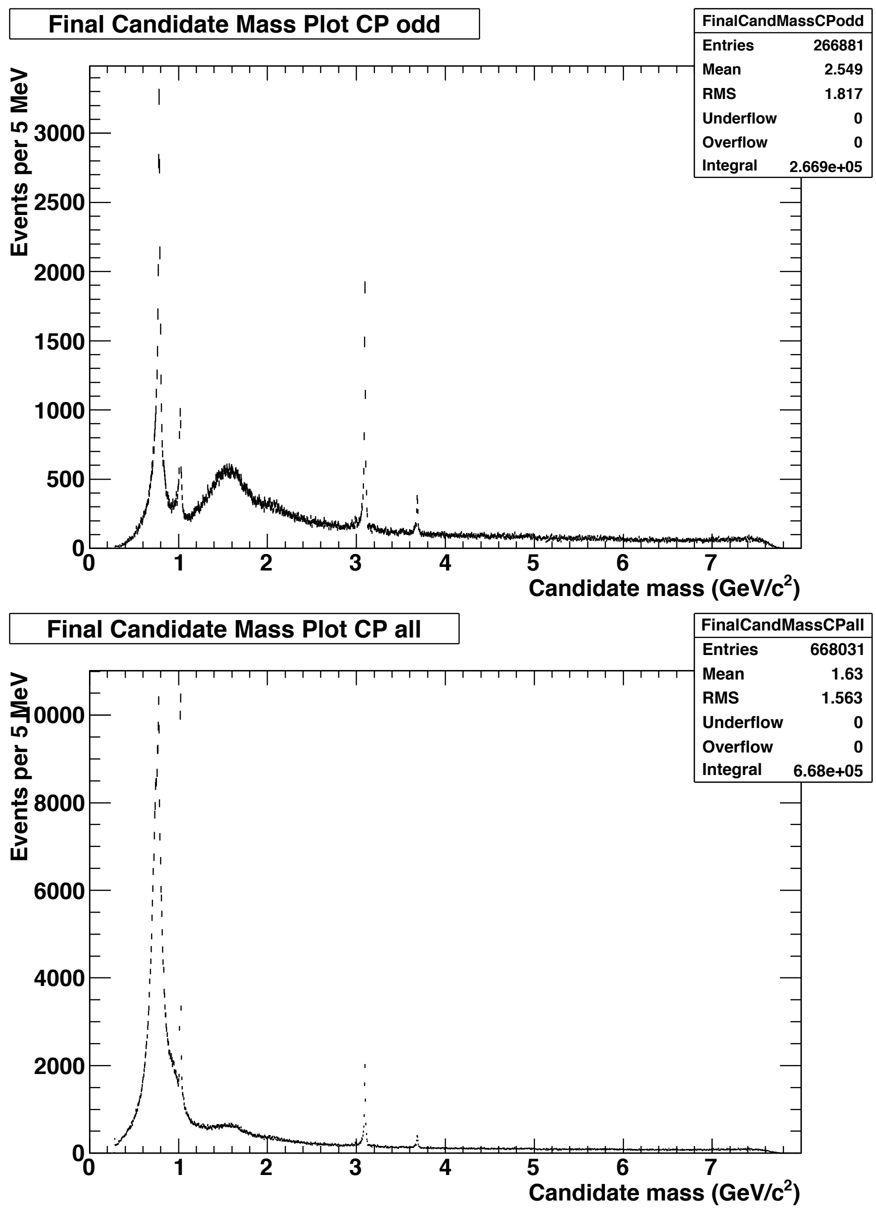

Figure 13: Candidate mass spectrum in the continuum subtraction data sample (Run 6 plus Run 7 off peak) for the (top) CP odd and (bottom) CP all selection criteria.

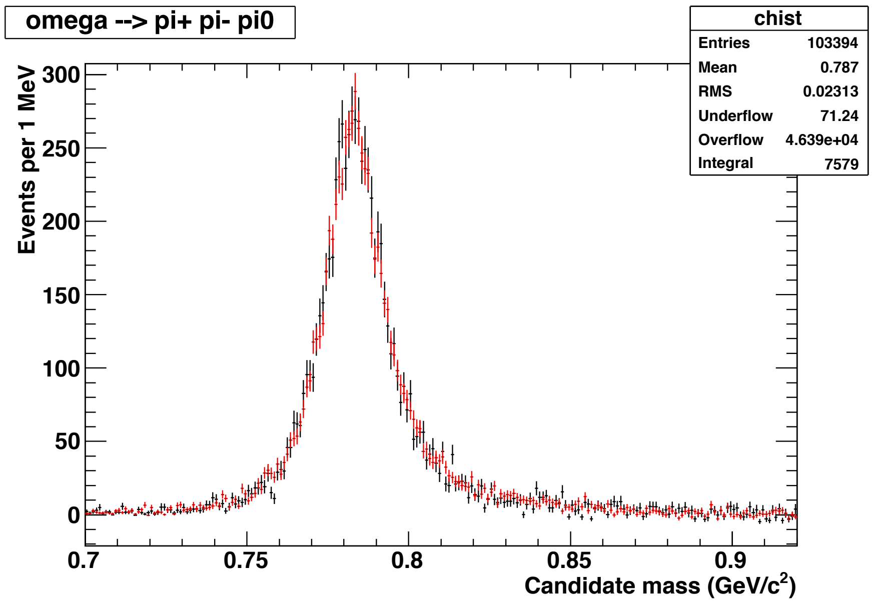

Figure 14: $\omega \to \pi^+\pi^-\pi^0$ in the Run 7 on-peak data (black) overlaid with the continuum sample (red) normalized to the same area.

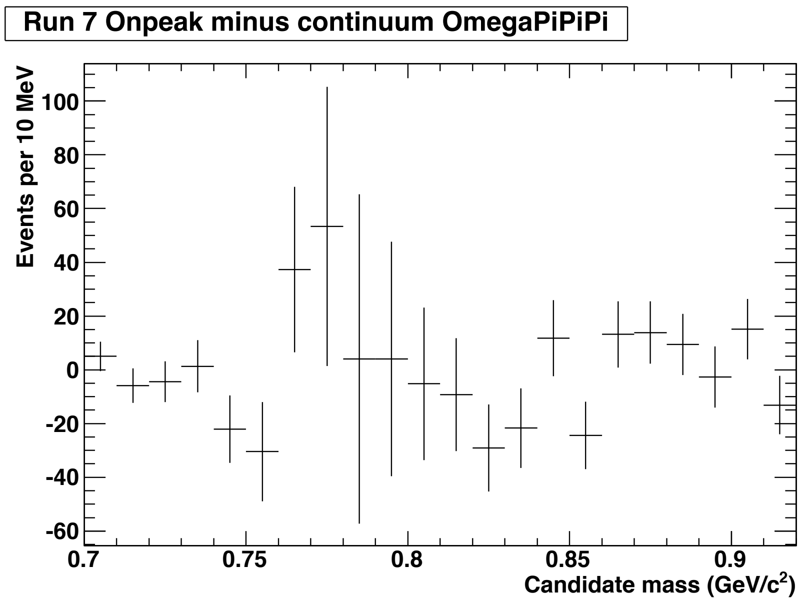

Figure 15: $\omega \to \pi^+\pi^-\pi^0$ in the Run 7 on-peak data minus the continuum sample.

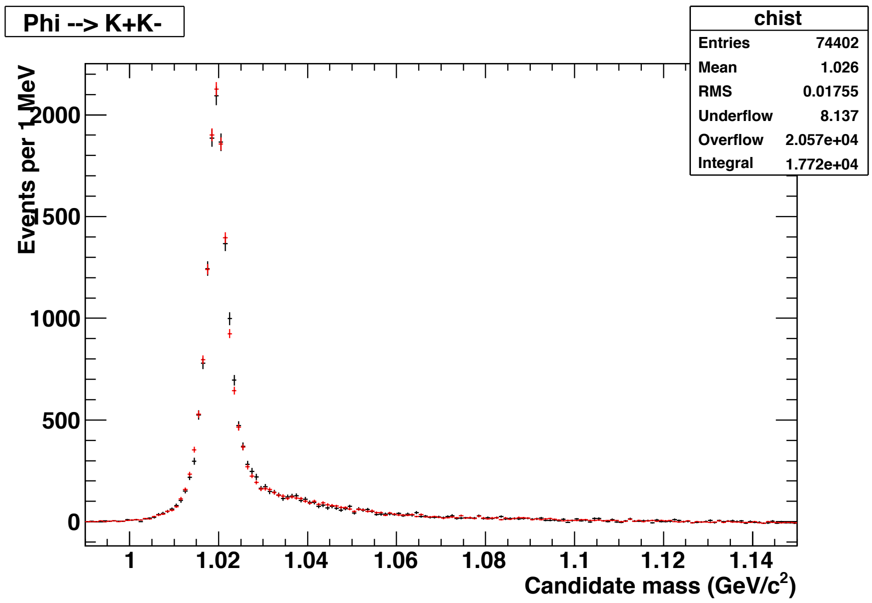

Figure 16: $\phi \to K^+K^-$ in the Run 7 on-peak data (black) overlaid with the continuum sample (red) normalized to the same area.

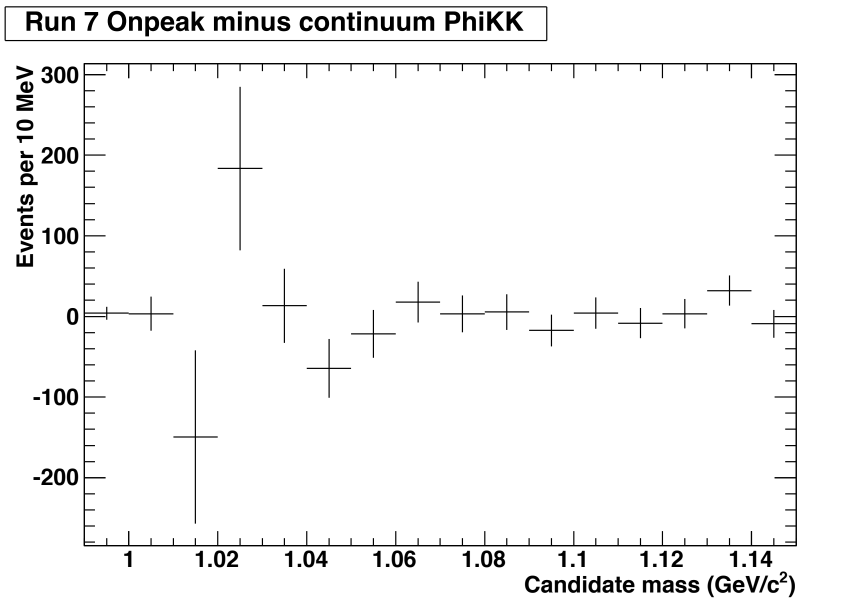

Figure 17: $\phi \to K^+K^-$ in the Run 7 on-peak data minus the continuum sample.

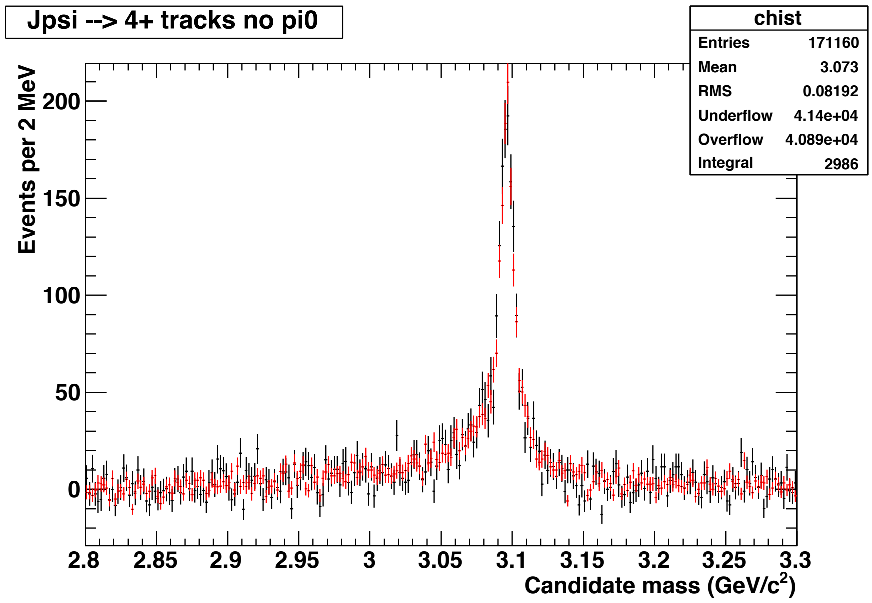

Figure 18: $J/\psi \rightarrow \geq 4\text{tracks}1\pi^0$ in the Run 7 on-peak data (black) overlaid with the continuum sample (red) normalized to the same area.

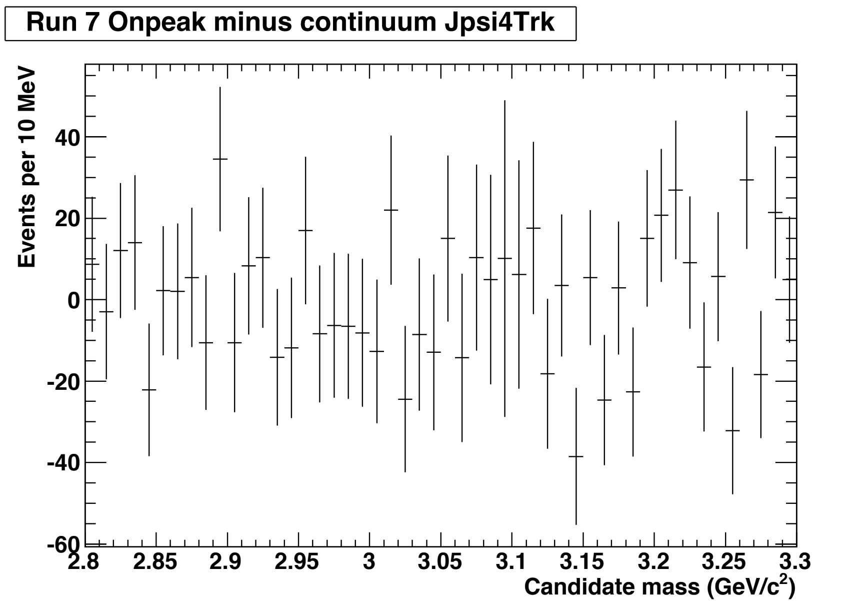

Figure 19: $J/\psi \rightarrow \geq 4\text{tracks}1\pi^0$ in the Run 7 on-peak data minus the continuum sample.

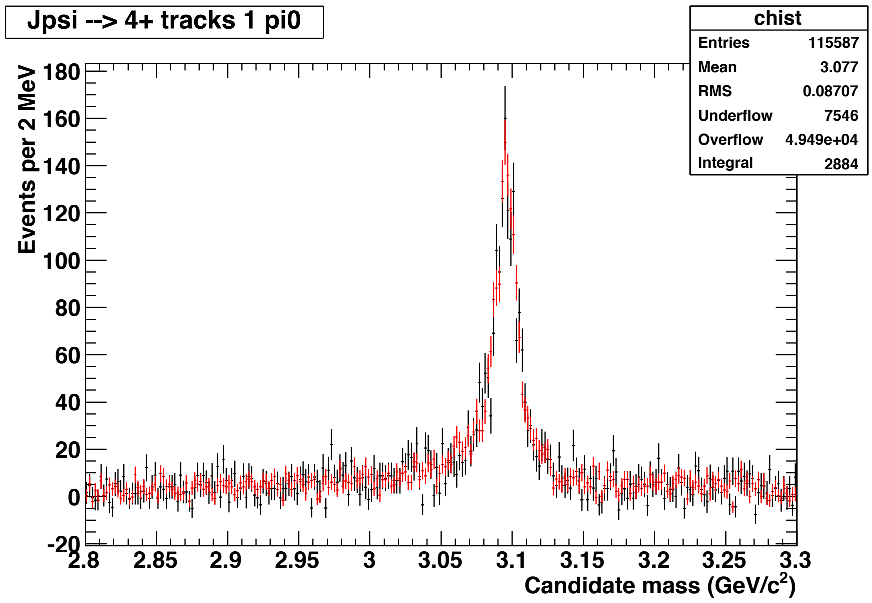

Figure 20: $J/\psi \rightarrow \geq 4\text{tracks}0\pi^0$ in the Run 7 on-peak data (black) overlaid with the continuum sample (red) normalized to the same area.

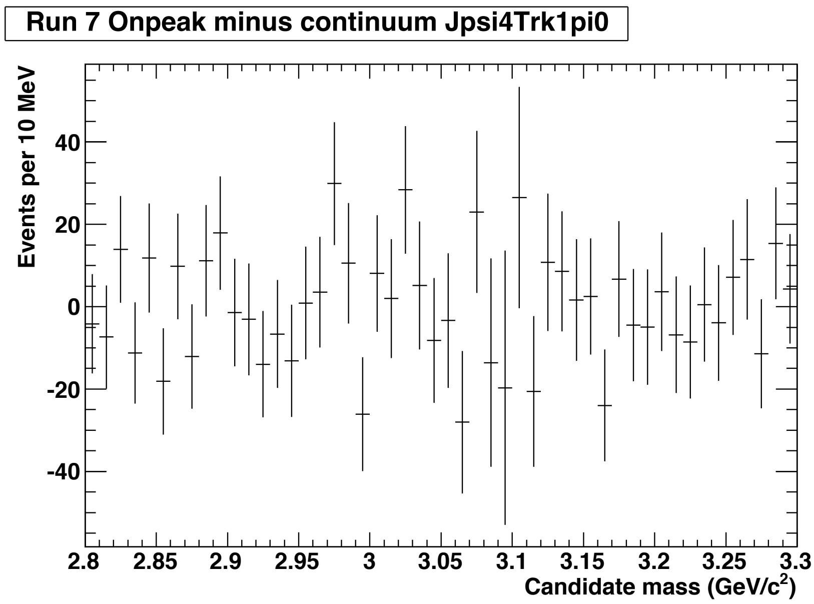

Figure 21: $J/\psi \rightarrow \geq 4\text{tracks}0\pi^0$ in the Run 7 on-peak data minus the continuum sample.

Table 4: Mass and widths [14] of the light resonances nominally included in the fit to the Υ spectrum, together with CLEO measurements of product branching fractions.

	M (MeV/c^2)	Γ (MeV)	CLEO measurement	BF (10^{-5})
$f_0(980)$	980 ± 10	70 ± 30	$\Upsilon(1S) \to \gamma f_0 \to \pi^+\pi^-$	$1.8^{+0.8}_{-0.7} \pm 0.1$
$f_2(1270)$	1275.1 ± 1.2	$185.1^{+2.9}_{-2.1}$	$\Upsilon(1S) \to \gamma f_2$	$10.2 \pm 0.8 \pm 0.7$
$f_2'(1525)$	1525 ± 5	73^{+6}_{-5}	$\Upsilon(1S) \to \gamma f_2'$	$3.7^{+0.9}_{-0.7} \pm 0.8$
$f_0(1710)$	1720 ± 6	135 ± 6	$\Upsilon(1S) \to \gamma f_0 \to K^+K^-$	$0.38 \pm 0.16 \pm 0.04$
$f_4(2050)$	2018 ± 11	237 ± 18	$\Upsilon(1S) \to \gamma f_4 \to \pi^+\pi^-$	$0.37 \pm 0.14 \pm 0.03$

rely on the product branching fractions measured by CLEO. The fit assumes no interference between the resonances.

The shape parameters of the resonances are fixed in the fit; only the normalizations are floated.

There are 11 other established light mesons with total angular momentum J even, charge conjugation quantum number $C = +1$, and Isospin $I = 0$, the quantum numbers expected for $\Upsilon \to \gamma X$ (Fig. 22). These are included in the fit for systematic studies. Belle saw no evidence [15] for radiative decays of the $\Upsilon(1S)$ to charmonium states, so we would not expect to see these decays.

8 Toy MC studies

8.1 Generating a simulated experiment

Simulated experiments are used to test the signal extraction techniques. An experiment consists of a randomly generated on-peak data set (specifically, the reconstructed Higgs candidate mass distribution), plus a randomly generated continuum sample.

The on peak data set has four components: signal, continuum, non-resonant $\Upsilon \to \gamma gg$, and resonant $\Upsilon \to \gamma X$. The continuum sample has only the one component.

The mean sizes of each component are listed in Table 5. The number of Υ decays (resonant plus non-resonant) has been estimated by the number of entries in the Y3S-Low mass distribution histograms; the plots themselves were blind at the time the studies were done. The split between resonant

LIGHT UNFLAVORED ($S = C = B = 0$)

	$I^G(J^{PC})$		$I^G(J^{PC})$
• $\pi^\pm$	$1^-(0^-)$	• $\pi_2(1670)$	$1^-(2^{-+})$
• π^0	$1^-(0^{-+})$	• $\phi(1680)$	$0^-(1^{--})$
• η	$0^+(0^{-+})$	• $\rho_3(1690)$	$1^+(3^{--})$
• $f_0(600)$	$0^+(0^{++})$	• $\rho(1700)$	$1^+(1^{--})$
• $\rho(770)$	$1^+(1^{--})$	$a_2(1700)$	$1^-(2^{++})$
• $\omega(782)$	$0^-(1^{--})$	• $f_0(1710)$	$0^+(0^{++})$
• $\eta'(958)$	$0^+(0^{-+})$	$\eta(1760)$	$0^+(0^{-+})$
• $f_0(980)$	$0^+(0^{++})$	• $\pi(1800)$	$1^-(0^{-+})$
• $a_0(980)$	$1^-(0^{++})$	$f_2(1810)$	$0^+(2^{++})$
• $\phi(1020)$	$0^-(1^{--})$	$X(1835)$	$?^?(?^{-+})$
• $h_1(1170)$	$0^-(1^{+-})$	• $\phi_3(1850)$	$0^-(3^{--})$
• $b_1(1235)$	$1^+(1^{+-})$	$\eta_2(1870)$	$0^+(2^{-+})$
• $a_1(1260)$	$1^-(1^{++})$	• $\pi_2(1880)$	$1^-(2^{-+})$
• $f_2(1270)$	$0^+(2^{++})$	$\rho(1900)$	$1^+(1^{--})$
• $f_1(1285)$	$0^+(1^{++})$	$f_2(1910)$	$0^+(2^{++})$
• $\eta(1295)$	$0^+(0^{-+})$	• $f_2(1950)$	$0^+(2^{++})$
• $\pi(1300)$	$1^-(0^{-+})$	$\rho_3(1990)$	$1^+(3^{--})$
• $a_2(1320)$	$1^-(2^{++})$	• $f_2(2010)$	$0^+(2^{++})$
• $f_0(1370)$	$0^+(0^{++})$	$f_0(2020)$	$0^+(0^{++})$
$h_1(1380)$	$?^-(1^{+-})$	• $a_4(2040)$	$1^-(4^{++})$
• $\pi_1(1400)$	$1^-(1^{-+})$	• $f_4(2050)$	$0^+(4^{++})$
• $\eta(1405)$	$0^+(0^{-+})$	$\pi_2(2100)$	$1^-(2^{-+})$
• $f_1(1420)$	$0^+(1^{++})$	$f_0(2100)$	$0^+(0^{++})$
• $\omega(1420)$	$0^-(1^{--})$	$f_2(2150)$	$0^+(2^{++})$
$f_2(1430)$	$0^+(2^{++})$	$\rho(2150)$	$1^+(1^{--})$
• $a_0(1450)$	$1^-(0^{++})$	• $\phi(2170)$	$0^-(1^{--})$
• $\rho(1450)$	$1^+(1^{--})$	$f_0(2200)$	$0^+(2^{++}$
• $\eta(1475)$	$0^+(0^{-+})$		or $4^{++})$
• $f_0(1500)$	$0^+(0^{++})$	$\eta(2225)$	$0^+(0^{-+})$
$f_1(1510)$	$0^+(1^{++})$	$\rho_3(2250)$	$1^+(3^{--})$
• $f_2'(1525)$	$0^+(2^{++})$	• $f_2(2300)$	$0^+(2^{++})$
$f_2(1565)$	$0^+(2^{++})$	$f_4(2300)$	$0^+(4^{++})$
$\rho(1570)$	$1^+(1^{--})$	$f_0(2330)$	$0^+(0^{++})$
$h_1(1595)$	$0^-(1^{+-})$	• $f_2(2340)$	$0^+(2^{++})$
• $\pi_1(1600)$	$1^-(1^{-+})$	$\rho_5(2350)$	$1^+(5^{--})$
$a_1(1640)$	$1^-(1^{++})$	$a_6(2450)$	$1^-(6^{++})$
$f_2(1640)$	$0^+(2^{++})$	$f_6(2510)$	$0^+(6^{++})$
• $\eta_2(1645)$	$0^+(2^{-+})$		
• $\omega(1650)$	$0^-(1^{--})$	**OTHER LIGHT**	
• $\omega_3(1670)$	$0^-(3^{--})$	Further States	

STRANGE ($S = \pm1$, $C = B = 0$)

	$I(J^P)$
• $K^\pm$	$1/2(0^-)$
• K^0	$1/2(0^-)$
• K^0_S	$1/2(0^-)$
• K^0_L	$1/2(0^-)$
$K_0^*(800)$	$1/2(0^+)$
• $K^*(892)$	$1/2(1^-)$
• $K_1(1270)$	$1/2(1^+)$
• $K_1(1400)$	$1/2(1^+)$
• $K^*(1410)$	$1/2(1^-)$
• $K_0^*(1430)$	$1/2(0^+)$
• $K_2^*(1430)$	$1/2(2^+)$
$K(1460)$	$1/2(0^-)$
$K_2(1580)$	$1/2(2^-)$
$K(1630)$	$1/2(?^?)$
$K_1(1650)$	$1/2(1^+)$
• $K^*(1680)$	$1/2(1^-)$
• $K_2(1770)$	$1/2(2^-)$
• $K_3^*(1780)$	$1/2(3^-)$
• $K_2(1820)$	$1/2(2^-)$
$K(1830)$	$1/2(0^-)$
$K_0^*(1950)$	$1/2(0^+)$
$K_2^*(1980)$	$1/2(2^+)$
• $K_4^*(2045)$	$1/2(4^+)$
$K_2(2250)$	$1/2(2^-)$
$K_3(2320)$	$1/2(3^+)$
$K_5^*(2380)$	$1/2(5^-)$
$K_4(2500)$	$1/2(4^-)$
$K(3100)$	$?^?(?^{??})$

CHARMED ($C = \pm1$)

• $D^\pm$	$1/2(0^-)$
• D^0	$1/2(0^-)$
• $D^*(2007)^0$	$1/2(1^-)$
• $D^*(2010)^\pm$	$1/2(1^-)$
• $D_0^*(2400)^0$	$1/2(0^+)$
$D_0^*(2400)^\pm$	$1/2(0^+)$
• $D_1(2420)^0$	$1/2(1^+)$
$D_1(2420)^\pm$	$1/2(?^?)$
$D_1(2430)^0$	$1/2(1^+)$
• $D_2^*(2460)^0$	$1/2(2^+)$
• $D_2^*(2460)^\pm$	$1/2(2^+)$
$D^*(2640)^\pm$	$1/2(?^?)$

CHARMED, STRANGE ($C = S = \pm1$)

	$I(J^P)$
• $D_s^\pm$	$0(0^-)$
• $D_s^{*\pm}$	$0(?^?)$
• $D_{s0}^*(2317)^\pm$	$0(0^+)$
• $D_{s1}(2460)^\pm$	$0(1^+)$
• $D_{s1}(2536)^\pm$	$0(1^+)$
• $D_{s2}(2573)$	$0(?^?)$
$D_{s1}^*(2700)^\pm$	$0(1^-)$
$D_{sJ}^*(2860)^\pm$	$0(?^?)$
$D_{sJ}(3040)^\pm$	$0(?^?)$

BOTTOM ($B = \pm1$)

• $B^\pm$	$1/2(0^-)$
• B^0	$1/2(0^-)$
• $B^\pm/B^0$ ADMIXTURE	
• $B^\pm/B^0/B_s^0/b$-baryon ADMIXTURE	
V_{cb} and V_{ub} CKM Matrix Elements	
• B^*	$1/2(1^-)$
$B_J^*(5732)$	$?(?^?)$
• $B_1(5721)^0$	$1/2(1^+)$
• $B_2^*(5747)^0$	$1/2(2^+)$

BOTTOM, STRANGE ($B = \pm1$, $S = \mp1$)

• B_s^0	$0(0^-)$
• B_s^*	$0(1^-)$
• $B_{s1}(5830)^0$	$1/2(1^+)$
• $B_{s2}^*(5840)^0$	$1/2(2^+)$
$B_{sJ}^*(5850)$	$?(?^?)$

BOTTOM, CHARMED ($B = C = \pm1$)

• $B_c^\pm$	$0(0^-)$

$c\overline{c}$

	$I^G(J^{PC})$
• $\eta_c(1S)$	$0^+(0^{-+})$
• $J/\psi(1S)$	$0^-(1^{--})$
• $\chi_{c0}(1P)$	$0^+(0^{++})$
• $\chi_{c1}(1P)$	$0^+(1^{++})$
• $h_c(1P)$	$?^?(1^{+-})$
• $\chi_{c2}(1P)$	$0^+(2^{++})$
• $\eta_c(2S)$	$0^+(0^{-+})$
• $\psi(2S)$	$0^-(1^{--})$
• $\psi(3770)$	$0^-(1^{--})$
• $X(3872)$	$0^?(?^{?+})$
$\chi_{c2}(2P)$	$0^+(2^{++})$
$X(3940)$	$?^?(?^{??})$
$X(3945)$	$0^+(?^{?+})$
• $\psi(4040)$	$0^-(1^{--})$
$X(4050)^\pm$	$?(?^?)$
$X(4140)$	$0^+(?^{?+})$
• $\psi(4160)$	$0^-(1^{--})$
$X(4160)$	$?^?(?^{??})$
$X(4250)^\pm$	$?(?^?)$
• $X(4260)$	$?^?(1^{--})$
$X(4350)$	$0^+(?^{?+})$
$X(4360)$	$?^?(1^{--})$
• $\psi(4415)$	$0^-(1^{--})$
$X(4430)^\pm$	$?(?^?)$
$X(4660)$	$?^?(1^{--})$

$b\overline{b}$

$\eta_b(1S)$	$0^+(0^{-+})$
• $\Upsilon(1S)$	$0^-(1^{--})$
• $\chi_{b0}(1P)$	$0^+(0^{++})$
• $\chi_{b1}(1P)$	$0^+(1^{++})$
• $\chi_{b2}(1P)$	$0^+(2^{++})$
• $\Upsilon(2S)$	$0^-(1^{--})$
$\Upsilon(1D)$	$0^-(2^{--})$
• $\chi_{b0}(2P)$	$0^+(0^{++})$
• $\chi_{b1}(2P)$	$0^+(1^{++})$
• $\chi_{b2}(2P)$	$0^+(2^{++})$
• $\Upsilon(3S)$	$0^-(1^{--})$
• $\Upsilon(4S)$	$0^-(1^{--})$
• $\Upsilon(10860)$	$0^-(1^{--})$
• $\Upsilon(11020)$	$0^-(1^{--})$

NON-$q\overline{q}$ CANDIDATES

NON-$q\overline{q}$ CANDIDATES

Figure 22: Meson summary from [14]. The five mesons marked in red are nominally included in the fit. The eleven others marked in blue are candidates to be included. Mesons marked with a dot are considered established.

Table 5: Mean number of events of each category used to generate simulated experiments. The last two rows give are illustrations of the number of signal events expected for a CP odd Higgs produced with a product branching fraction of 10^{-5}. The numbers for the combined data set toys are sum of the $\Upsilon(2S)$ and $\Upsilon(3S)$ numbers. The Run 1–6 continuum sample used to generate the simulated experiments contains 1.03M CP odd and 2.53M CP all events.

	CP odd			CP all		
	Y3S	Y2S	Continuum	Y3S	Y2S	Continuum
Continuum	82,737	46,051	260,365	201,654	113,019	639,086
Ups non res	19,000	19,000	-	19,000	19,000	-
Ups resonant	1,764	1,764	-	14,378	14,378	-
A0 2 GeV CP odd	72	60	-	72	60	-
A0 4 GeV CP odd	14	12	-	14	12	-

and non-resonant is arbitrary, as is the relative weight of the various resonances. The continuum numbers are scaled using luminosity from the actual continuum sample.

The non-signal probability distribution functions (pdfs) for the $\Upsilon(3S)$ studies are shown in Fig. 23. $\Upsilon(2S)$ and combined data set plots are similar. Some examples of signal pdfs are in Fig. 24. The signal shapes are the mass distributions reconstructed using signal MC. The continuum pdf consists of the full Run 1–6 on peak plus off peak data sample. The non-resonant Υ shapes are smooth threshold functions convolved with an efficiency that drops linearly with mass. The resulting shape is consistent with the distribution observed above 2 GeV/c^2 in generic Υ MC but is essentially arbitrary at lower masses. The resonant Υ distribution is a sum of the five included resonances (Table 4). Each resonance is a relativistic Breit-Wigner.

The various components are combined with appropriate weights to give the mean number of events expected in each 1 MeV/c^2 bin of reconstructed candidate mass. The number of events in each bin in a particular simulated experiment is taken from a Poisson distribution about this mean.

8.2 A sample simulated experiment

An example of a simulated experiment, and an illustration of the steps involved in signal extraction, is shown in Fig. 25–30. It represents the $\Upsilon(3S)$ data set, with the CP odd hypothesis, and includes a 4 GeV/c^2 Higgs. The nominal significance of the signal (i.e., the number of events divided by statistical error) is 6.2σ. This corresponds to 5.2σ after accounting for the

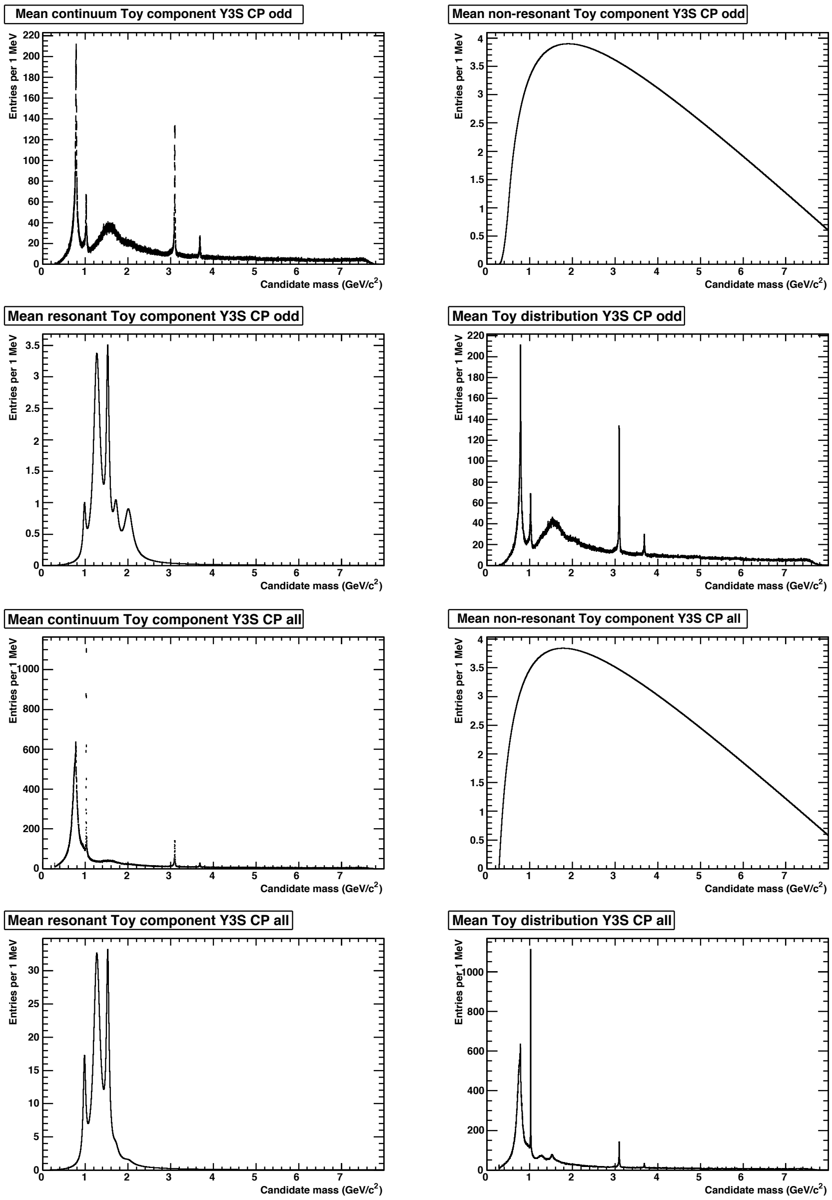

Figure 23: Continuum, Υ non-resonant, Υ resonant, and total contribution to the mean candidate mass distribution used to generate simulated experiments with no signal. Top set of plots is for $\Upsilon(3S)$ CP odd; bottom set is for $\Upsilon(3S)$ CP all. The plots are normalized to the $\Upsilon(3S)$ luminosity.

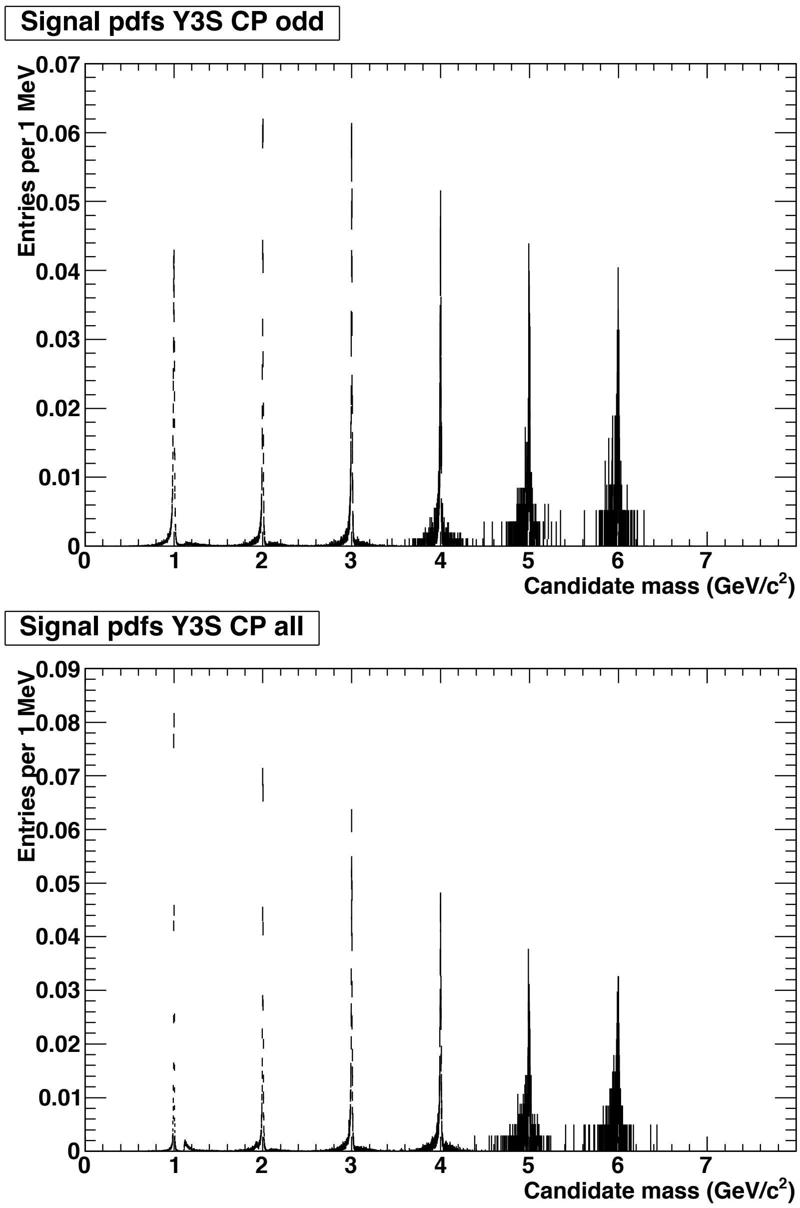

Figure 24: Examples of mass distributions for signal MC. Top plot is CP odd; bottom is CP all. In these plots, the 1 GeV/c^2 A^0 decays to gg, 2 through 4 GeV/c^2 decays 50% to gg and 50% to $s\bar{s}$, and 5 and 6 GeV/c^2 to $c\bar{c}$. The curve for each decay is normalize to unit area.

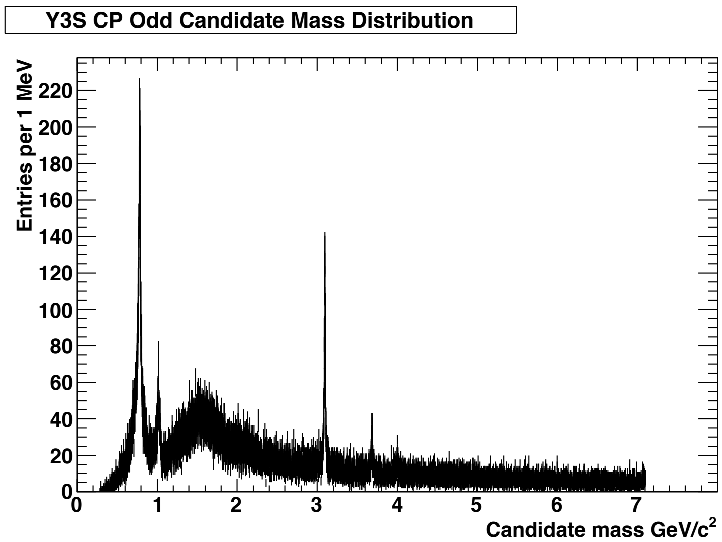

Figure 25: Candidate mass distribution in a simulated $\Upsilon(3S)$ CP odd data set.

trials penalty, and so would be considered an observation if this were the real data.

8.3 Tests of bias with no signal

Simulated experiments generated with no included signal are used to estimate the bias of the of signal extraction procedure in the most likely circumstance, when there is no signal present. In the next section, they are used to quantify the probability that a particular apparent signal is the result of a statistical fluctuation of the background.

100,000 experiments are generated for each of the $\Upsilon(3S)$ CP odd and CP all cases, and 20,000 for the $\Upsilon(2S)$ and combined studies. The fit the Υ spectrum fails (probability $\chi^2 < 10^{-6}$) in a small fraction of the cases (0.1–0.2%). A typical failure is shown in Fig. 31. In the handful of such examples studied, the fit is fine after the initial parameters are manually adjusted. These fits are included in the results presented in this section, which considers average quantities, but are excluded from the next section, which is considering tails of distributions. There are also a significant number of fits to toys that give a good χ^2, but in which the error matrix is not positive

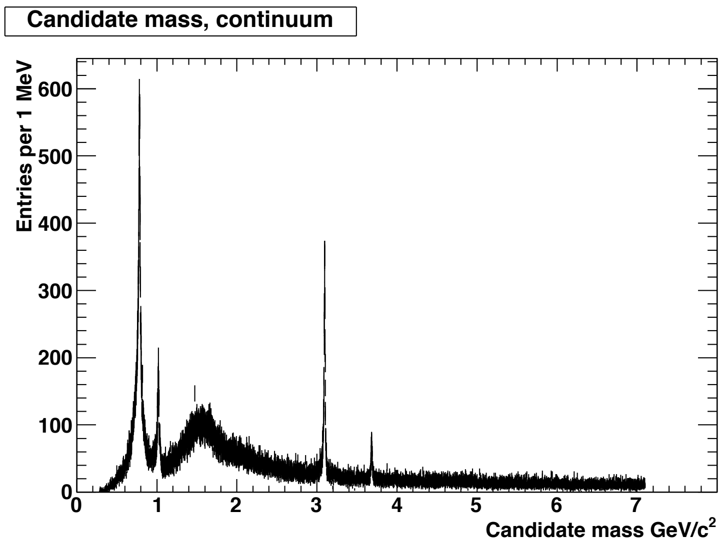

Figure 26: Candidate mass distribution in the simulated continuum sample corresponding to the simulated data set in Fig. 25.

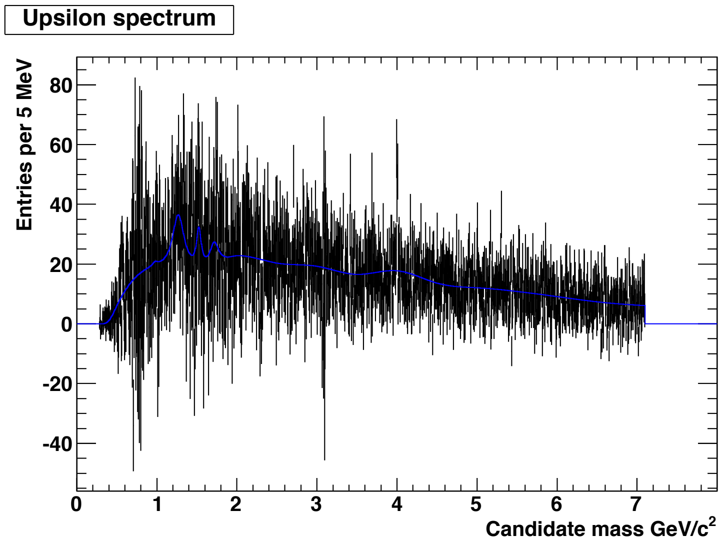

Figure 27: Candidate mass distribution for radiative decays of the simulated $\Upsilon(3S)$ data set obtained by subtracting the continuum sample in Fig. 26 from the data in Fig. 25. The solid blue line is the fit to the spectrum. Note the 5 MeV/c^2 bins, versus the 1 MeV/c^2 bins in the earlier two plots.

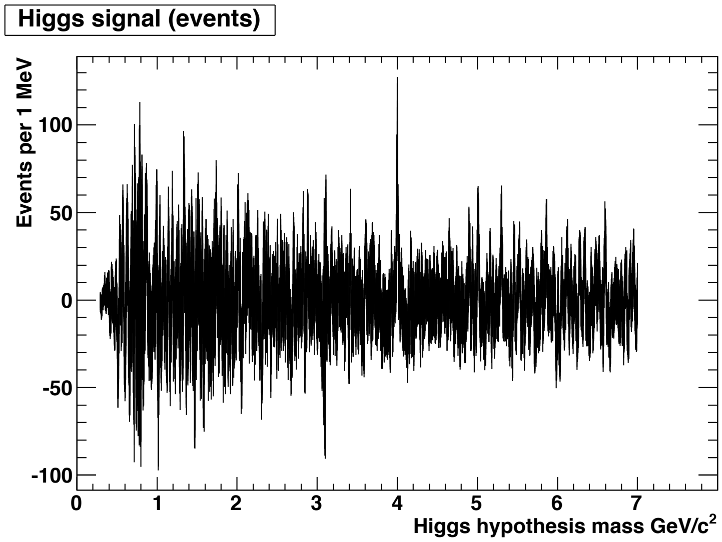

Figure 28: Higgs signal (events) in the simulated sample versus hypothesis mass.

definite. This is probably due to the large correlations between the resonant and non resonant parameters, and among the non resonant parameters.

Figures 32–37 summarize the results. In all cases, the bias is less than 1.5 events for all Higgs hypothesis masses, corresponding to less than 0.1σ. The histograms of all Higgs measurements in σ (bottom left hand plots) are close to being normal distributions of zero mean and unit width, although with small low-side tails due to Poisson fluctuations in low statistics bins. The fit qualities (probability χ^2) are biased low, so it would not be unexpected if the fit to actual data is low quality. Since the resonance fits use the same pdfs for generation and for fitting, the poor quality is presumably due to the cubic spline fit to the Υ spectrum. Note, however, that the fit is good enough to not bias the Higgs signal, which is the point of the analysis.

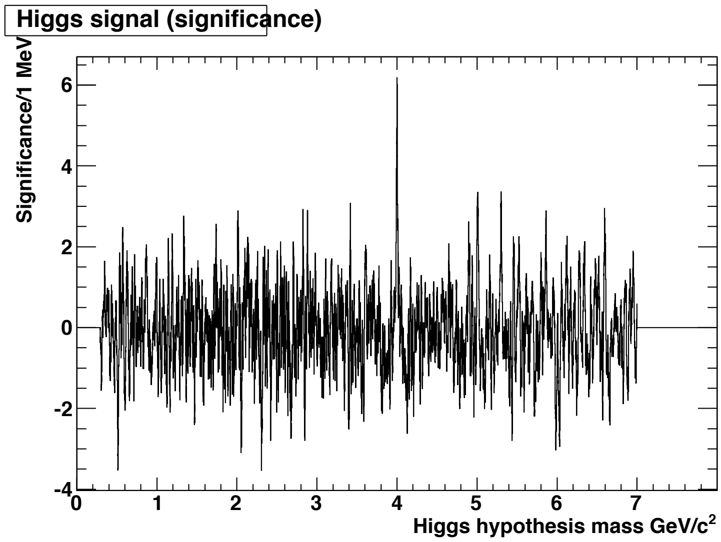

Figure 29: Higgs signal significance ($\mathcal{S}$ = signal/statistical error) in the simulated sample versus hypothesis mass. The signal at 4 GeV/c^2 is 110$\pm$18 events, or 6.2σ nominal, 5.2σ after accounting for trials penalty.

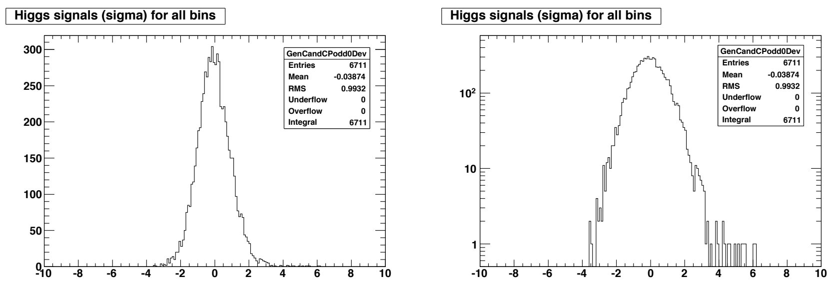

Figure 30: Histogram of the significance of the 6711 Higgs measurements in Fig. 29, linear and log versions. The high-side tail extending beyond 6 indicates the presence of a signal.

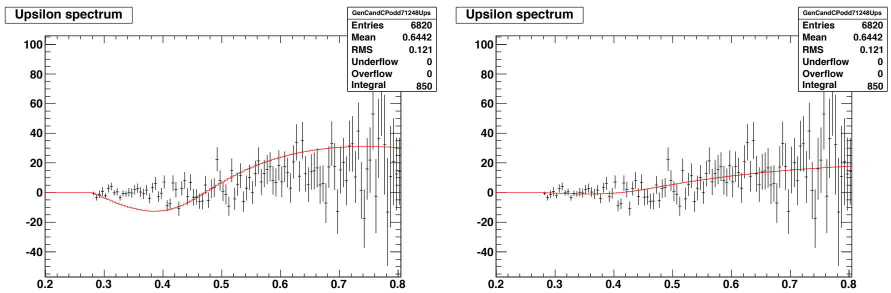

Figure 31: A detail of the candidate mass spectrum for the Υ radiative decays in a simulated experiment. The left plot shows a typical example of a fit that initially fails. The right plot shows the fit after the initial parameters are manually adjusted.

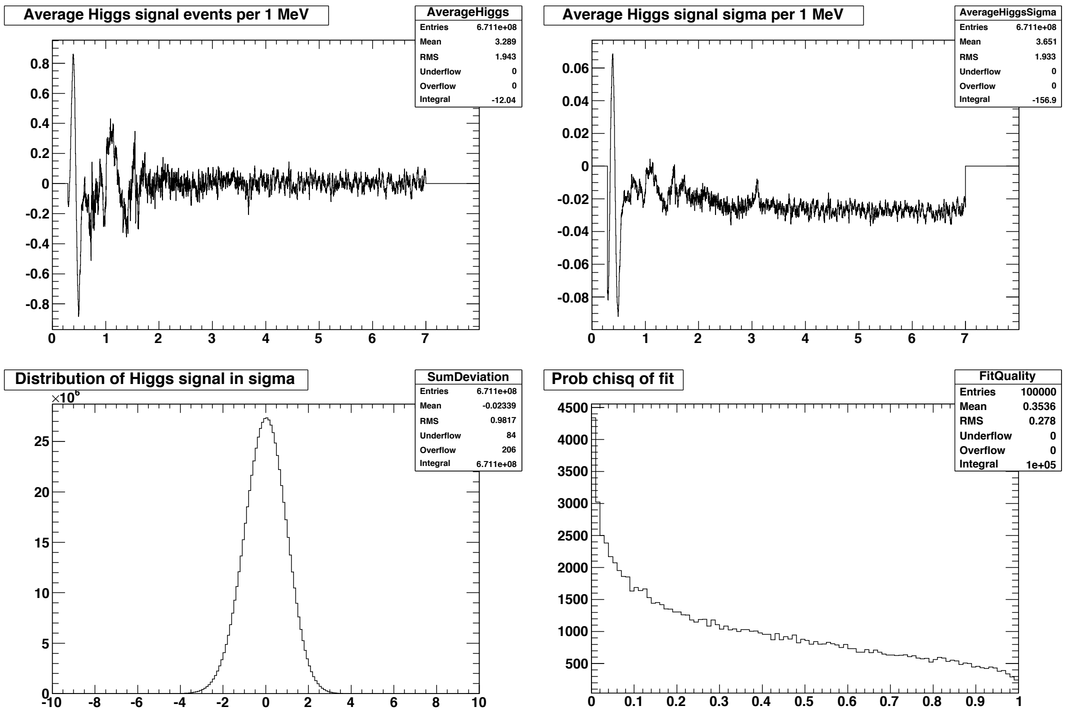

Figure 32: $\Upsilon(3S)$ CP odd toy results. (Upper left) Average Higgs signal in events as a function of hypothesis mass. (Upper right) Average Higgs signal in σ as a function of hypothesis mass. (Bottom left) Summary of all Higgs signals in σ. (Bottom right) Probability χ^2 of the fit to the Υ candidate mass spectrum.

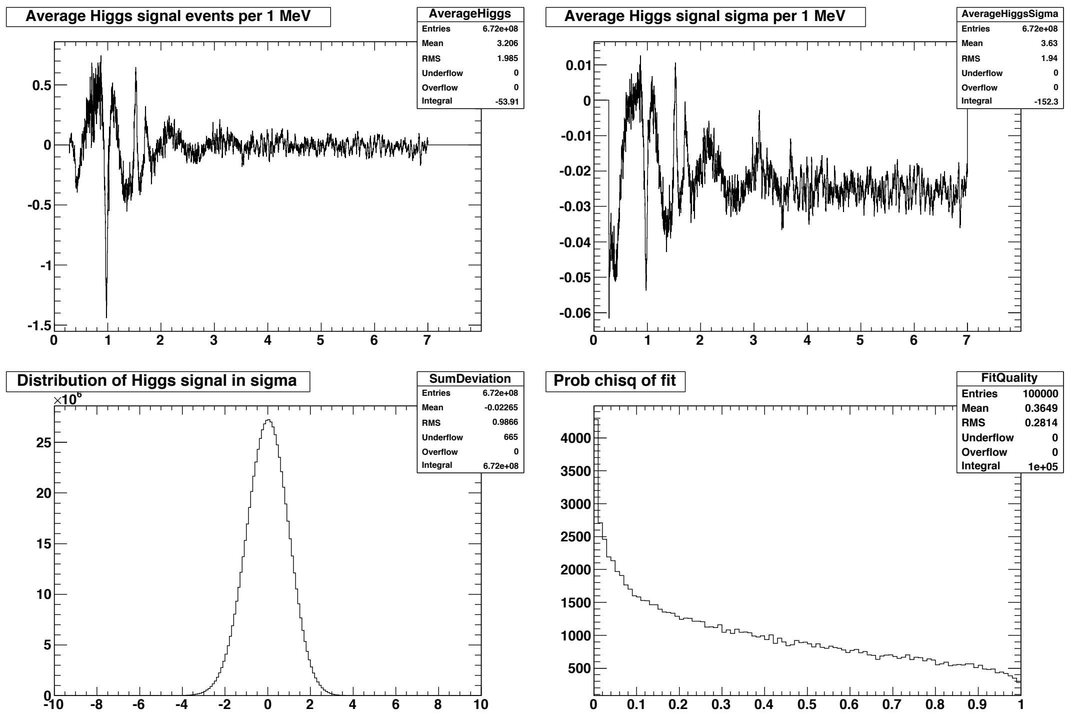

Figure 33: $\Upsilon(3S)$ CP all toy results. (Upper left) Average Higgs signal in events as a function of hypothesis mass. (Upper right) Average Higgs signal in σ as a function of hypothesis mass. (Bottom left) Summary of all Higgs signals in σ. (Bottom right) Probability χ^2 of the fit to the Υ candidate mass spectrum.

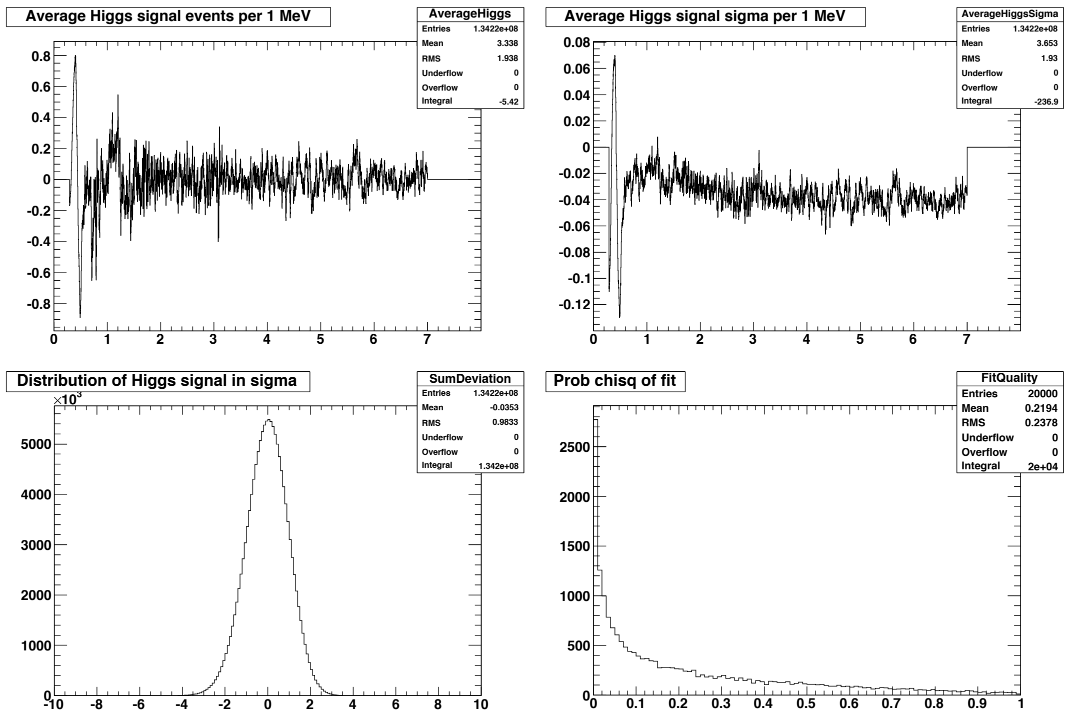

Figure 34: $\Upsilon(2S)$ CP odd toy results. (Upper left) Average Higgs signal in events as a function of hypothesis mass. (Upper right) Average Higgs signal in σ as a function of hypothesis mass. (Bottom left) Summary of all Higgs signals in σ. (Bottom right) Probability χ^2 of the fit to the Υ candidate mass spectrum.

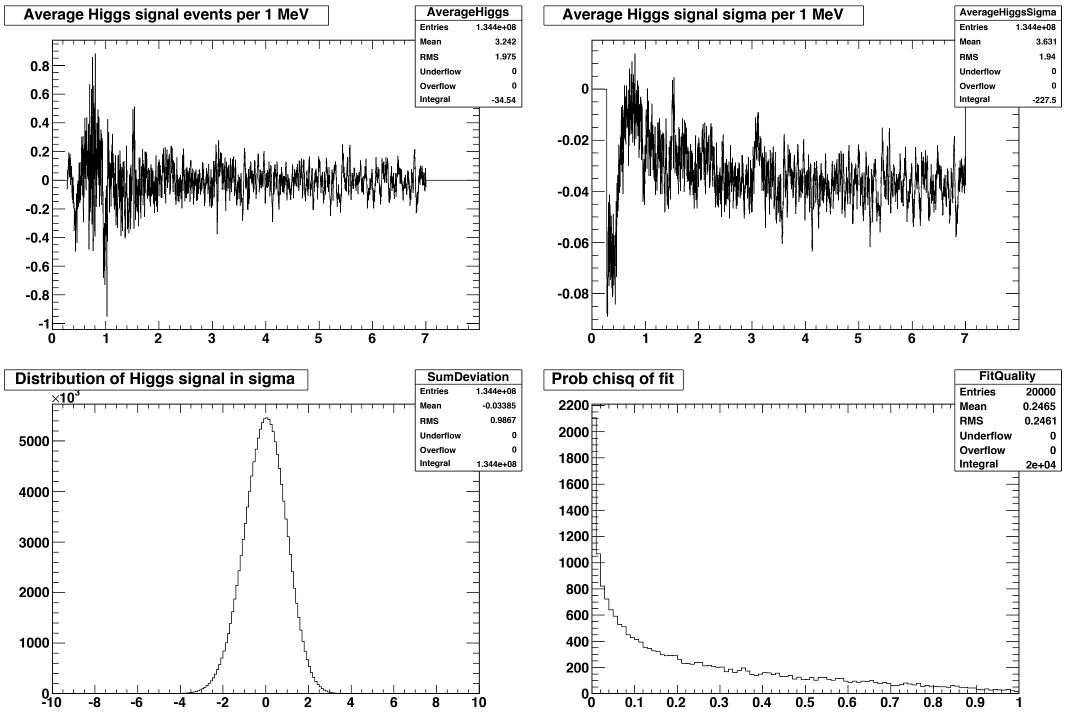

Figure 35: $\Upsilon(2S)$ CP all toy results. (Upper left) Average Higgs signal in events as a function of hypothesis mass. (Upper right) Average Higgs signal in σ as a function of hypothesis mass. (Bottom left) Summary of all Higgs signals in σ. (Bottom right) Probability χ^2 of the fit to the Υ candidate mass spectrum.

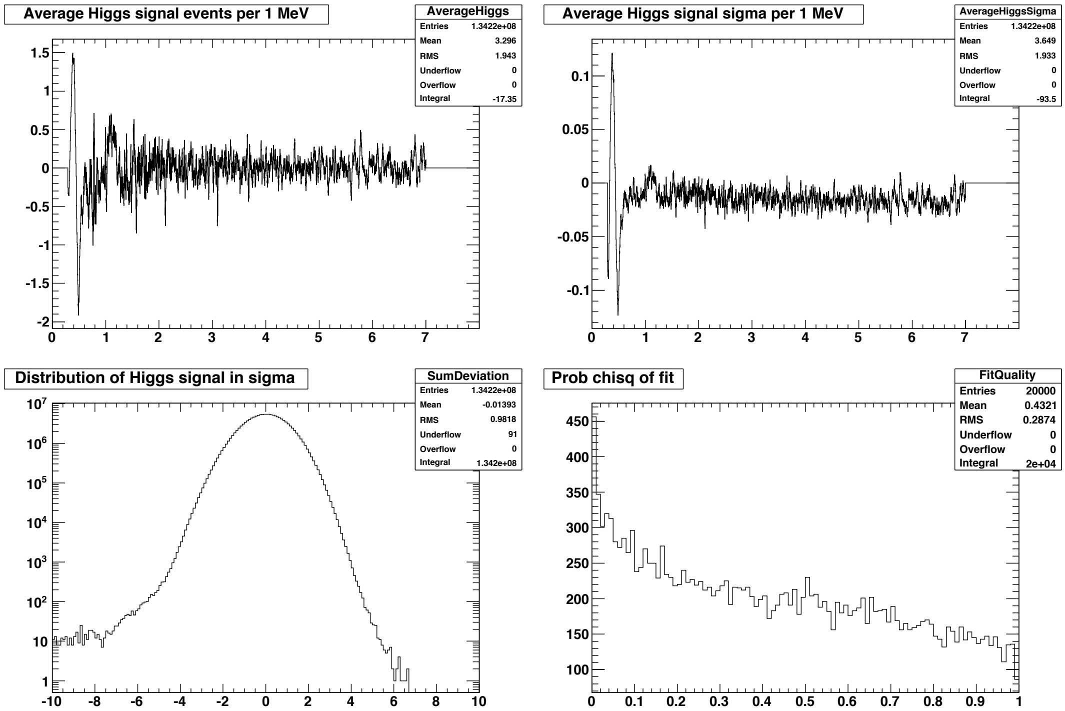

Figure 36: Run 7 on peak CP odd toy results. (Upper left) Average Higgs signal in events as a function of hypothesis mass. (Upper right) Average Higgs signal in σ as a function of hypothesis mass. (Bottom left) Summary of all Higgs signals in σ. (Bottom right) Probability χ^2 of the fit to the Υ candidate mass spectrum.

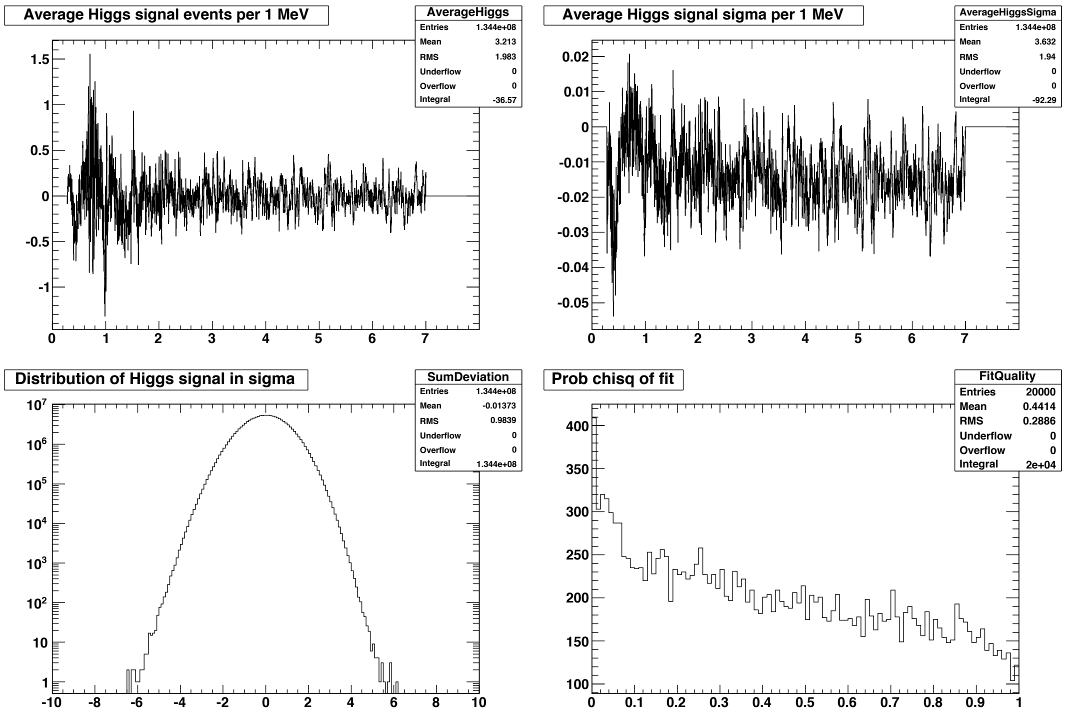

Figure 37: Run 7 on peak CP all toy results. (Upper left) Average Higgs signal in events as a function of hypothesis mass. (Upper right) Average Higgs signal in σ as a function of hypothesis mass. (Bottom left) Summary of all Higgs signals in σ. (Bottom right) Probability χ^2 of the fit to the Υ candidate mass spectrum.

8.4 Significance of signal / trials penalty

Even if there is no light Higgs, there is a chance of seeing a significant upwards fluctuation at one of the ~ 6700 hypothesis masses. The true significance of an apparent signal, therefore, is not the size of the signal divided by its statistical error, but rather by its p-value, the probability of observing such a signal or more due to statistical fluctuations of the background. This reduction in significance can be characterized by the "trials penalty" t. The true significance $\mathcal{S}'$ is obtained by subtracting t in quadrature from the apparent significance, $\mathcal{S}' = \sqrt{\mathcal{S}^2 - t^2}$, where S is the most significant upwards fluctuation among the signals $\mathcal{S}_i \equiv H_i/\delta_i$ at each mass m_i.

Toy experiments with no signal included are used to calculate the distribution of S expected from the statistical fluctuations of the background. Figure 38 shows the distribution of S for each of the six different cases (so there is one entry in a plot per toy experiment). A statement that an experiment contains 3σ evidence for a Higgs actually means that the probability that the signal is due to a background fluctuation is 0.00135, the area of a Normal curve above 3. From the $\Upsilon(3S)$ CP odd plot in Fig. 38, for example, we see that 0.135% of experiments have a maximum signal of 4.57σ or more, implying a trials penalty $t = \sqrt{4.57^2 - 3^2} = 3.45$. Looking at the all of the cases, for 2σ (2.25%) and 3σ fluctuations, the derived trials penalty ranges from 3.25 to 3.65 σ, with an average value of 3.5σ. Higher statistics studies could be done if the presence of a signal in the actual data demands it.

Figure 39 shows the opposite quantity, the minimum signal in each toy experiment.

8.4.1 The number of mass hypotheses

Fewer mass hypotheses would produce a smaller trials penalty, but could also produce a smaller signal, if none of the corresponding Higgs mass windows were centered on the actual signal. To study this tradeoff, 20000 $\Upsilon(3S)$ CP odd toys were generated with no signal, and 4000 were generated with 100 signal events at 4 GeV/c^2. The toys were analyzed with the nominal 1 MeV/c^2 steps, and with steps that were a fraction of the Higgs mass window full width shown in Fig. 9. The results, shown in Table 6, indicate that the 1 MeV/c^2 step gives the most significant average signal after subtracting the trials penalty.

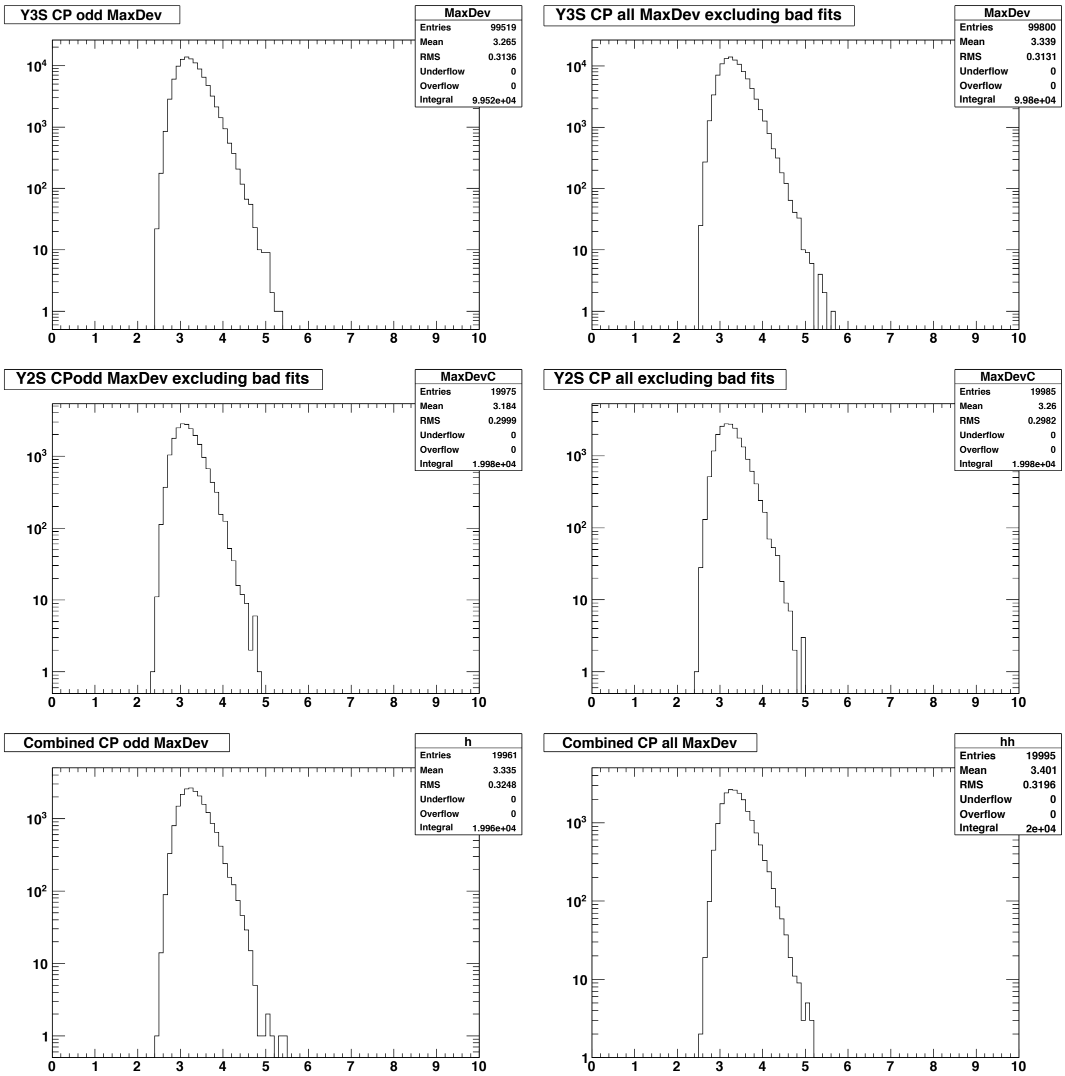

Figure 38: Maximum Higgs signal (σ) in simulated background-only experiments for (top row) $\Upsilon(3S)$, (middle row) $\Upsilon(2S)$, and (bottom row) combined data. CP odd is on the left, CP all is on the right.

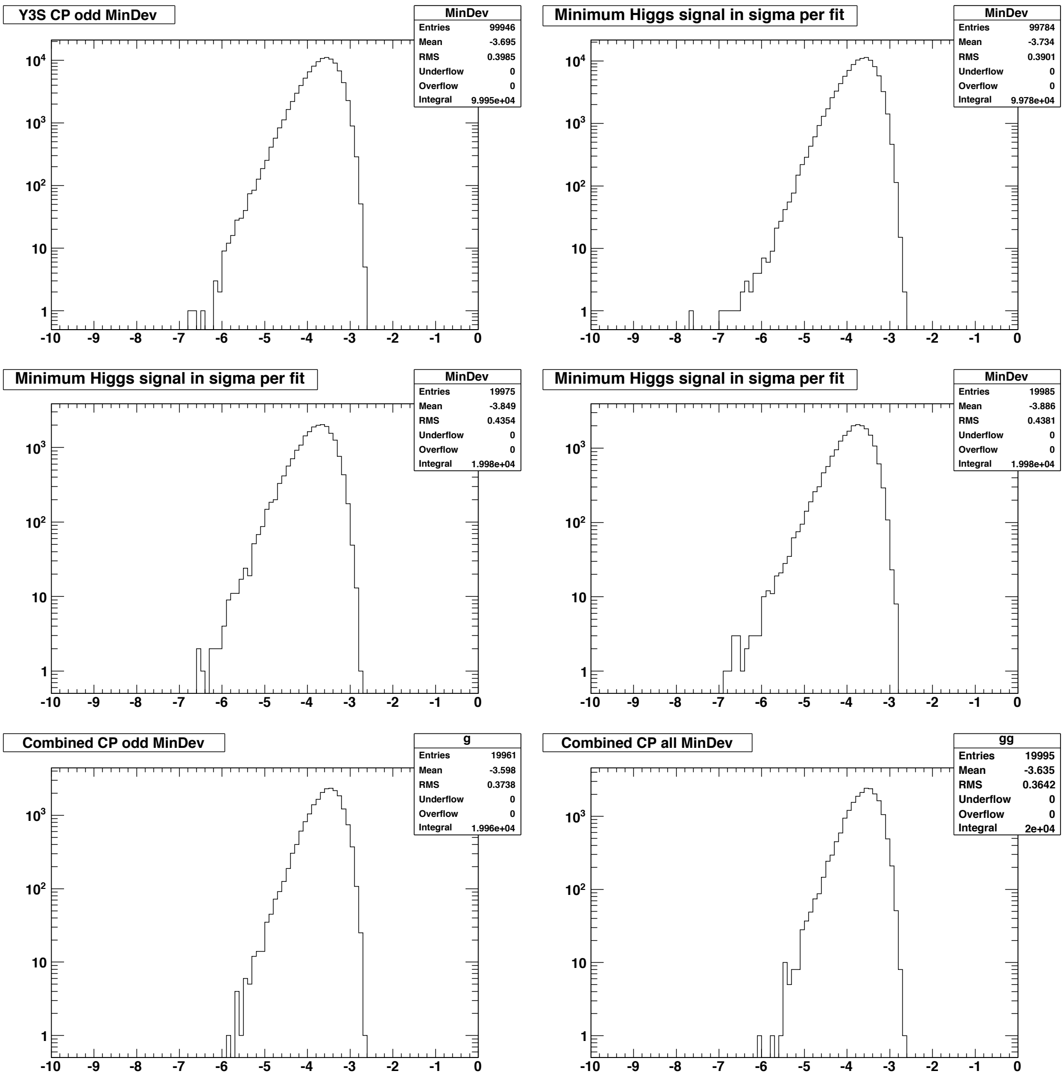

Figure 39: Minimum Higgs signal (σ) in simulated background-only experiments for (top row) $\Upsilon(3S)$, (middle row) $\Upsilon(2S)$, and (bottom row) combined data. CP odd is on the left, CP all is on the right.

Table 6: Average signal (in events and sigma) and trials penalty for various numbers of mass hypotheses. The first row is for 1 MeV/c^2 steps; in the other rows, the step size is a function of mass, and is calculated as a fraction of the mass window.

Step size	# hypotheses	Signal Events	Signal Sig	Trials penaly	Net
none	6711	99.2	5.75	3.45	4.60
0.125	3798	97.6	5.67	3.38	4.55
0.25	1802	96.1	5.59	3.27	4.53
0.5	888	91.8	5.37	3.12	4.37
0.75	591	87.6	5.17	3.02	4.19

8.5 Tests of bias on signal

The bias on a non-zero Higgs signal is studied by comparing the number of signal events reconstructed in simulated experiments to the number known to have been included. An example of one such experiment was shown in Sec. 8.2, which included 100 4 GeV/c^2 Higgs events passing all cuts. Figure 40 shows the number of Higgs events measured in an ensemble of such simulated experiments. The bias in this case is negligible.

Note, however, that this plot shows the largest Higgs signal in each experiment. Due to fluctuations in the background, the reconstructed mass may be slightly different from the true 4 GeV/c^2 value. If the reconstructed mass is constrained to be 4 GeV/c^2, the average number of events is 94.4, compared to the true value of 100. This small bias is consistent with the non-resonant component of the fit being pulled slightly by the presence of the signal.

This brief study indicates that the signal extraction works reasonably well. If necessitated by the presence of a signal in data, additional studies could be undertaken. It could also be possible to modify the fitting procedure by excluding the narrow mass region of the signal.

8.6 Fits to known light mesons

Table 7 summarizes the fit results regarding the light resonances included in $\Upsilon(3S)$ simulated experiments, when there is no Higgs signal present. The table lists the mean number of each resonance included; the actual number in a particular experiment is distributed about this mean, as opposed to Sec. 8.5, in which the number of signal events was constrained to be exactly 100 in all experiments. The fits are not significantly biased with respect to the mean, but the mean errors in all cases are significantly low compared to the true rms. Because these resonances are broad compared to the Higgs

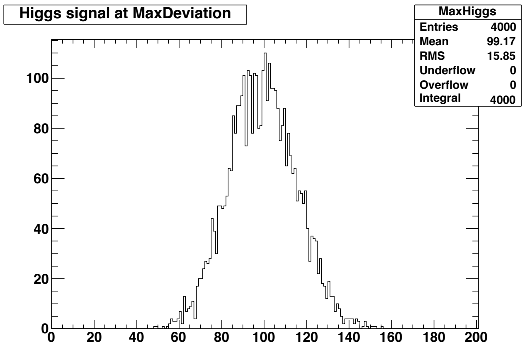

Figure 40: Number of Higgs events reconstructed in simulated $\Upsilon(3S)$ experiments containing 100 4 GeV/c^2 CP odd Higgs events passing all cuts.

signal, there are substantial correlations with the non-resonant component. It is also worth noting that the systematic error on f_L produces a large uncertainty in the total number of Υ decays in the sample. An analysis looking at particular final states, such as that being done by Rocky So, would be a better way of measuring the properties of light resonances produced in radiative decays of the Υ.

Table 7: Fit results for the light resonances included in simulated experiments of the $\Upsilon(3S)$, for CP odd and CP all hypotheses. No Higgs signal is included in these studies. Means, biases, and rms are in events; masses and widths are in MeV/c^2.

Y3S CP odd						
	Mass	Width	True mean	Bias	rms(bias)	Mean fit error
f0(980)	980	70	82	6	135	32
f2(1270)	1275.1	185.1	930	3	289	86
f'2(1525)	1525	73	337	-4	164	47
f0(1710)	1720	135	139	-6	235	64
f4(2050)	2018	237	277	-2	381	118
Y3S CP all						
	Mass	Width	True mean	Bias	rms(bias)	Mean fit error
f0(980)	980	70	1630	30	393	75
f2(1270)	1275.1	185.1	8999	8	604	57
f'2(1525)	1525	73	3264	-12	237	35
f0(1710)	1720	135	282	-16	306	35
f4(2050)	2018	237	203	1	428	158

9 Fit results for Run 7 on peak data

A total of 371,740 events in the Run 7 on peak data satisfy the CP all selection criteria with candidate mass in the region 0.29–7.1 GeV/c^2, with 171,136 of these in the CP odd subset. Figure 41 shows the candidate mass distribution overlaid with the fit and the normalized continuum distribution. The fit results are summarized in Table 8.

Subtracting the normalized continuum from the on peak data and from the fit gives the candidate mass spectrum from Υ decay (Fig. 42).

The number of Higgs events as a function of Higgs mass is shown in Fig. 43, and the corresponding statistical significance (signal events divided by statistical error) is shown as a function of mass in Fig. 44, and is summarized in Fig. 45. The largest upwards fluctuations (considering only statistical errors) are 3.5σ at 3.107 GeV/c^2 for CP-all and 3.2σ at 0.772 GeV/c^2 for CP-odd. The most negative fluctuations are are -3.6σ at 0.914 GeV/c^2 for CP-all and -3.9σ at 0.575 GeV/c^2 for CP-odd (Table 9). The corresponding locations candidate mass distributions are shown in Fig 46–47. The fraction of zero-signal Toys with fluctuations at least this large are 33% (CP-all) and 63% (CP-odd) for the upwards fluctuations, and 49% (CP-all) and 19% (CP-odd) for the downwards fluctuations. Note that the size and location of the maximum deviations are changed by the inclusion of systematic errors on the background (Sec. 11).

Although the uncertainties on the yields of the five resonances are not reliable, it is nevertheless clear that there are no significant signals present. There is fairly large negative fluctuation in the $f_0(980)$ in the Run 7 on peak CP all fit.

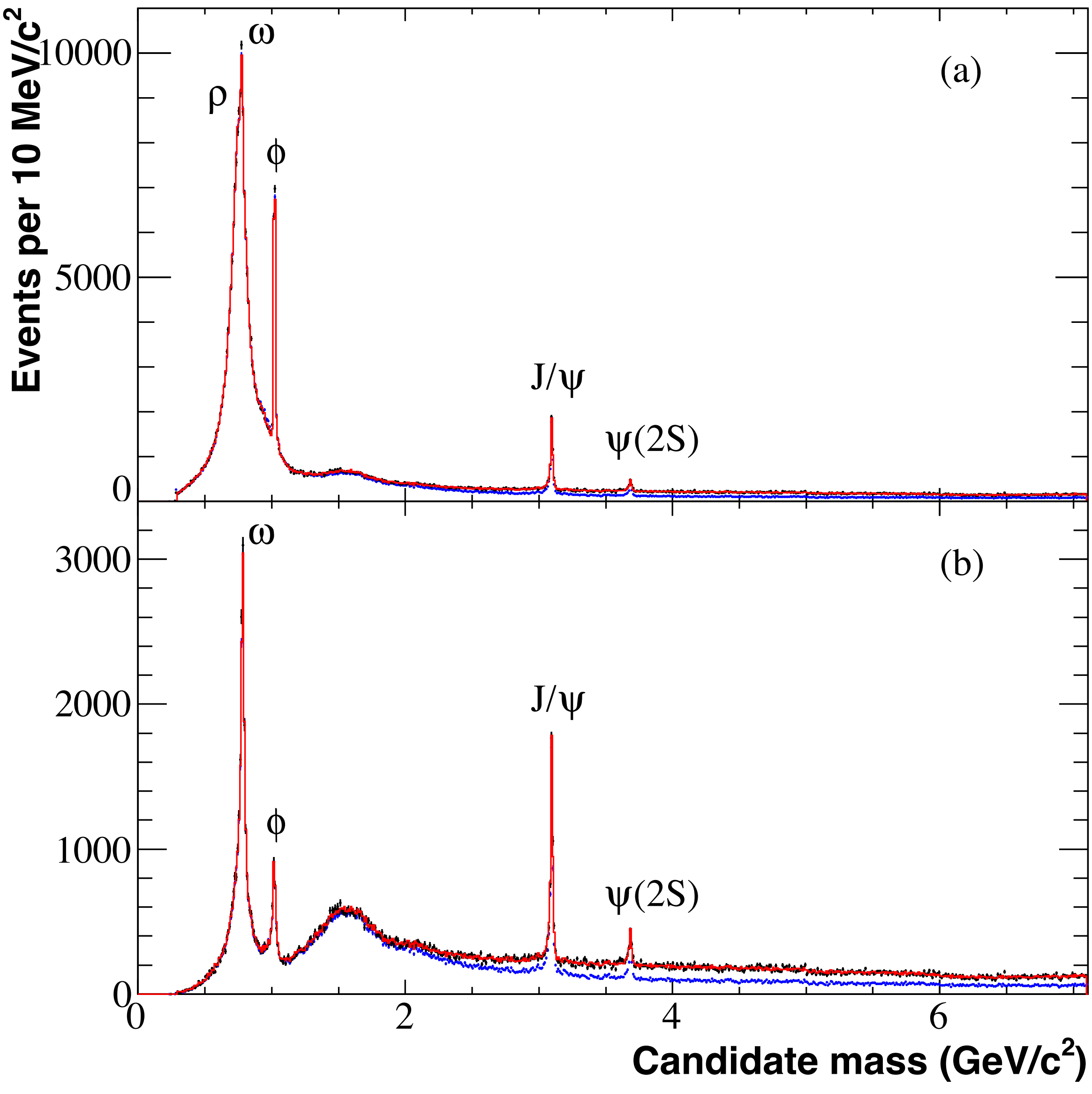

Figure 41: Run 7 on peak candidate mass spectrum in the (a) CP-all and (b) CP-odd analyses. The top curve in each plot is the on-peak data overlaid (in red) with the fit described below, while the bottom curve (blue) is the scaled continuum data. The prominent initial state radiation resonances are labeled.

Table 8: Results of the fits to the candidate mass spectra for the (top) Run 7 on-peak data, (middle) $\Upsilon(3S)$ data, and (bottom) $\Upsilon(2S)$ data. Numbers of events are for the fit region, 0.29–7.1 GeV/c^2.

Run 7 On Peak	CP odd	+/-	CP all	+/-
# events on peak	171,136		371,740	
# events continuum	259,794		658,262	
χ^2 / dof	1268 / 1341		1293 / 1341	
probability χ^2	0.921		0.824	
continuum	130,907	1,085	326,128	1,073
non-resonant	40,349	1,368	46,643	485
f0(980)	-144	111	-1345	250
f2(1270)	-16	302	189	343
f2'(1525)	91	172	267	177
f0(1710)	24	244	-149	240
f4(2050)	-71	435	12	408
Y3S On Peak	CP odd	+/-	CP all	+/-
# events on peak	102,796		230,838	
# events continuum	259,794		658,262	
χ^2 / dof	1265 / 1341		1263 / 1341	
probability χ^2	0.931		0.936	
continuum	85,548	873	210,557	1,020
non-resonant	17,483	1,078	21,410	1,220
f0(980)	-156	98	-846	210
f2(1270)	154	243	32	340
f2'(1525)	76	137	162	154
f0(1710)	-18	199	-136	219
f4(2050)	-290	357	-341	368
YSS On Peak	CP odd	+/-	CP all	+/-
# events on peak	68,340		140,902	
# events continuum	259,794		658,262	
χ^2 / dof	1367 / 1341		1409 / 1341	
probability χ^2	0.307		0.095	
continuum	45,258	634	115,557	800
non-resonant	22,955	817	25,187	1,065
f0(980)	10	75	-489	154
f2(1270)	-180	181	172	297
f2'(1525)	14	108	106	130
f0(1710)	47	156	-4	178
f4(2050)	236	277	377	287

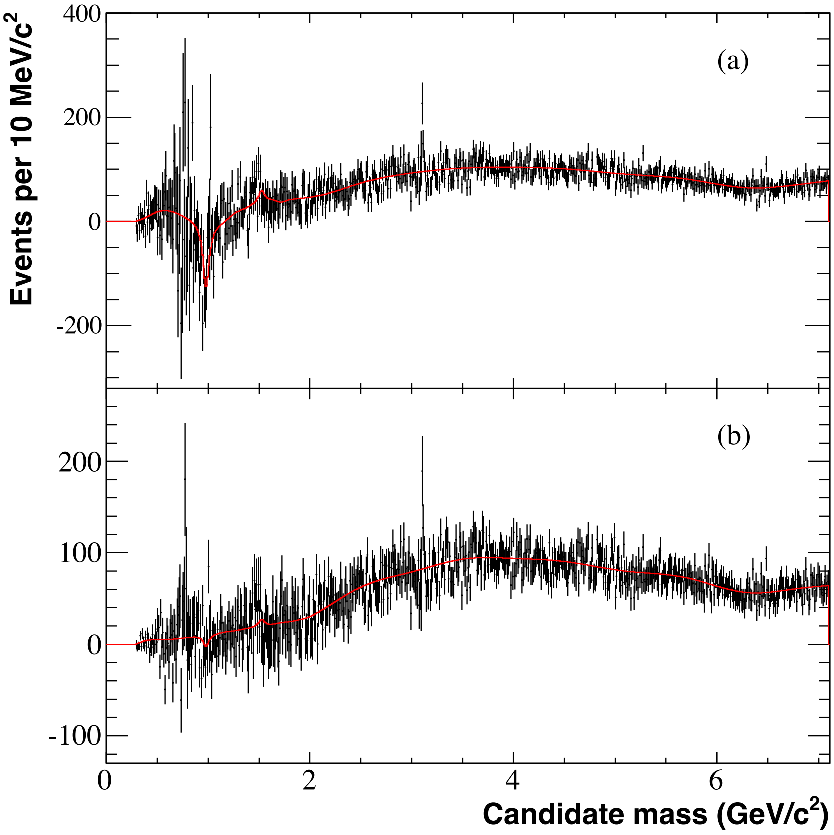

Figure 42: A^0 candidate mass spectrum after continuum subtraction, overlaid with fit. (a) CP-all analysis; (b) CP-odd analysis.

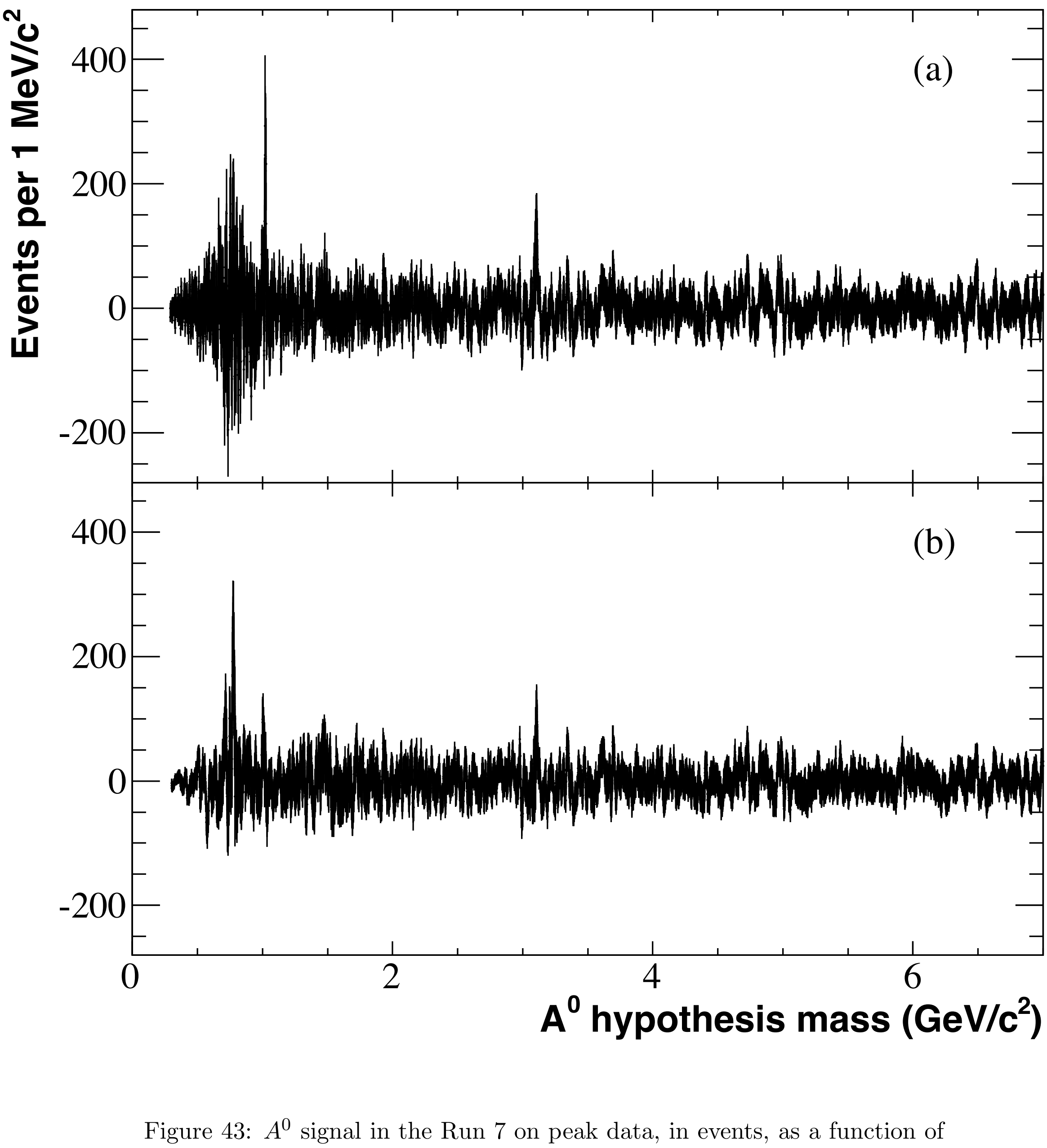

Figure 43: A^0 signal in the Run 7 on peak data, in events, as a function of hypothesis mass, for (a) CP-all analysis, and (b) CP-odd analysis.

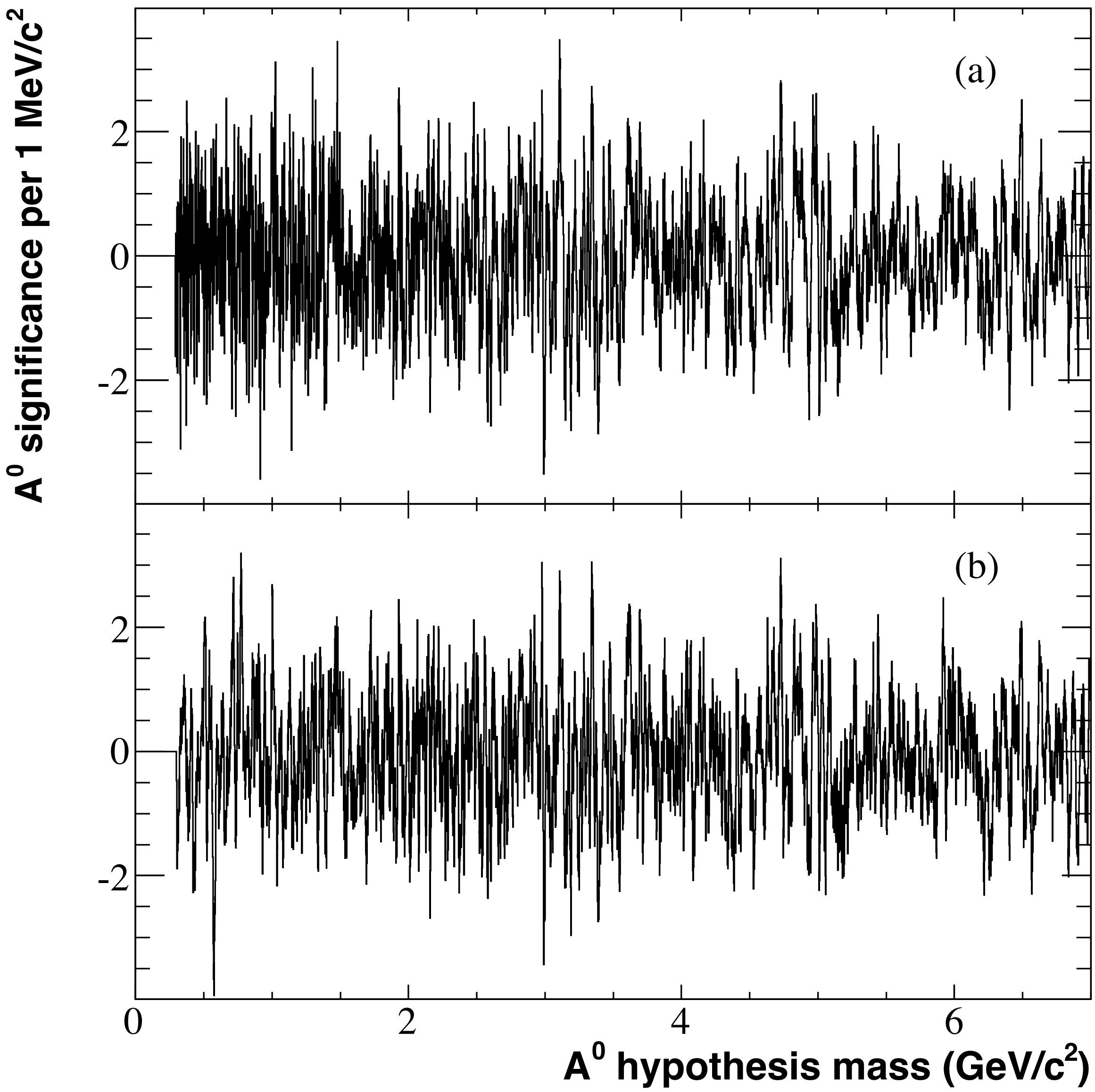

Figure 44: Statistical significance (events divided by statistical error) of the A^0 signal in the Run 7 on peak data as a function of mass, for (a) CP-all analysis, and (b) CP-odd analysis.

Table 9: Largest and most-negative fluctuations in A^0 statistical significance in the (top) Run 7 on-peak data, (middle) $\Upsilon(3S)$ data, and (bottom) $\Upsilon(2S)$ data. The mass is given in GeV/c^2. P-values are the fraction of zero-signal Toy experiments that have fluctuations at least that magnitude.

	CP odd			**CP all**		
Run 7 On Peak	Sigma	Mass	p-value	Sigma	Mass	p-value
Maximum	3.2	0.772	0.63	3.5	3.107	0.33
Minimum	-3.9	0.575	0.19	-3.6	0.914	0.49
Y3S On Peak						
Maximum	3.1	0.717	0.67	3.1	2.557	0.77
Minimum	-4.7	0.572	0.02	-3.9	0.914	0.29
Y2S On Peak						
Maximum	3.2	2.300	0.43	4.3	1.477	0.004
Minimum	-3.3	3.042	0.93	-3.6	1.889	0.73

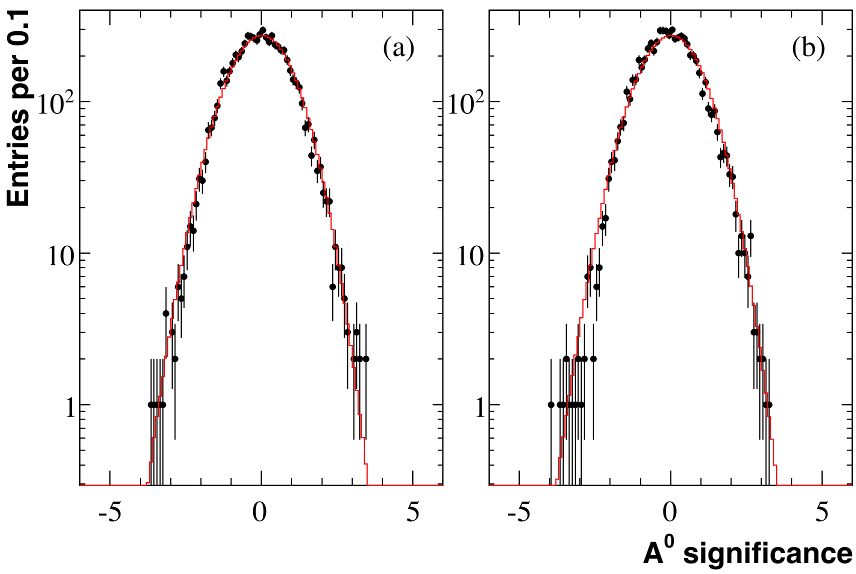

Figure 45: Histogram of the statistical significance of the A^0 signal in the Run 7 on peak data for (a) the 6710 masses considered in the CP-all analysis, and for (b) the 6701 masses in the CP-odd analysis. The overlaid curve shows the distribution expected in the absence of signal.

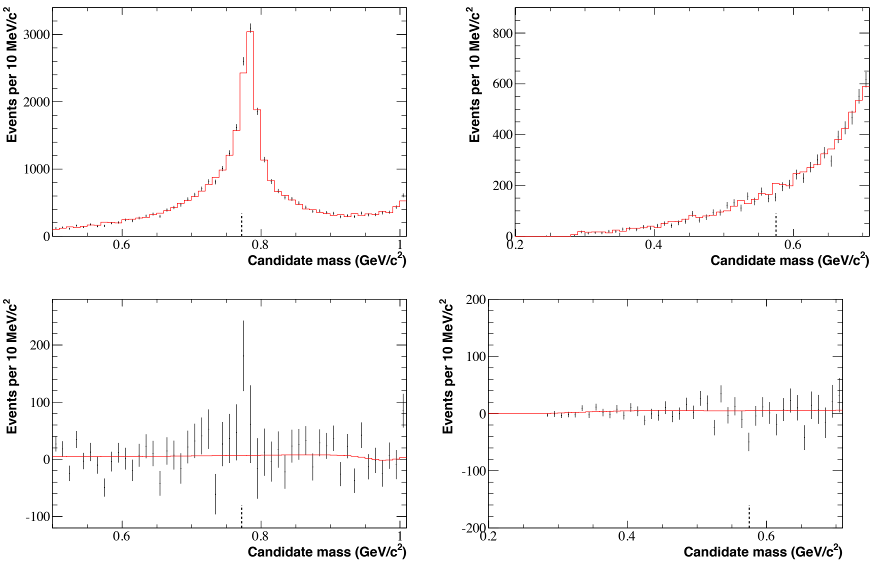

Figure 46: Locations of (left) maximum and (right) minimum Higgs signals in the Run 7 on peak CP odd analysis. Black points are data, red line is the fit. Lower row shows the same distributions after subtracting the continuum background. The location of the deviation is marked by a dashed line on the horizontal axis.

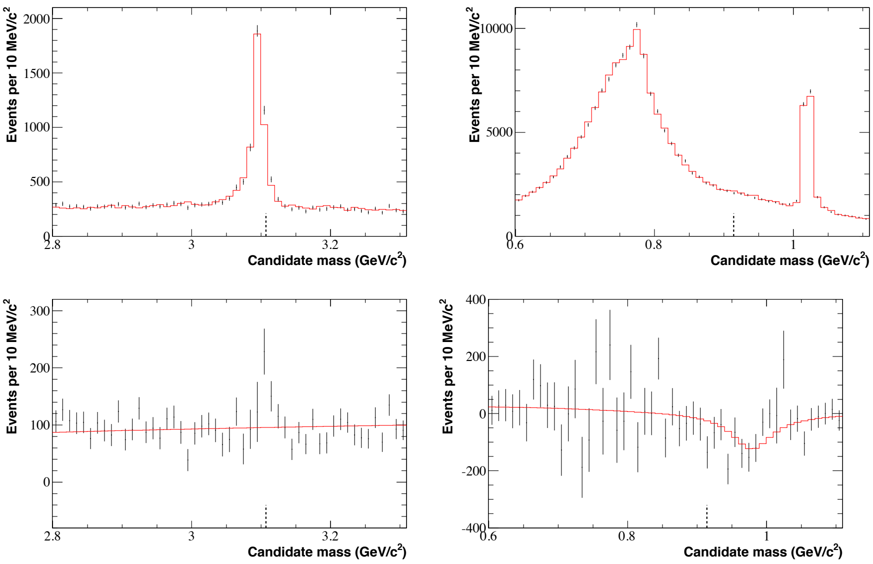

Figure 47: Locations of (left) maximum and (right) minimum Higgs signals in the Run 7 on peak CP all analysis. Black points are data, red line is the fit. Lower row shows the same distributions after subtracting the continuum background. The location of the deviation is marked by a dashed line on the horizontal axis.

9.1 Fit results for the $\Upsilon(3S)$ and $\Upsilon(2S)$ samples

The results of separate fits to the $\Upsilon(3S)$ and $\Upsilon(2S)$ data sets are summarized in Table 8, and in Fig. 48–57.

The most and least significant Higgs signals in these samples are listed in Table 9. The largest magnitude deviation among off the fits is the nominal 4.3σ upwards fluctuation in the $\Upsilon(2S)$ CP all analysis. The corresponding p-value of 0.4%, found using Toy experiments, is equivalent to 2.5σ.

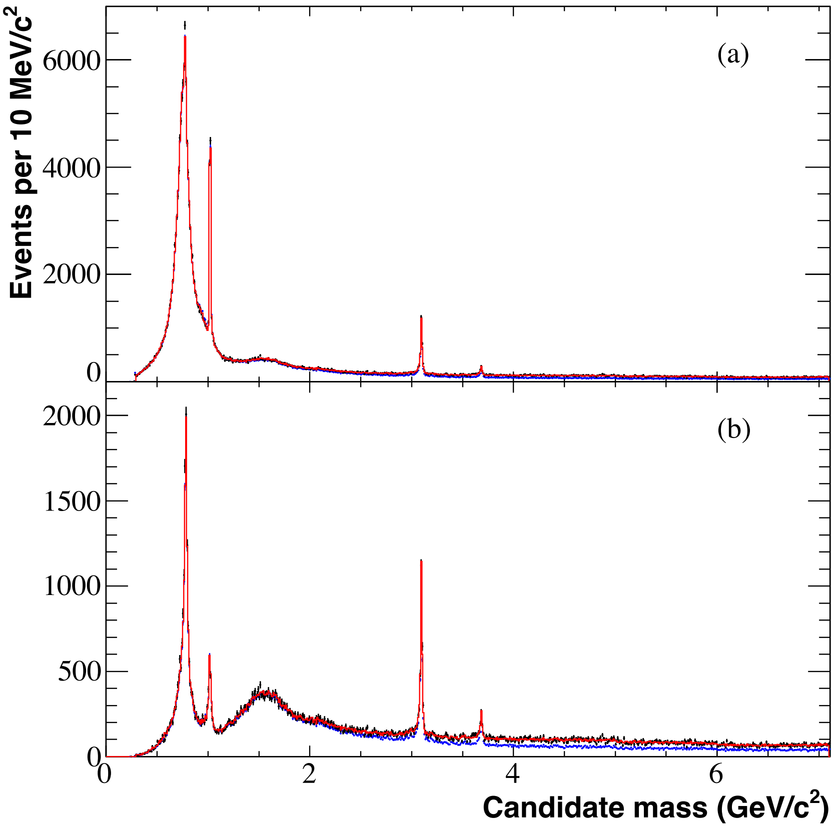

Figure 48: $\Upsilon(3S)$ candidate mass spectrum in the (a) CP-all and (b) CP-odd analyses. The top curve in each plot is the on-peak data overlaid (in red) with the fit described below, while the bottom curve (blue) is the scaled continuum data.

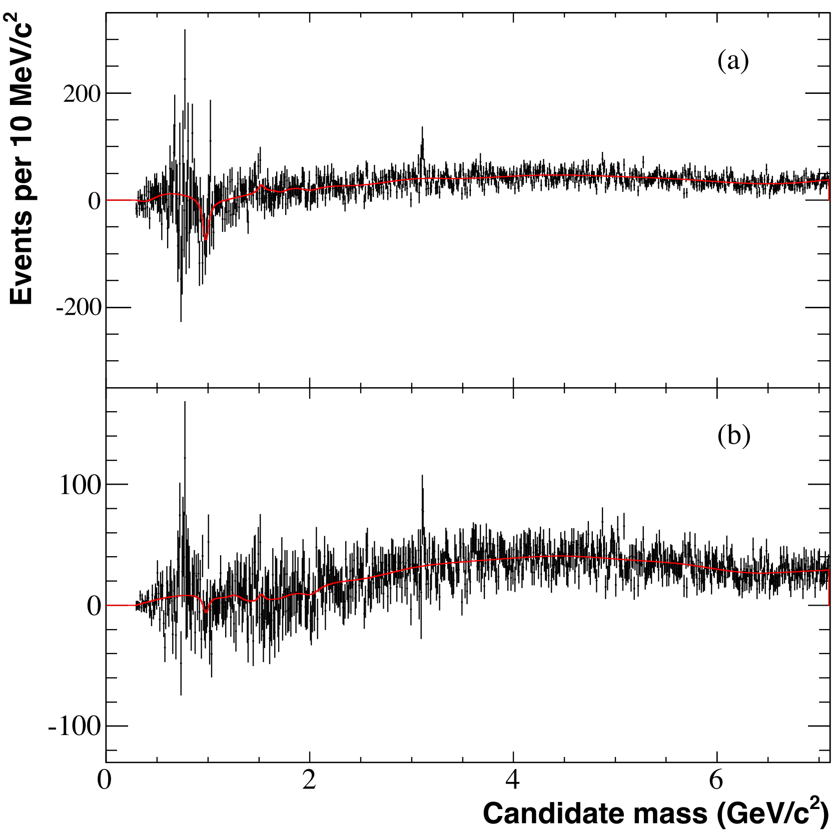

Figure 49: $\Upsilon(3S)$ A^0 candidate mass spectrum after continuum subtraction, overlaid with fit. (a) CP-all analysis; (b) CP-odd analysis.

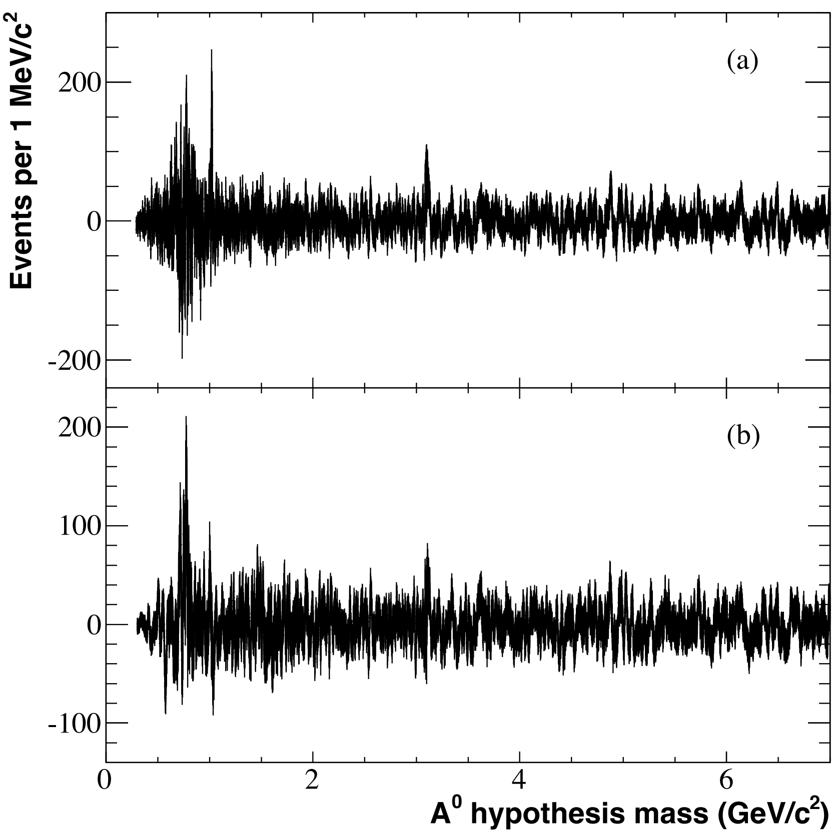

Figure 50: $\Upsilon(3S)$ A^0 signal, in events, as a function of hypothesis mass, for (a) CP-all analysis, and (b) CP-odd analysis.

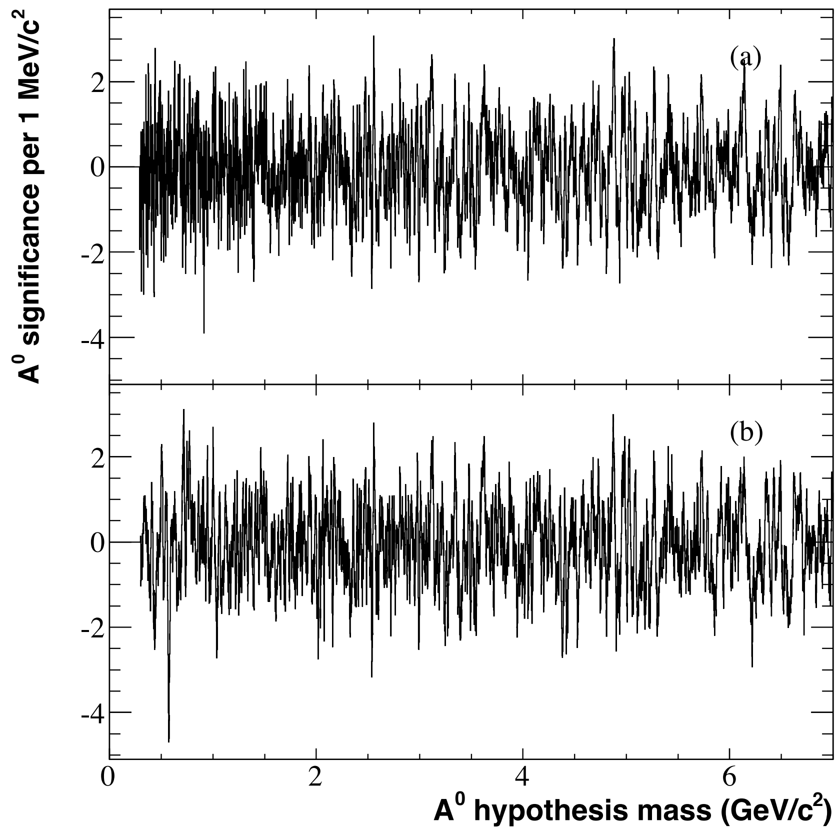

Figure 51: Statistical significance (events divided by statistical error) of the $\Upsilon(3S)$ A^0 signal as a function of mass, for (a) CP-all analysis, and (b) CP-odd analysis.

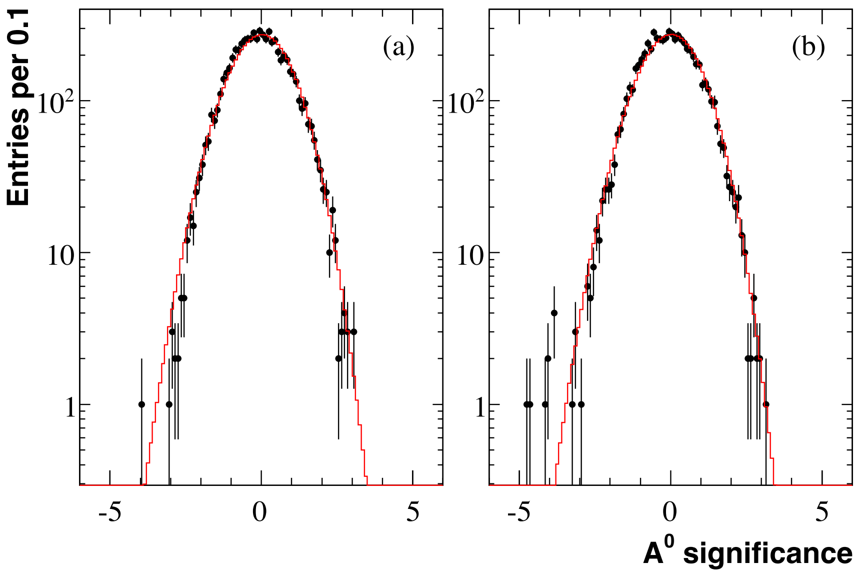

Figure 52: Histogram of the statistical significance of the A^0 signals in the $\Upsilon(3S)$ data set for (a) the 6710 masses considered in the CP-all analysis, and for (b) the 6701 masses in the CP-odd analysis. The overlaid curve shows the distribution expected in the absence of signal.

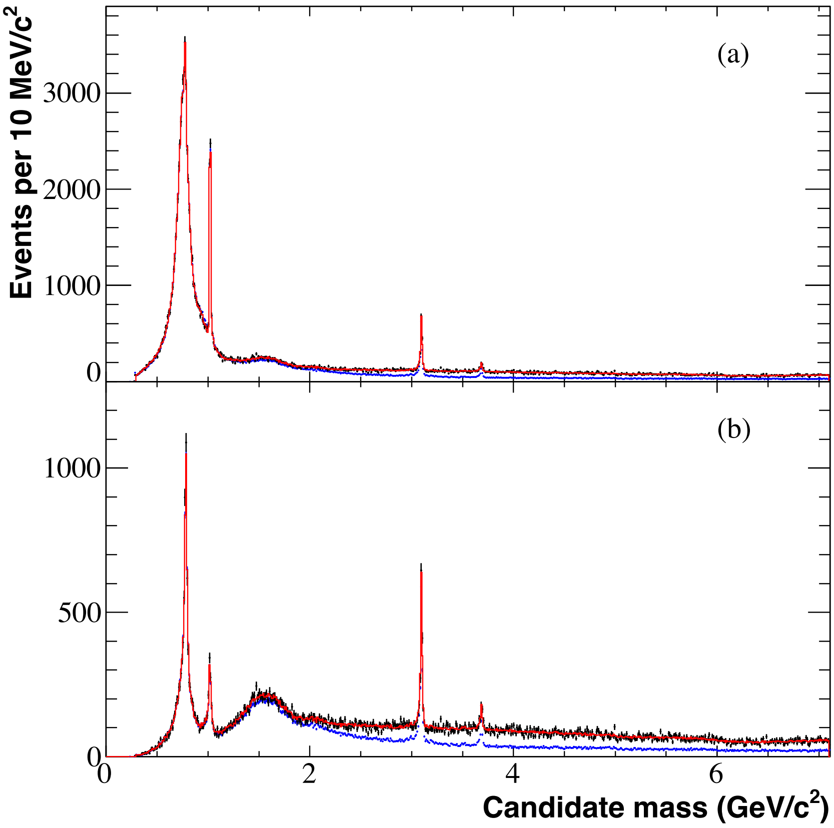

Figure 53: $\Upsilon(2S)$ candidate mass spectrum in the (a) CP-all and (b) CP-odd analyses. The top curve in each plot is the on-peak data overlaid (in red) with the fit described below, while the bottom curve (blue) is the scaled continuum data.

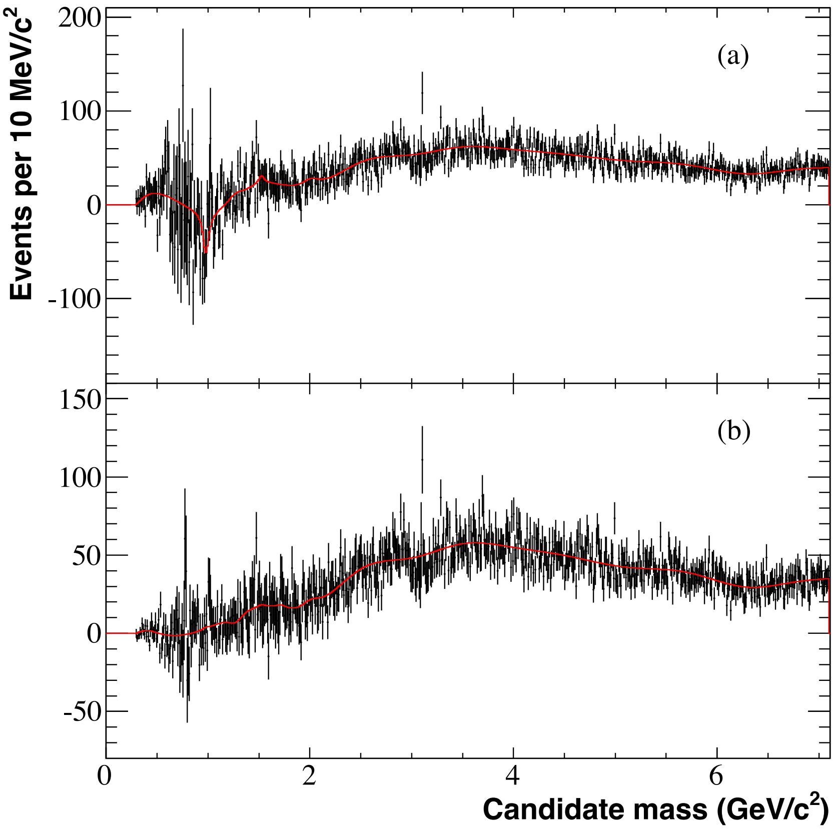

Figure 54: $\Upsilon(2S)$ A^0 candidate mass spectrum after continuum subtraction, overlaid with fit. (a) CP-all analysis; (b) CP-odd analysis.

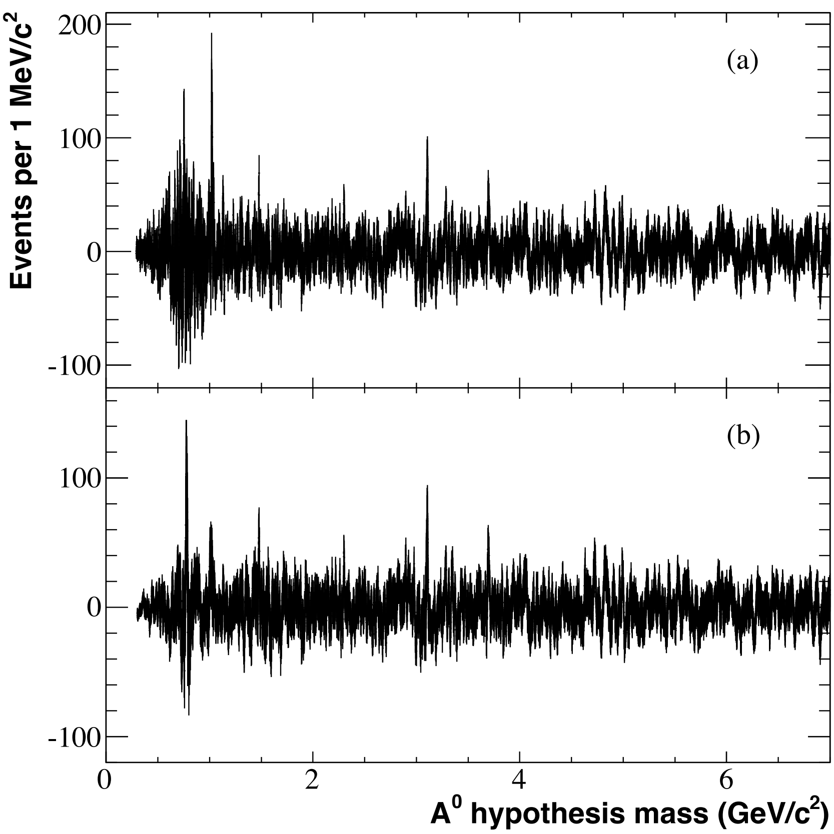

Figure 55: $\Upsilon(2S)$ A^0 signal, in events, as a function of hypothesis mass, for (a) CP-all analysis, and (b) CP-odd analysis.

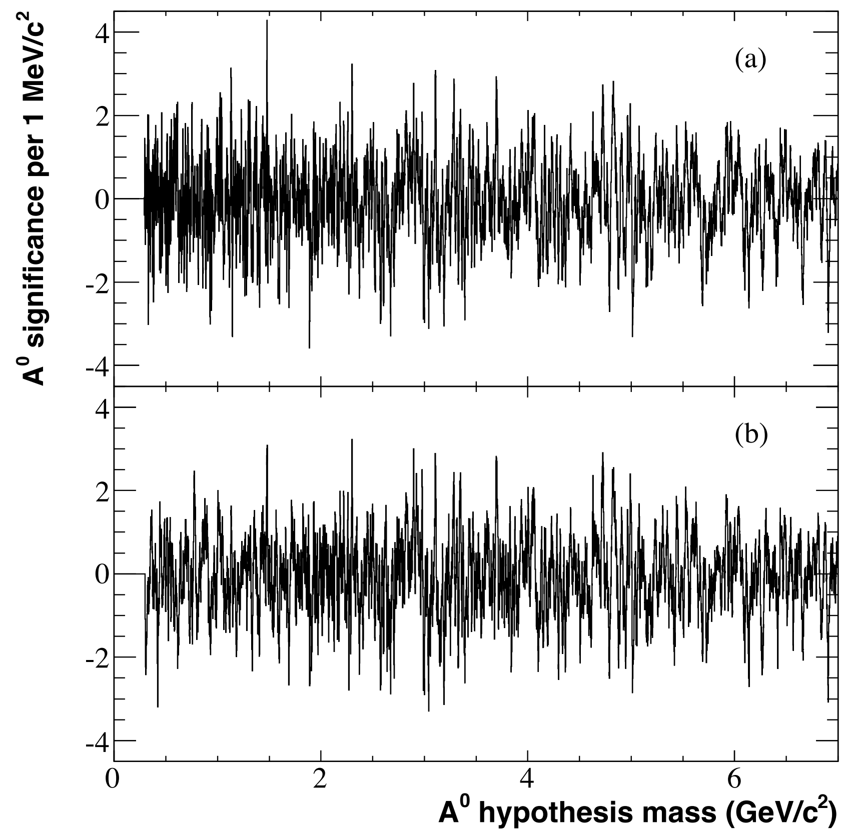

Figure 56: Statistical significance (events divided by statistical error) of the $\Upsilon(2S)$ A^0 signal as a function of mass, for (a) CP-all analysis, and (b) CP-odd analysis.

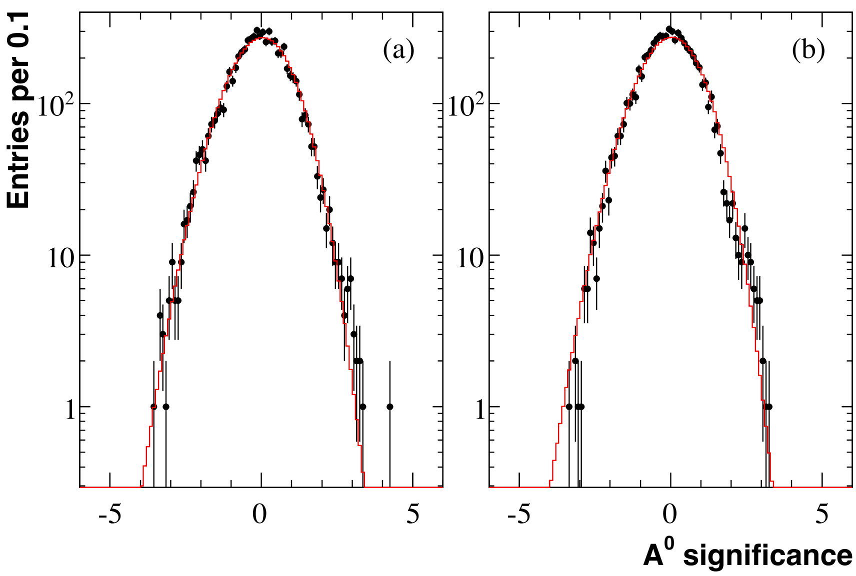

Figure 57: Histogram of the statistical significance of the A^0 signals in the $\Upsilon(2S)$ data set for (a) the 6710 masses considered in the CP-all analysis, and for (b) the 6701 masses in the CP-odd analysis. The overlaid curve shows the distribution expected in the absence of signal.

10 Efficiency and systematic error on efficiency

The signal efficiency is calculated at the various masses for which signal MC is available. Events are counted towards the efficiency if they satisfy the selection criteria and have reconstructed masses in the signal window for that Higgs mass.

Signal MC is available for one, two, or three Higgs decays modes, depending on its mass: 50% gg and 50% $s\bar{s}$; 100% gg; and 100% $c\bar{c}$. There are decay mode predictions available in some SUSY models (depending on $\tan\beta$ and other parameters), but clearly the actual decay modes are not known. The procedure that has been adopted is that at each mass, one combination of these three MC samples is taken to be the nominal value of the efficiency. A second combination is used to study the systematic error. Since this is an important and ill-defined uncertainty, a conservative approach is taken in terms of assigning a value.

For masses less than $3.5\,\mathrm{GeV}/c^2$ and above $s\bar{s}$ threshold, the nominal combination is 50% $s\bar{s}$ and 50% gg, and the variation is 100% gg. For masses above this, nominal is one-third for each of $s\bar{s}$, gg, and $c\bar{c}$ (i.e. two-thirds weight for the 50/50 $gg/s\bar{s}$ sample and one-third weight for the $c\bar{c}$ sample), and the variation is one-half weight each for the 50/50 $gg/s\bar{s}$ sample and the $c\bar{c}$ sample.

Among the CP odd samples at low mass, the change in efficiency ranges from 1.5% to 8.2%, with the largest change at a mass of $1.5\,\mathrm{GeV}/c^2$. 8.2% is taken as the systematic error for all CP odd samples with mass $\leq 3.5\,\mathrm{GeV}/c^2$. At higher masses, $c\bar{c}$ has significantly lower efficency, and the change in efficiency ranges from 18% to 21%, with 21% taken as the systematic error.

For CP all at low masses, the efficiency change ranges from less than 1% to 4.1% in the 2.5–$3.5\,\mathrm{GeV}/c^2$ region, with 4.1% taken as the systematic error at low masses. At high masses, there is little difference between the CP odd and CP all efficiencies, and the same systematic error is taken for both cases.

Other systematic errors on the efficiency are due to uncertainties in particle reconstruction and identification. Each of the items below is evaluated separately for each signal MC Higgs mass. The efficiency per particle is reduced by the amount listed, and the reduction in overall efficiency is taken as the systematic error.

1. Tracking: 0.6% per charged track
2. Photon reconstruction: 1% per photon

3. pion identification: 1% per pion

4. kaon identification: 1% per kaon

Table 10 summarizes the efficiency and systematic errors for each signal MC mass. The upper limit calculations require these quantities for each (1 MeV/c^2) Higgs mass hypothesis. These are found by fitting a cubic spline to the values in the table as a function of mass. The resulting efficiencies and systematic errors are plotted in Fig. 58 and Fig. 59.

As is clear from these figures, the efficiencies and uncertainties are essentially identical for the $\Upsilon(2S)$ and the $\Upsilon(3S)$. The efficiency for the combined sample is the average of the separate efficiencies, and the systematic error is the average of the systematic errors.

11 Systematic error on backgrounds

The systematic error on the background is found by repeating the fit to the candidate mass spectrum with variations in the background modeling. The five nominal resonances are removed one at a time, and eleven different resonances, marked in blue in Fig. 22, are added one at a time. Finally, f_L is fixed to the "best estimate" value found in Sec. 11.1. The total systematic error is the sum in quadrature of the changes in the total background resulting from each of these variations.

11.1 Continuum normalization

The normalization of the continuum sample is floated in the nominal fit, but fixed in an alternative fit used to estimate systematic errors. Luminosity alone is not sufficient to obtain the normalization parameter f_L because both the cross section and reconstruction efficiencies of the ISR processes vary with $\sqrt{s}$. The value for f_L used in the alternative fit is taken to be the mid-point of the range of values found using a variety of methods. The first two are the values obtained from the nominal fits to the CP odd and CP all Run 7 on-peak data (Sec. 7). The normalization parameter is also determined from fits to narrow ISR resonances in data (Sec. 11.1.1), and from MC calculations of these same ISR resonances (Sec. 11.1.2) . Finally, f_L can be estimated from the requirement that the number of Υ decays in the CP odd sample be less than or equal to the number in the CP all sample (Sec. 11.1.3). The results are summarized and combined in Sec. 11.1.4.

Table 10: Efficiency and systematic errors on efficiency

Y2S CP Odd	Efficiency		Systematic errors (%)						
Mass	Nominal	Alternative	Decay mode	MC statistics	Tracking	Photon	Pion	Kaon	Total uncertainty %
0.5	0.1054	0.1054	8.2	0.8	1.2	7.0	3.0	0.0	11.3
1	0.1227	0.1227	8.2	0.7	1.2	7.1	3.0	0.0	11.4
1.5	0.0799	0.0864	8.2	0.9	1.7	5.1	2.0	1.0	10.1
2	0.0611	0.0621	8.2	1.0	2.0	4.9	1.9	1.3	10.1
2.5	0.0451	0.0474	8.2	1.2	2.2	6.1	2.5	1.3	10.9
3	0.0323	0.0333	8.2	1.4	2.4	7.0	2.9	1.4	11.6
3.5	0.0234	0.0238	8.2	2.4	2.7	7.7	3.3	1.4	12.3
4	0.0120	0.0094	21.0	2.7	2.9	8.4	3.6	1.5	23.3
4.5	0.0093	0.0074	21.0	3.1	3.1	9.1	3.9	1.6	23.7
5	0.0066	0.0053	21.0	3.6	3.3	9.6	4.2	1.7	24.0
5.5	0.0045	0.0036	21.0	4.4	3.5	10.4	4.5	1.7	24.6
6	0.0038	0.0031	21.0	4.8	3.5	10.4	4.5	1.9	24.6
6.5	0.0032	0.0027	21.0	5.2	3.8	10.8	4.7	2.1	25.0
7	0.0022	0.0018	21.0	6.2	3.9	11.2	4.9	2.0	25.5
Y2S CP All	Efficiency		Systematic errors (%)						
Mass	Nominal	Alternative	Decay mode	MC statistics	Tracking	Photon	Pion	Kaon	Total uncertainty %
0.35	0.1736	0.1736	4.1	0.8	1.2	5.0	2.0	0.0	6.9
0.5	0.2166	0.2166	4.1	0.4	1.2	5.0	2.0	0.0	6.9
1	0.1624	0.1624	4.1	0.6	1.2	5.1	2.0	0.1	7.0
1.5	0.1108	0.1166	4.1	1.0	1.4	3.6	1.3	1.1	6.0
2	0.0755	0.0758	4.1	0.9	1.8	3.8	1.4	1.5	6.3
2.5	0.0470	0.0489	4.1	1.2	2.2	6.1	2.5	1.2	8.3
3	0.0340	0.0354	4.1	1.4	2.4	7.0	2.9	1.3	9.2
3.5	0.0247	0.0248	4.1	2.8	2.7	7.9	3.3	1.3	10.3
4	0.0124	0.0100	21.0	2.6	2.9	8.5	3.6	1.5	23.3
4.5	0.0094	0.0076	21.0	3.0	3.1	9.0	3.9	1.5	23.6
5	0.0070	0.0056	21.0	4.0	3.3	9.5	4.1	1.7	24.0
5.5	0.0049	0.0040	21.0	5.1	3.4	10.1	4.3	1.8	24.6
6	0.0043	0.0035	21.0	4.5	3.7	10.7	4.6	1.9	24.8
6.5	0.0038	0.0030	21.0	6.4	3.7	11.2	4.9	1.9	25.5
7	0.0026	0.0020	21.0	12.0	4.0	12.4	5.4	1.9	28.1
Y3S CP Odd	Efficiency		Systematic errors (%)						
Mass	Nominal	Alternative	Decay mode	MC statistics	Tracking	Photon	Pion	Kaon	Total uncertainty %
0.5	0.0969	0.0969	8.2	0.8	1.2	7.0	3.0	0.0	11.3
1	0.1185	0.1185	8.2	0.7	1.2	7.1	3.0	0.0	11.4
1.5	0.0770	0.0831	8.2	0.8	1.7	5.1	2.0	1.1	10.1
2	0.0593	0.0607	8.2	1.0	2.0	4.9	1.9	1.2	10.1
2.5	0.0446	0.0463	8.2	1.1	2.2	6.2	2.5	1.2	10.9
3	0.0323	0.0331	8.2	1.3	2.4	7.0	2.9	1.3	11.6
3.5	0.0223	0.0230	8.2	1.9	2.7	7.8	3.3	1.4	12.3
4	0.0112	0.0088	21.0	3.3	2.9	8.5	3.6	1.5	23.4
4.5	0.0084	0.0067	21.0	2.4	3.1	9.2	3.9	1.6	23.6
5	0.0063	0.0050	21.0	2.4	3.3	9.7	4.2	1.7	23.9
5.5	0.0043	0.0034	21.0	3.0	3.5	10.3	4.4	1.8	24.3
6	0.0036	0.0029	21.0	3.2	3.7	10.6	4.6	1.9	24.6
6.5	0.0030	0.0025	21.0	3.5	3.8	11.0	4.8	2.0	24.8
7	0.0026	0.0021	21.0	3.8	3.8	11.3	4.9	2.0	25.0
Y3S CP All	Efficiency		Systematic errors (%)						
Mass	Nominal	Alternative	Decay mode	MC statistics	Tracking	Photon	Pion	Kaon	Total uncertainty %
0.35	0.1627	0.1627	4.1	0.5	1.2	5.0	2.0	0.0	6.9
0.5	0.2085	0.2085	4.1	0.4	1.2	5.0	2.0	0.0	6.9
1	0.1582	0.1582	4.1	0.5	1.2	5.1	2.0	0.1	7.0
1.5	0.1070	0.1129	4.1	0.7	1.4	3.5	1.2	1.1	5.9
2	0.0733	0.0722	4.1	0.8	1.8	3.8	1.3	1.5	6.2
2.5	0.0457	0.0475	4.1	1.0	2.2	6.1	2.5	1.2	8.2
3	0.0333	0.0342	4.1	1.2	2.4	7.0	2.9	1.3	9.2
3.5	0.0235	0.0243	4.1	1.6	2.6	7.7	3.3	1.4	9.9
4	0.0123	0.0099	21.0	1.7	2.9	8.4	3.6	1.5	23.2
4.5	0.0089	0.0072	21.0	2.0	3.1	9.0	3.9	1.6	23.5
5	0.0066	0.0053	21.0	2.4	3.3	9.8	4.2	1.6	24.0
5.5	0.0050	0.0040	21.0	2.7	3.4	9.8	4.2	1.9	24.0
6	0.0039	0.0031	21.0	3.1	3.6	10.5	4.5	1.9	24.5
6.5	0.0031	0.0025	21.0	3.5	3.8	11.1	4.8	1.9	24.8
7	0.0029	0.0024	21.0	3.6	3.8	11.0	4.7	2.1	24.8

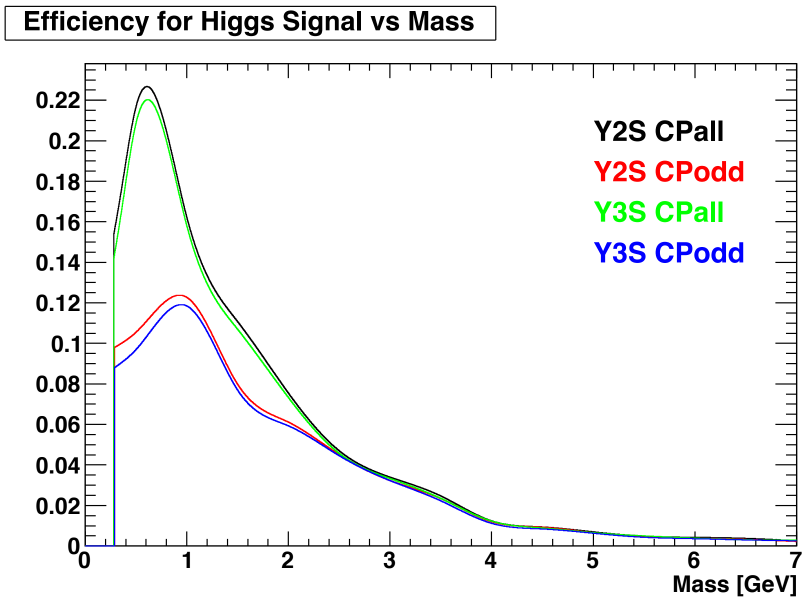

Figure 58: Signal efficiency as a function of mass for the two data set ($\Upsilon(2S)$ and $\Upsilon(3S)$) and two CP hypotheses. Efficiency for the combined data set is the average of the $\Upsilon(2S)$ and $\Upsilon(3S)$ values.

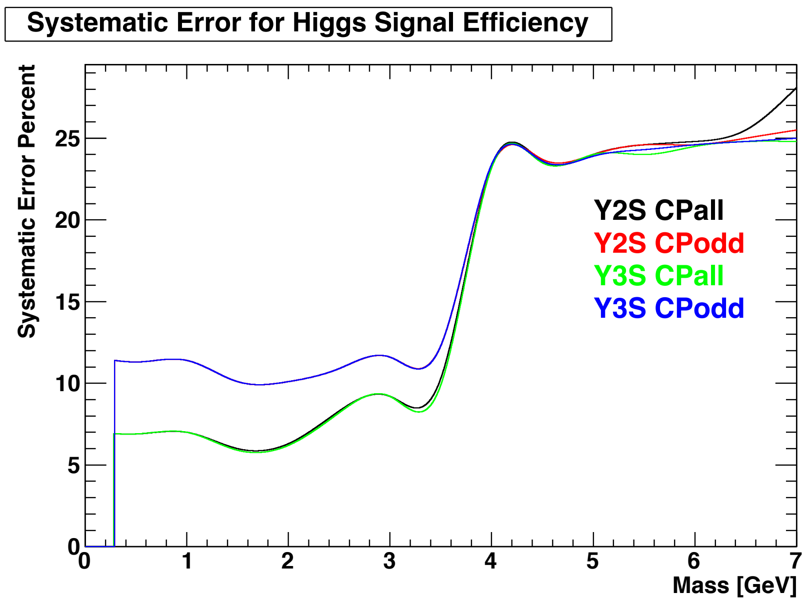

Figure 59: Systematic error (percent) on the efficiency as a function of mass.

Table 11: Number of narrow resonance events found in the continuum and on-peak data samples. The continuum sample is Run 6 plus Run 7 off peak.

	Continuum	±	Y3S onpeak	±	f_L	±	Y2S onpeak	±	f_L	±	Run 7 onpeak	±	f_L	±
omega to pi pi pi	14,258	127	4,968	76	0.348	0.006	2,618	54	0.184	0.004	7,579	93	0.532	0.008
Phi to K K	32,667	190	11,355	113	0.348	0.004	6,367	83	0.195	0.003	17,721	140	0.542	0.005
Jpsi to 4 tracks	5,513	116	1,954	71	0.354	0.015	1,041	56	0.189	0.011	2,990	91	0.542	0.020
Jpsi to 4 tracks 1 pi0	5,249	110	1,918	70	0.366	0.015	968	53	0.184	0.011	2,887	88	0.550	0.020
average					0.349	0.003			0.191	0.002			0.540	0.004

11.1.1 Fits to narrow resonances produced in ISR

The four ISR resonances used for normalization purposes are described in Sec. 7. The number of events of each type is found by a fit to the data. The pdf for the signal is a mass histogram filled by the appropriate ISR MC mode, with a mass offset between data and MC being one of the free parameters of the fit. Background is assumed to be linear in mass, giving a total of four fit parameters (mass offset, normalization, and two background parameters).

The fits to the continuum, $\Upsilon(2S)$, $\Upsilon(3S)$, and combined $\Upsilon(2S)$ plus $\Upsilon(3S)$ data are shown in Fig. 60–91, and are summarized in Table 11.

The fit does not allow for resolution smearing between MC and data, although the J/ψ plots look like such smearing would help the fit. However, it does not look like the inclusion of such smearing would noticeably change the data/continuum ratio. Also, the final value of f_L is only weakly dependent on the J/ψ fits. For these reasons, it was decided to not pursue more complicated fits to the narrow resonances.

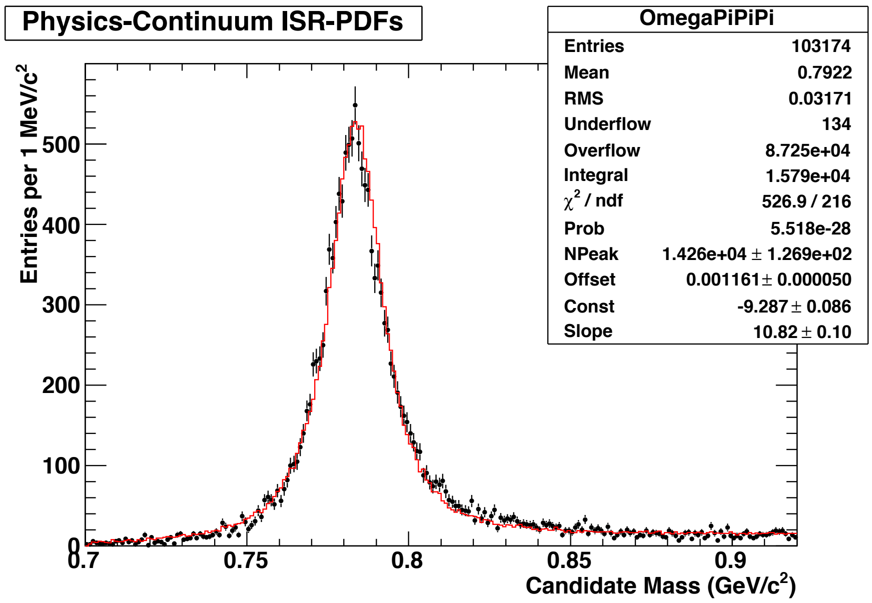

Figure 60: Fit to $\omega \to \pi^+\pi^-\pi^0$ in the continuum sample. Red curve is the fit, consisting of ISR MC plus linear background.

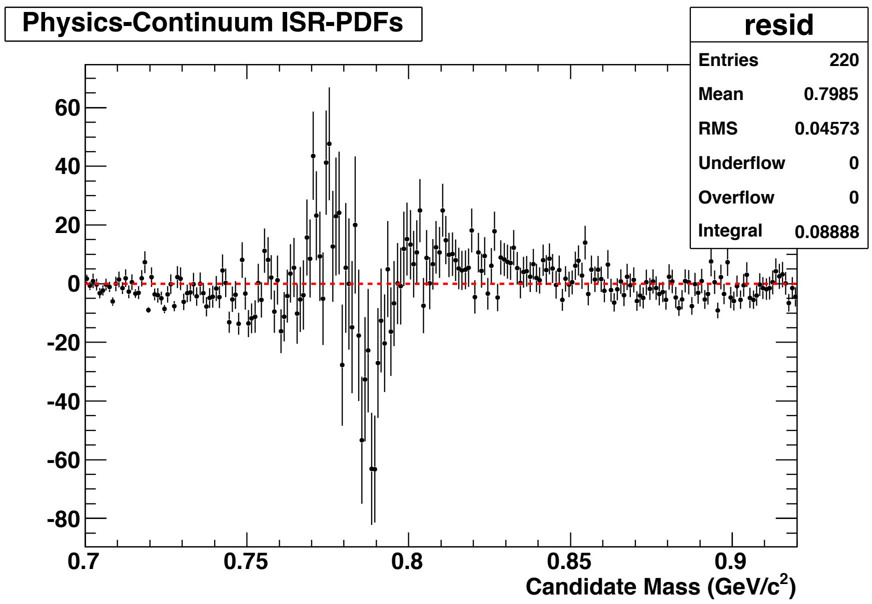

Figure 61: Residual of fit to $\omega \to \pi^+\pi^-\pi^0$ in the continuum sample.

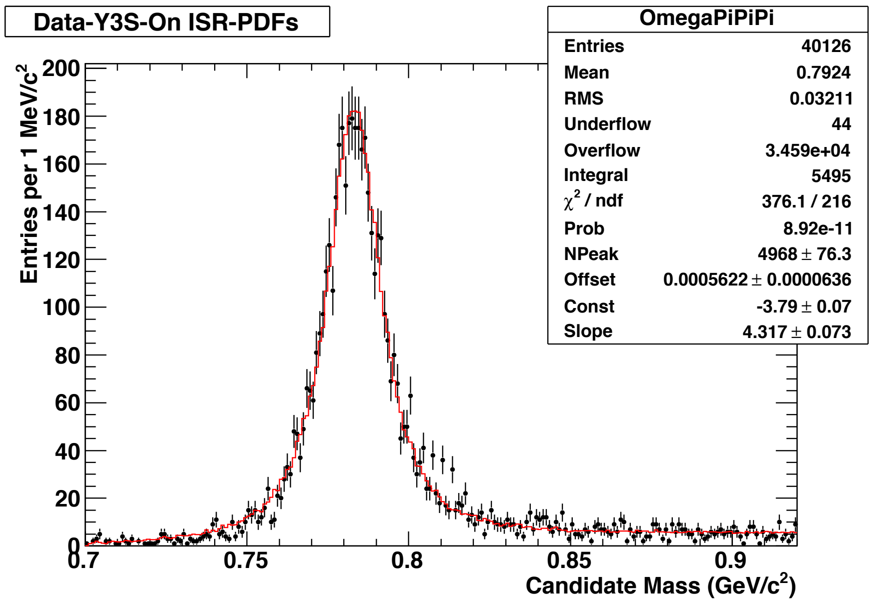

Figure 62: Fit to $\omega \to \pi^+\pi^-\pi^0$ in the $\Upsilon(3S)$ on peak sample. Red curve is the fit, consisting of ISR MC plus linear background.

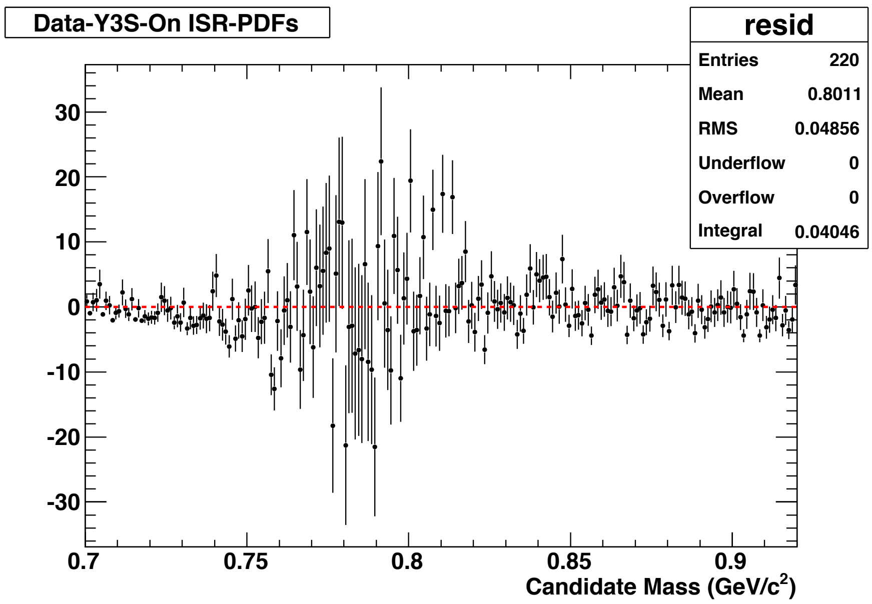

Figure 63: Residual of fit to $\omega \to \pi^+\pi^-\pi^0$ in the $\Upsilon(3S)$ on peak sample.

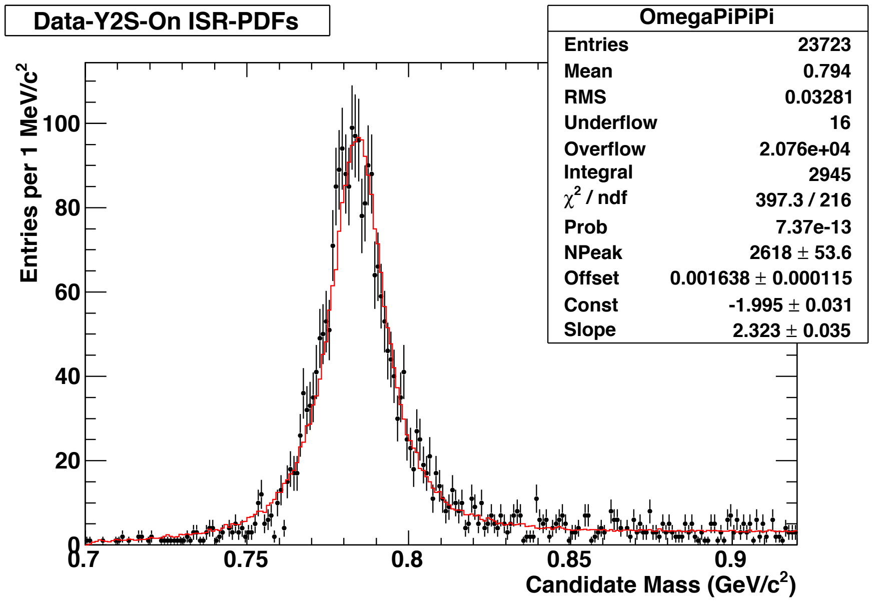

Figure 64: Fit to $\omega \to \pi^+\pi^-\pi^0$ in the $\Upsilon(2S)$ on peak sample. Red curve is the fit, ISR MC plus linear background.

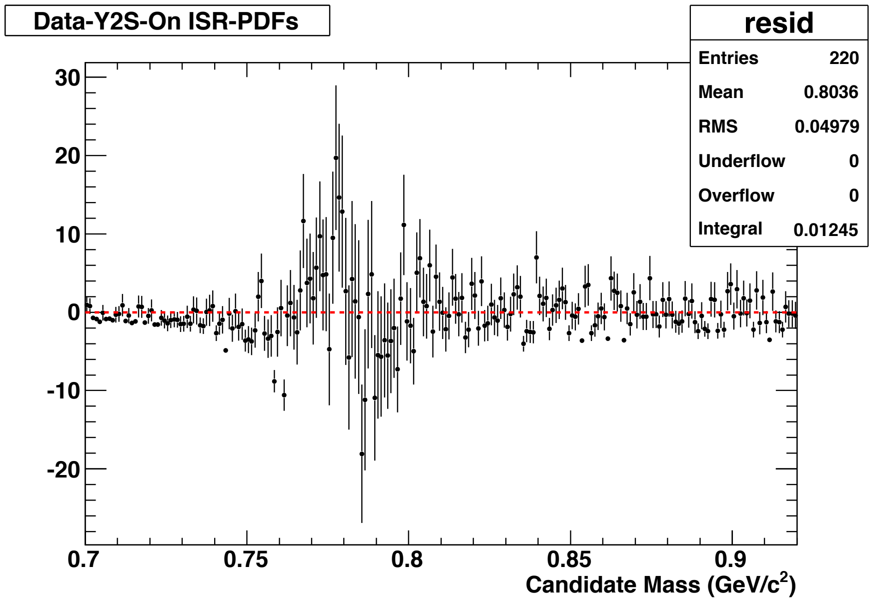

Figure 65: Residual of fit to $\omega \to \pi^+\pi^-\pi^0$ in the $\Upsilon(2S)$ on peak sample.

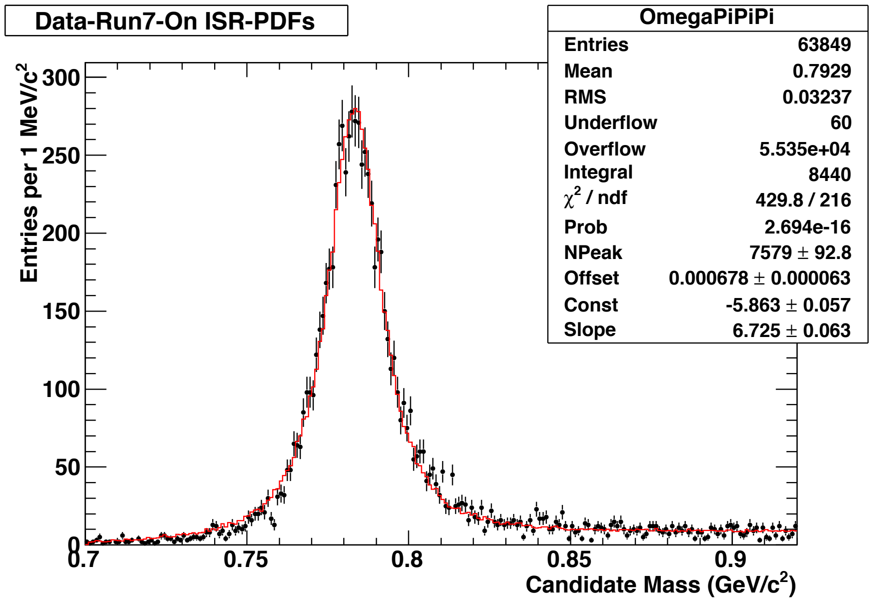

Figure 66: Fit to $\omega \rightarrow \pi^+\pi^-\pi^0$ in the Run 7 on peak sample. Red curve is the fit, ISR MC plus linear background.

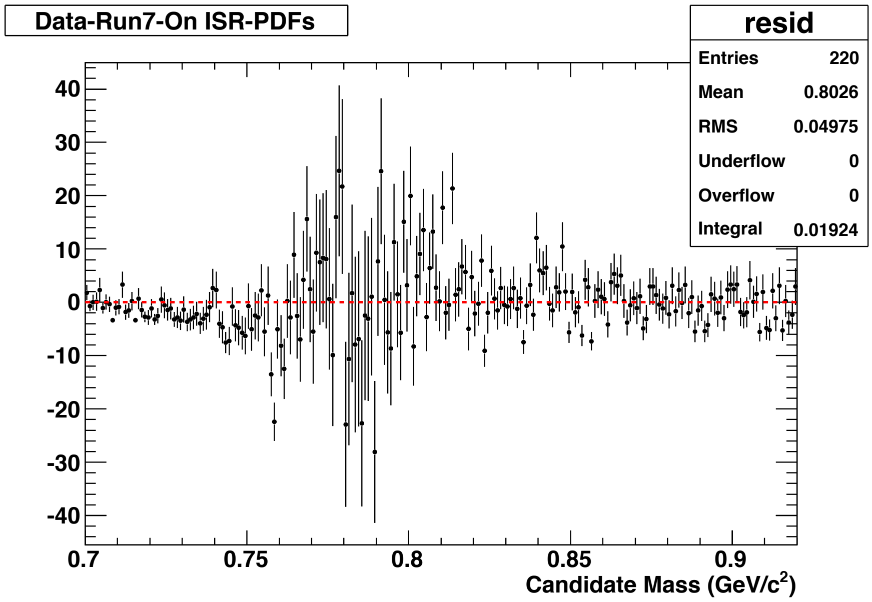

Figure 67: Residual of fit to $\omega \rightarrow \pi^+\pi^-\pi^0$ in the Run 7 on peak sample.

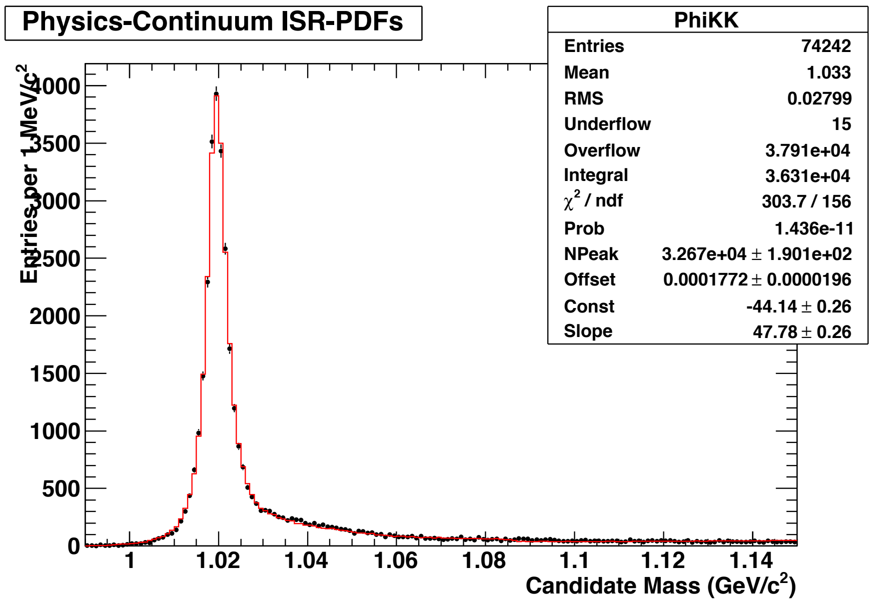

Figure 68: Fit to $\phi \to K^+K^-$ in the continuum sample. Red curve is the fit, ISR MC plus linear background.

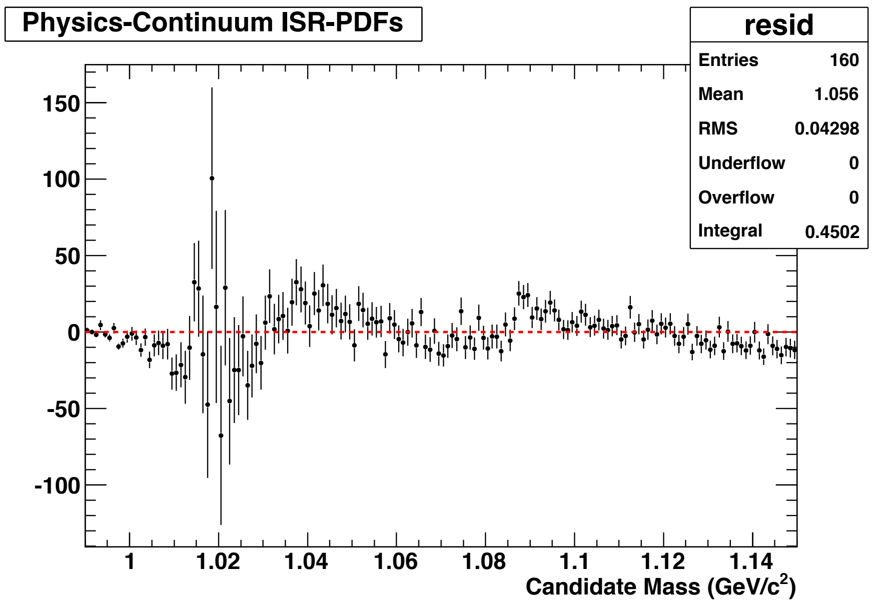

Figure 69: Residual of fit to $\phi \to K^+K^-$ in the continuum sample.

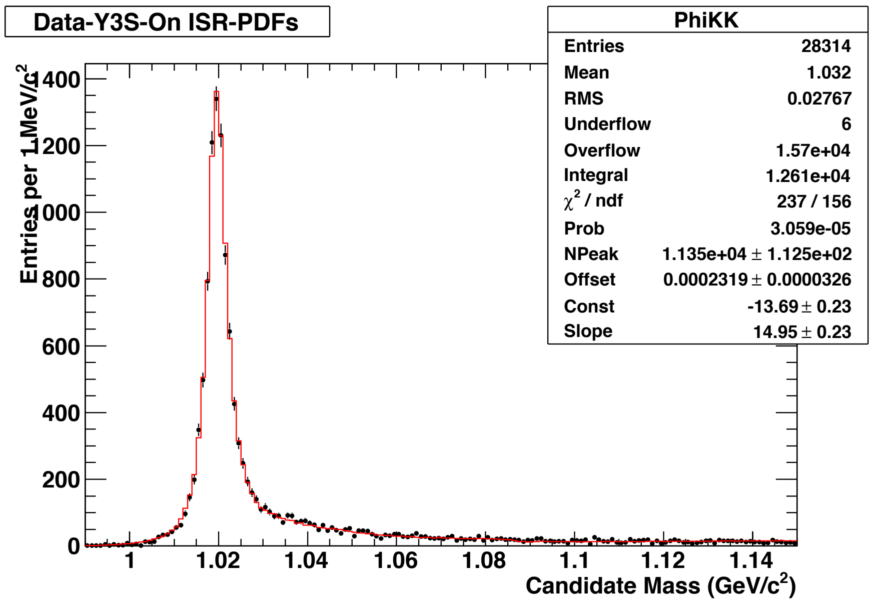

Figure 70: Fit to $\phi \to K^+K^-$ in the $\Upsilon(3S)$ on peak sample. Red curve is the fit, ISR MC plus linear background.

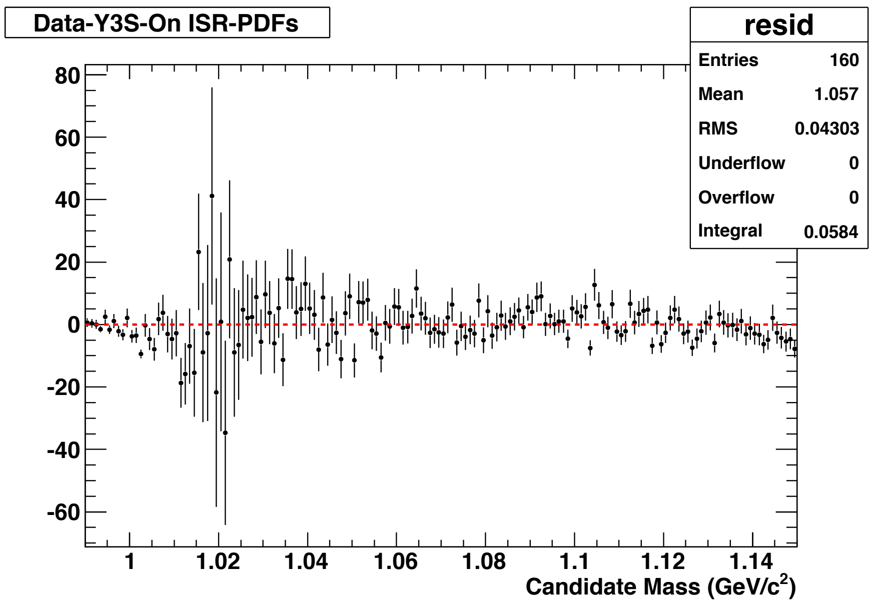

Figure 71: Residual of fit to $\phi \to K^+K^-$ in the $\Upsilon(3S)$ on peak sample.

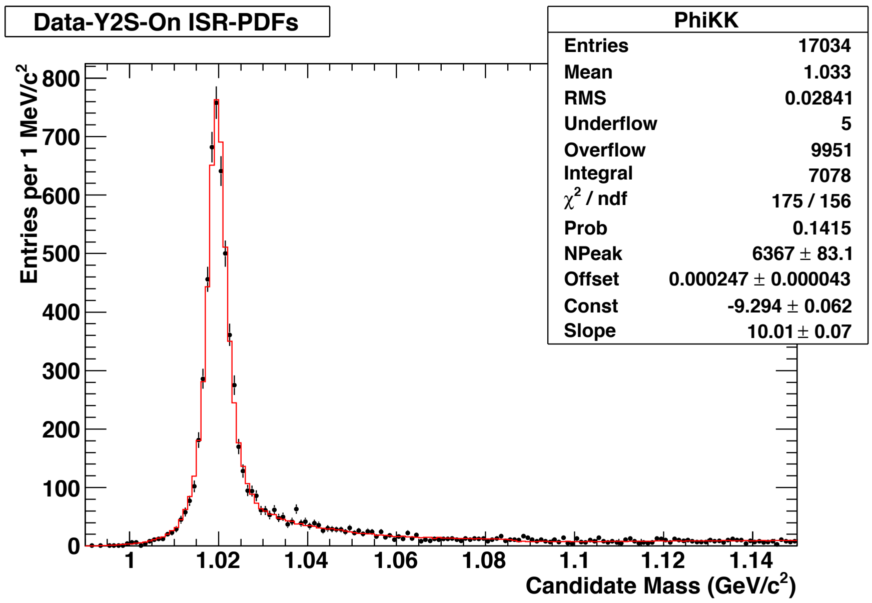

Figure 72: Fit to $\phi \to K^+K^-$ in the $\Upsilon(2S)$ on peak sample. Red curve is the fit, ISR MC plus linear background.

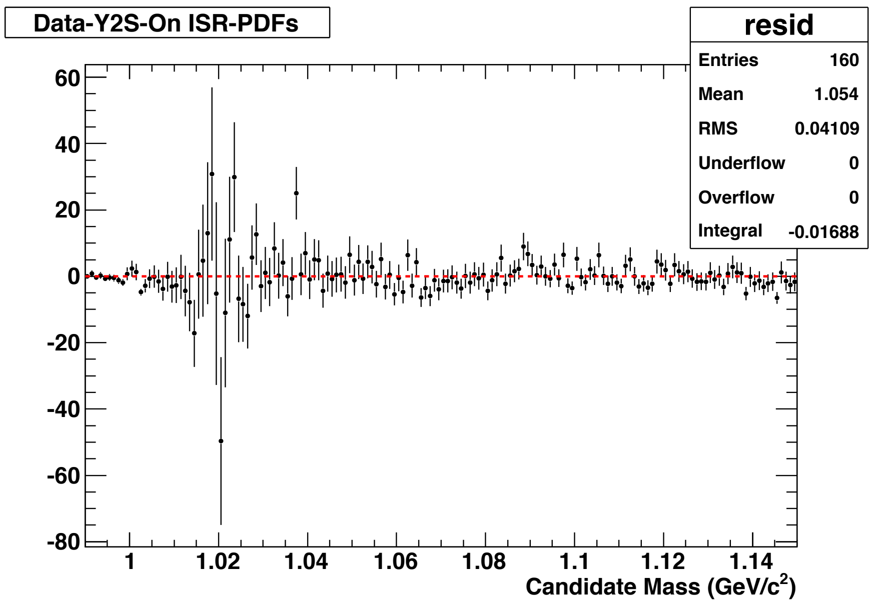

Figure 73: Residual of fit to $\phi \to K^+K^-$ in the $\Upsilon(2S)$ on peak sample.

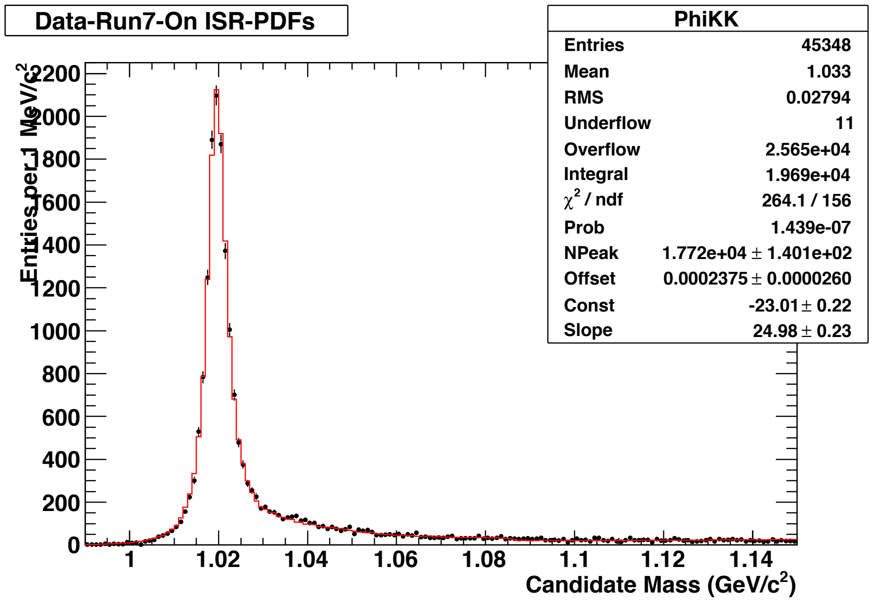

Figure 74: Fit to $\phi \to K^+K^-$ in the Run 7 on peak sample. Red curve is the fit, ISR MC plus linear background.

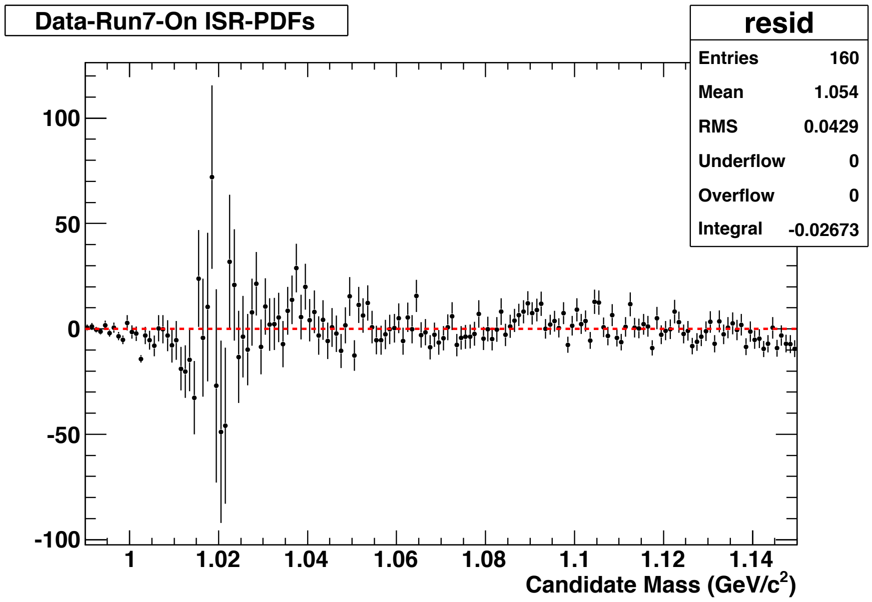

Figure 75: Residual of fit to $\phi \to K^+K^-$ in the Run 7 on peak sample.

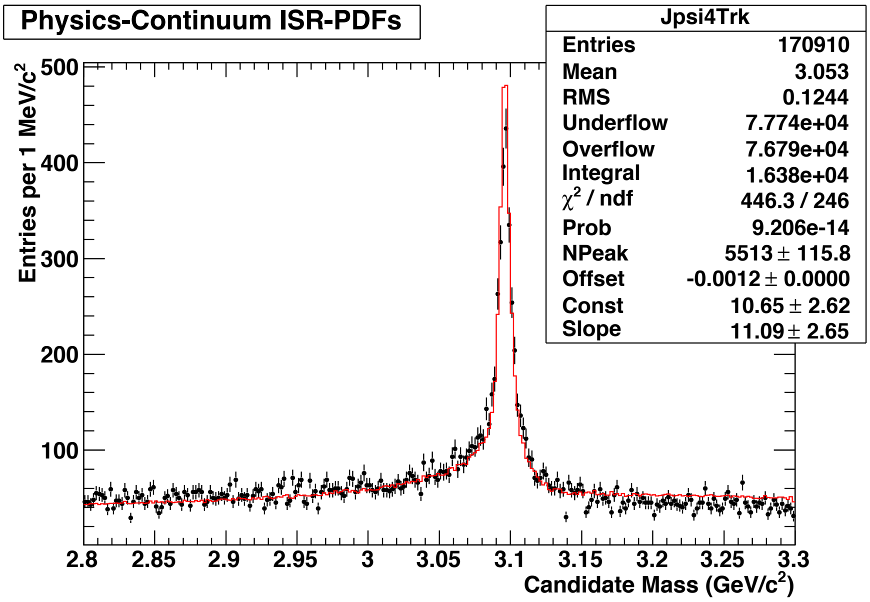

Figure 76: Fit to $J/\psi \rightarrow \geq 4 \text{tracks} 0 \pi^0$ in the continuum sample. Red curve is the fit, ISR MC plus linear background.

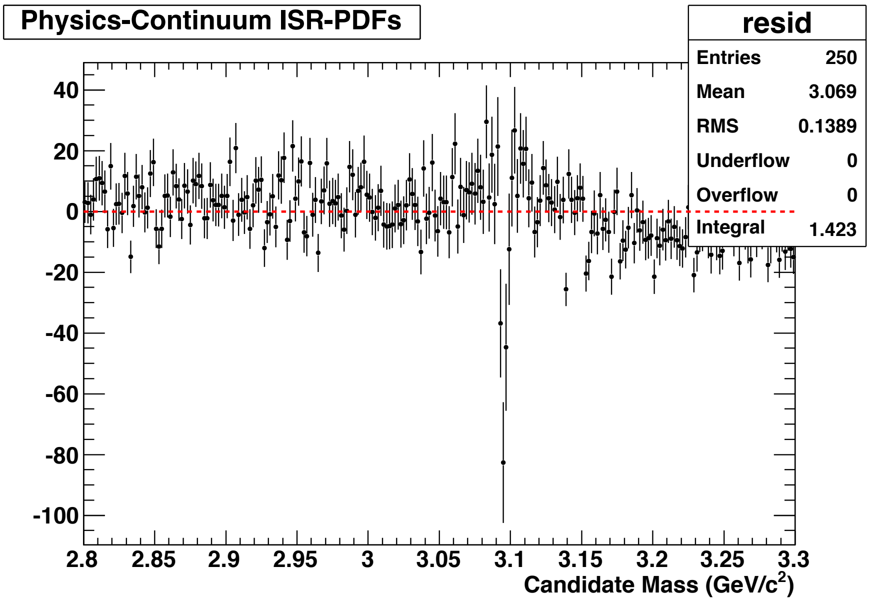

Figure 77: Residual of fit to $J/\psi \rightarrow \geq 4 \text{tracks} 0 \pi^0$.

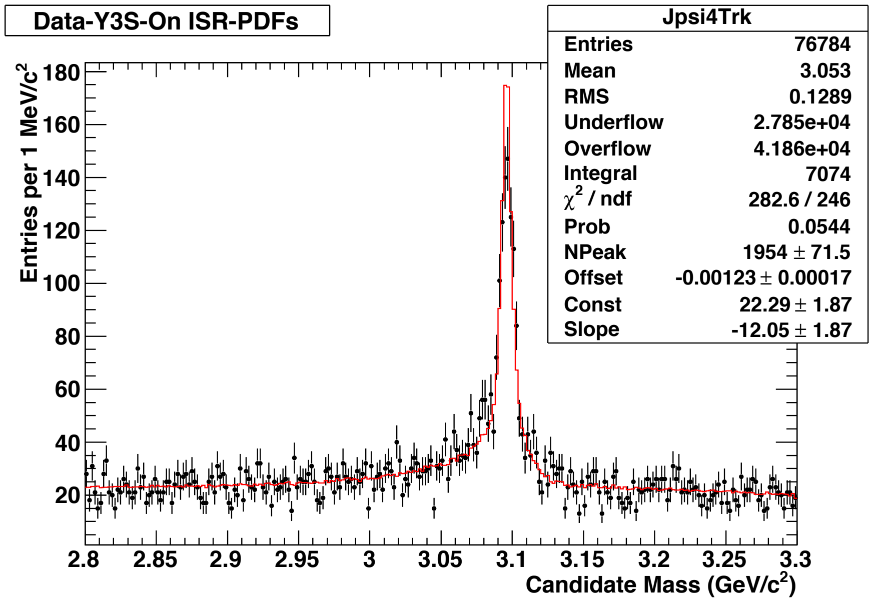

Figure 78: Fit to $J/\psi \to \geq$ 4tracks0π^0 in the $\Upsilon(3S)$ on peak sample. Red curve is the fit, ISR MC plus linear background.

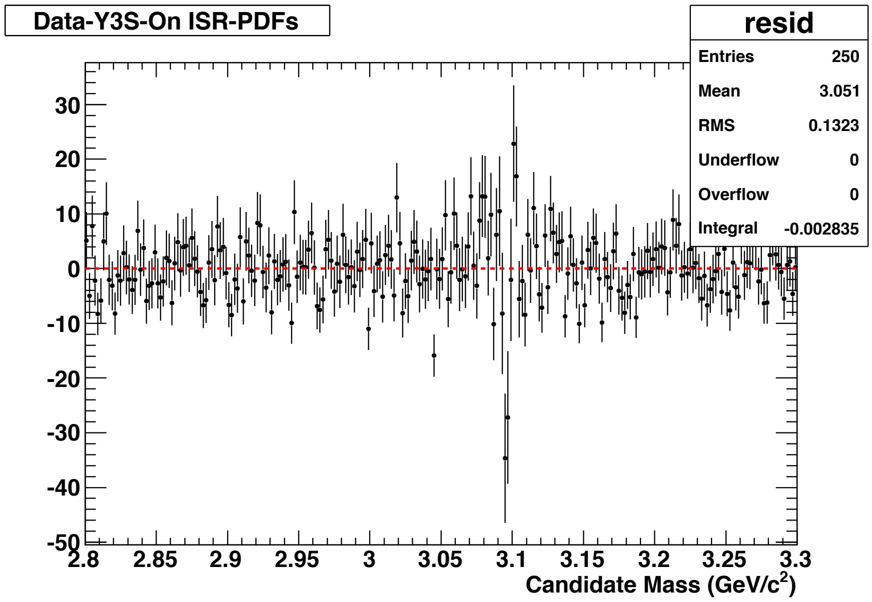

Figure 79: Residual of fit to $J/\psi \to \geq$ 4tracks0π^0.

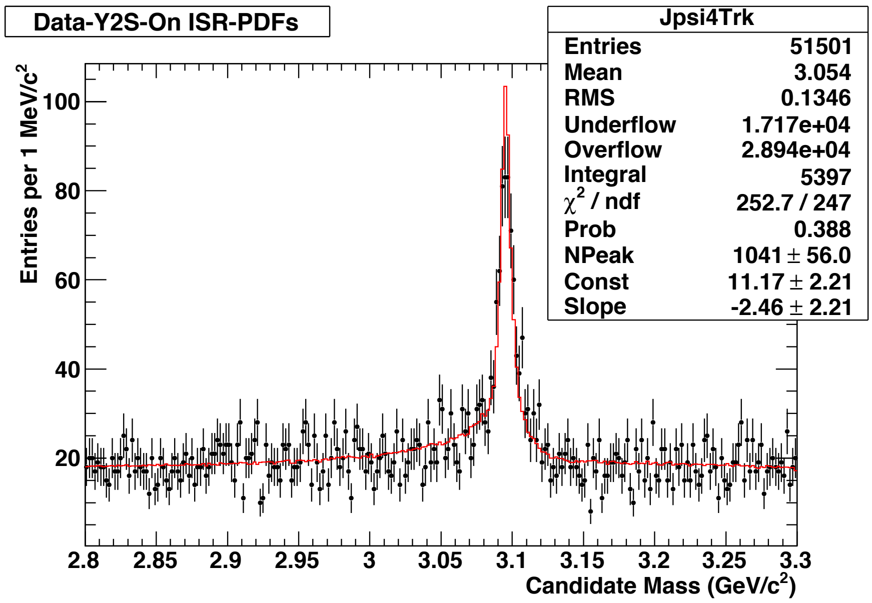

Figure 80: Fit to $J/\psi \to \geq 4\text{tracks}0\pi^0$ in the $\Upsilon(2S)$ on peak sample. Red curve is the fit, ISR MC plus linear background.

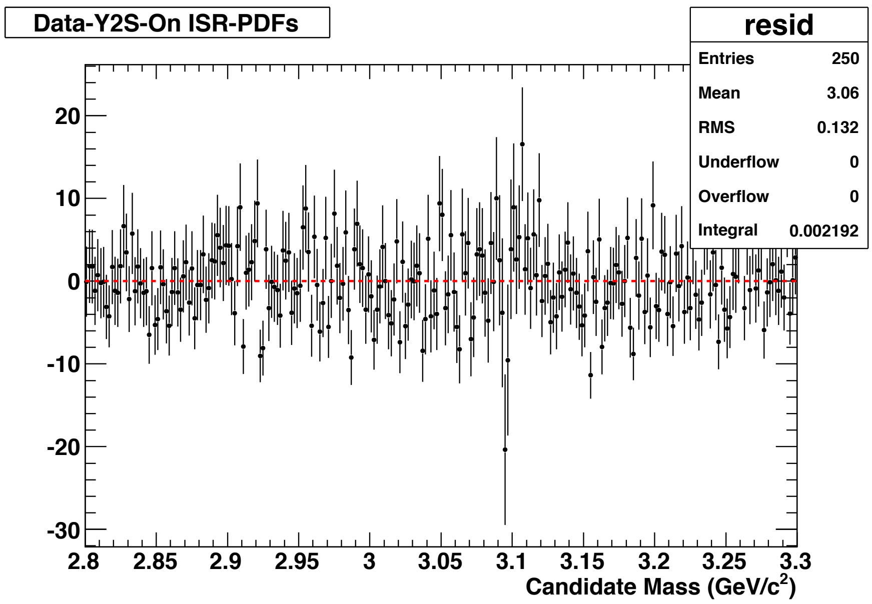

Figure 81: Residual of fit to $J/\psi \to \geq 4\text{tracks}0\pi^0$.

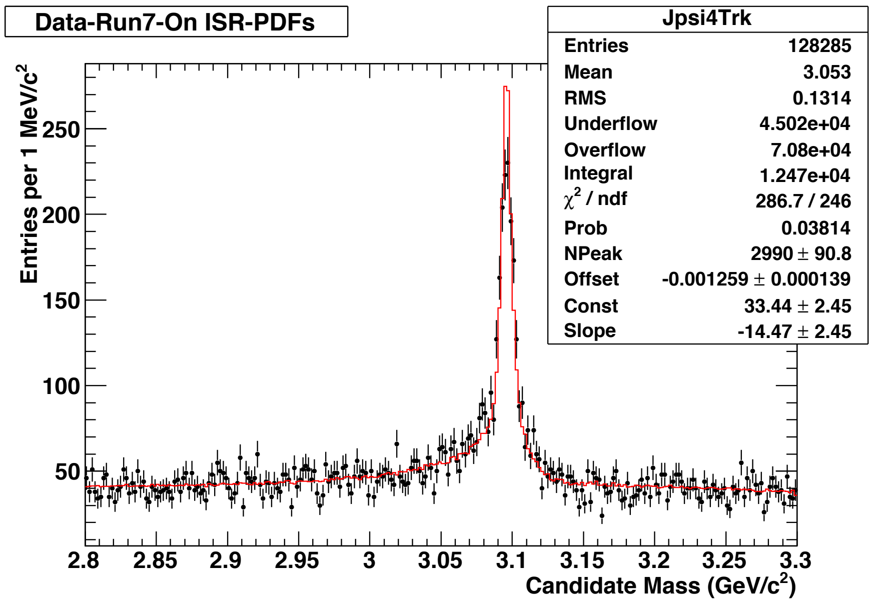

Figure 82: Fit to $J/\psi \rightarrow \geq$ 4tracks0π^0 in the Run 7 on peak sample. Red curve is the fit, ISR MC plus linear background.

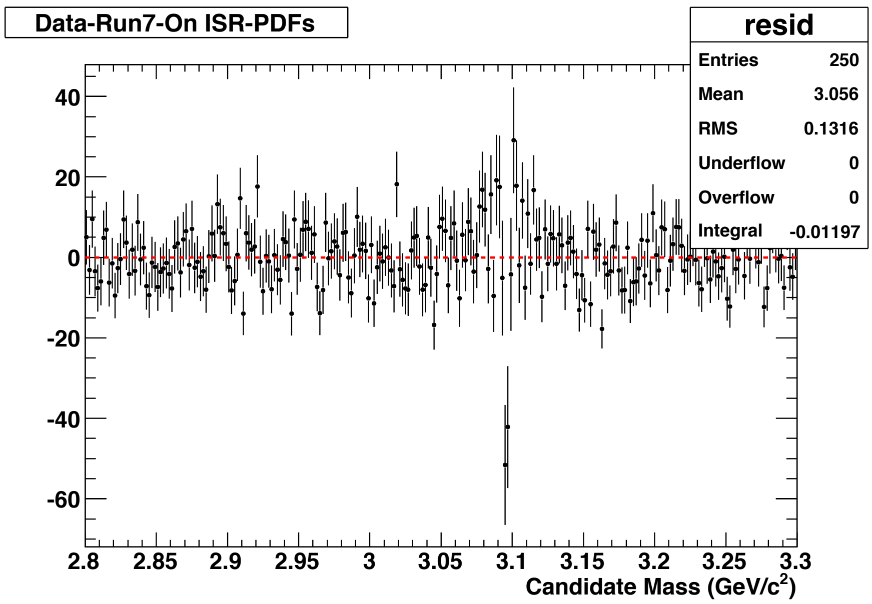

Figure 83: Residual of fit to $J/\psi \rightarrow \geq$ 4tracks0π^0.

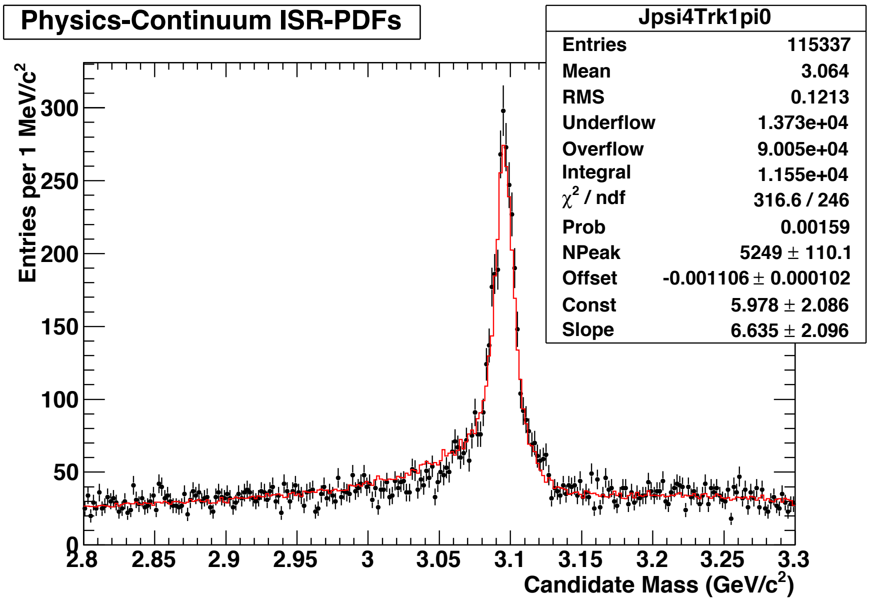

Figure 84: Fit to $J/\psi \to \geq$ 4tracks1π^0 in the continuum sample. Red curve is the fit, ISR MC plus linear background.

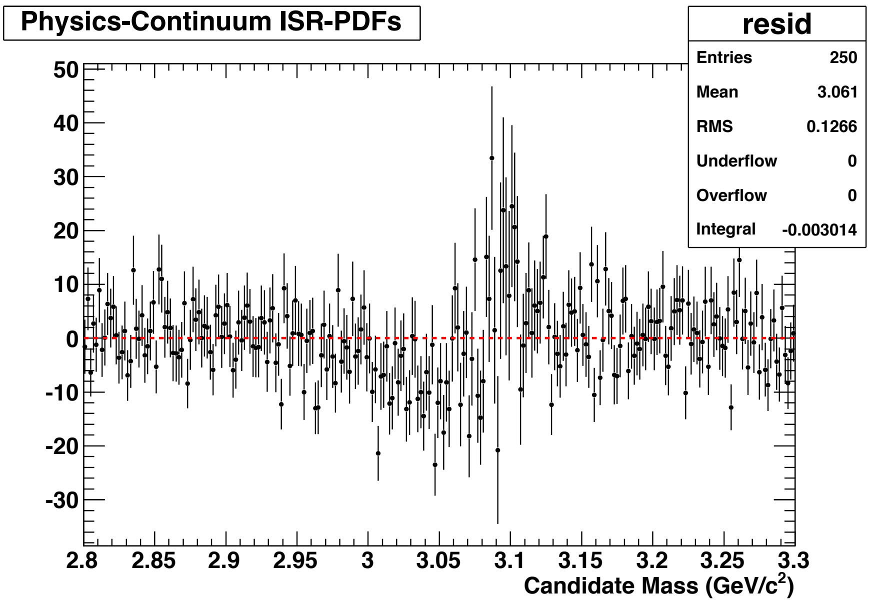

Figure 85: Residual of fit to $J/\psi \to \geq$ 4tracks1π^0.

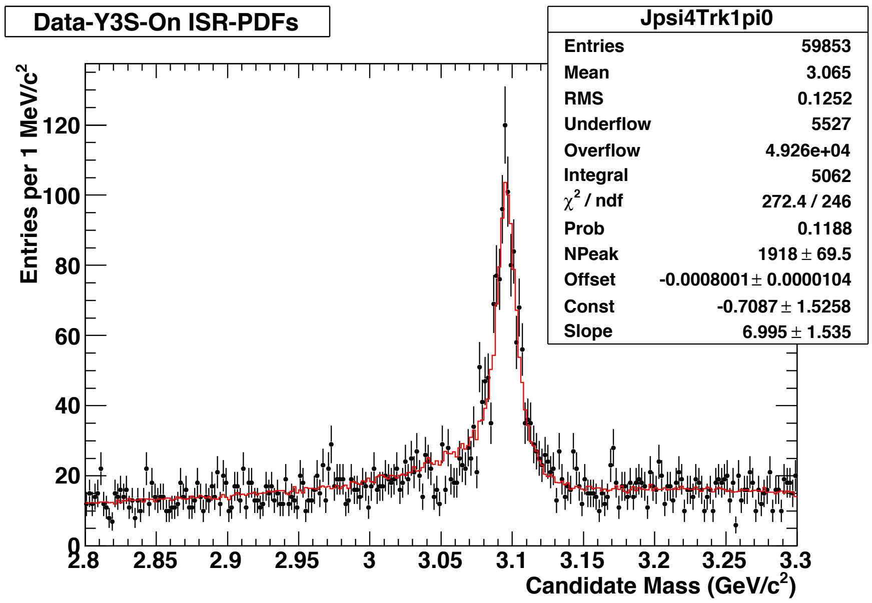

Figure 86: Fit to $J/\psi \rightarrow \geq 4\text{tracks}1\pi^0$ in the $\Upsilon(3S)$ on peak sample. Red curve is the fit, ISR MC plus linear background.

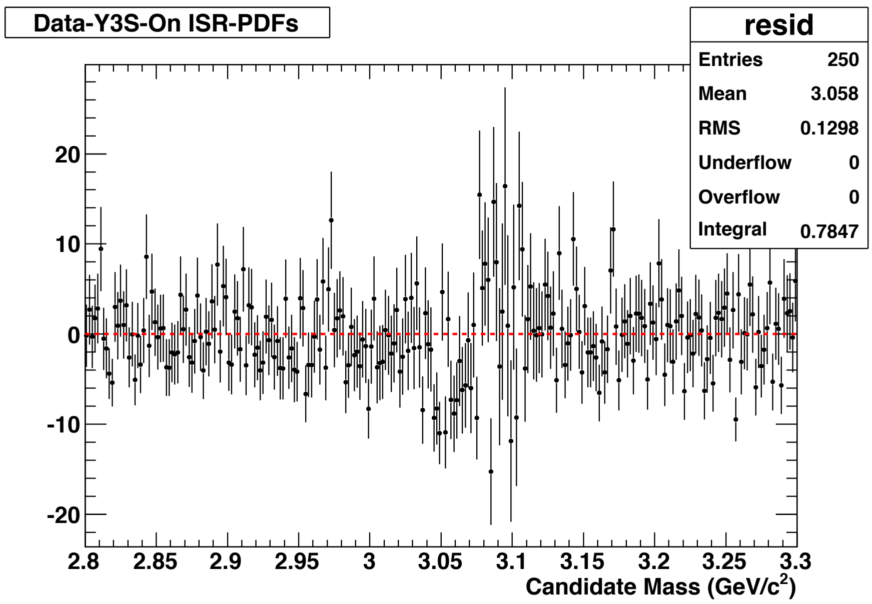

Figure 87: Residual of fit to $J/\psi \rightarrow \geq 4\text{tracks}1\pi^0$.

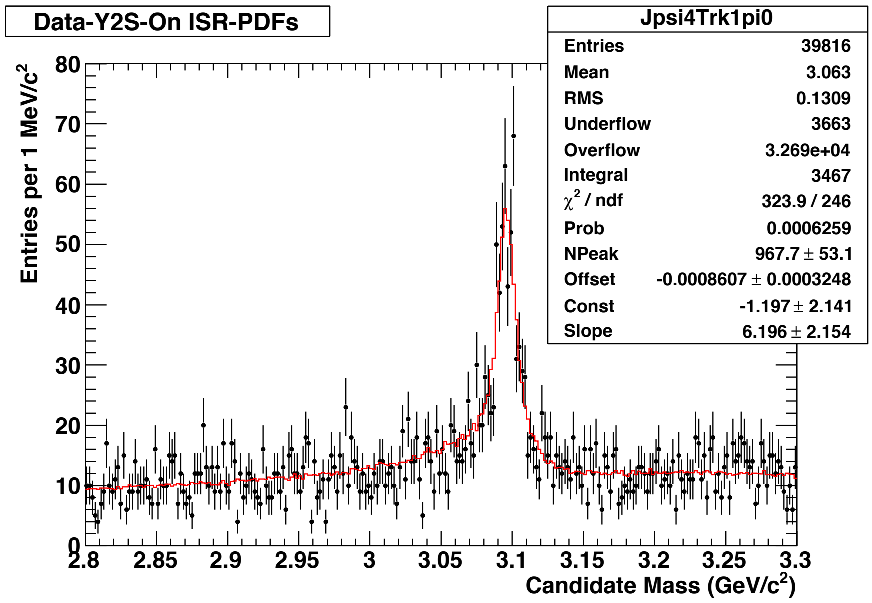

Figure 88: Fit to $J/\psi \to \geq 4\text{tracks}1\pi^0$ in the $\Upsilon(2S)$ on peak sample. Red curve is the fit, ISR MC plus linear background.

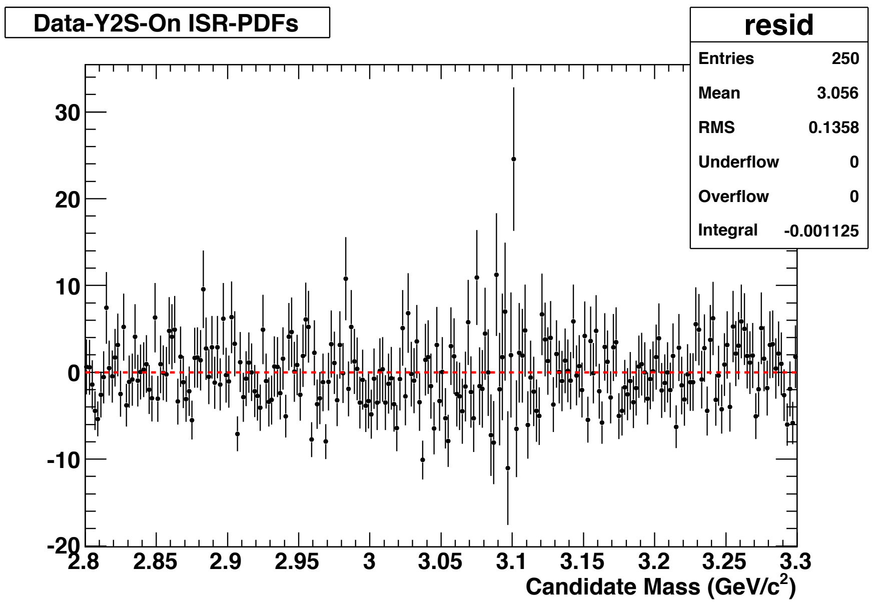

Figure 89: Residual of fit to $J/\psi \to \geq 4\text{tracks}1\pi^0$.

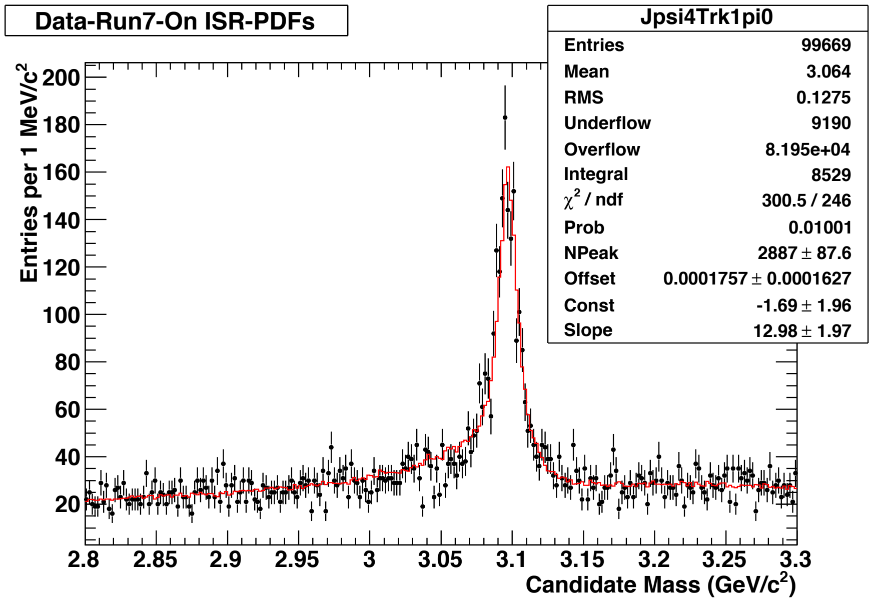

Figure 90: Fit to $J/\psi \rightarrow \geq$ 4tracks1π^0 in the Run 7 on peak sample. Red curve is the fit, ISR MC plus linear background.

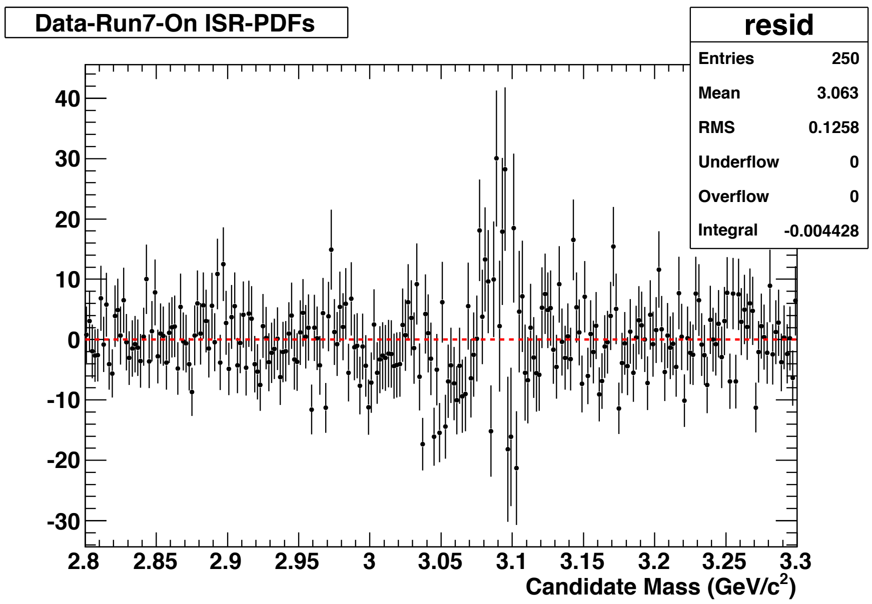

Figure 91: Residual of fit to $J/\psi \rightarrow \geq$ 4tracks1π^0.

Table 12: Number of narrow resonance events predicted in the continuum and on-peak data samples by calculations using ISR cross sections, measured luminosities, and efficiencies from MC ISR events.

			Y3S				Y2S				Run 7			
	Continuum	±	onpeak	±	f_L	±	onpeak	±	f_L	±	onpeak	±	f_L	±
omega to pi pi pi	25,171	159	8,384	68	0.333	0.003	4,571	43	0.182	0.002	12,955	81	0.515	0.005
Phi to K K	52,678	273	17,561	124	0.333	0.003	9,651	77	0.183	0.002	27,212	146	0.517	0.004
Jpsi to 4 tracks	8,745	304	2,997	32	0.343	0.012	1,586	15	0.181	0.007	4,583	36	0.524	0.019
Jpsi to 4 tracks 1 pi0	8,151	293	2,589	29	0.318	0.012	1,404	14	0.172	0.006	3,994	33	0.490	0.018
average					0.333	0.002			0.182	0.001			0.515	0.003

11.1.2 Calculating f_L using MC ISR samples

The second method uses MC samples of the same four ISR-produced resonances, together with calculated cross sections and known luminosities, to calculate f_L. For each resonance X, the scaling factor f_{LX} is:

$$f_{LX} = \frac{\mathcal{L}(s_\Upsilon) \cdot \sigma_{e^+e^- \to \gamma X}(s_\Upsilon) \cdot B_X \cdot \epsilon(s_\Upsilon)}{\sum_i \mathcal{L}(s_i) \cdot \sigma_{e^+e^- \to \gamma X}(s_i) \cdot B_X \cdot \epsilon(s_i)}, \tag{2}$$

where $\mathcal{L}(s)$ is the luminosity for the data recorded at center-of-mass energy s, $\sigma_{e^+e^- \to \gamma X}$ is the ISR production cross section for the resonance X, B_X is the branching fraction for X to decay into the relevant final state, and ϵ is the efficiency for reconstructing the decay of X. The index i runs over the four center-of-mass energies s_i that make up the continuum sample, Run 6 on peak, Run 6 off peak, $\Upsilon(3S)$ off peak, and $\Upsilon(2S)$ off peak.

The luminosities are nominally final, and are found using BbkLumi. The production cross sections are calculated using Ref. [16], and background MC samples are used to find the efficiencies.

The uncertainty on f_{LX} is due to MC statistics and the uncertainty on the luminosity. f_L for this method is the weighted average of the four f_{LX}. Results are summarized in Table 12.

Note that a comparison between Table 12 and Table 11 indicates that the actual number of observed events is approximately 60% of that predicted by the calculation. This problem has previously been observed [17].

The secondary branching fractions are not necessarily correct in DECAY.DEC for the J/ψ, but they should be correct for the ω and the ϕ. Note that this calculation of f_L does not depend on the absolute normalization being correct, but rather only on its variation with $\sqrt{s}$.

Table 13: Summary of the different methods used to calculate the continuum subtraction normalization factor f_L. The midpoint of the range is the value used for f_L in systematic error studies.

	Y3S	Y2S	Combined
Fits to narrow resonances	0.349	0.191	0.540
MC/luminosity	0.333	0.182	0.515
Fit continuum to CP odd spectrum	0.329	0.174	0.504
Fit continuum to CP all spectrum	0.320	0.176	0.495
N_Y(CP all) ≥ N_Y(CP odd)	0.321	0.182	0.503
Midpoint fL (alternative)	0.334	0.183	0.518

11.1.3 f_L from consistency between CP odd and CP all samples

The CP odd sample is a strict subset of the CP all sample for each center of mass energy. Therefore, the number of CP all Υ decays, after continuum subtraction, should be greater than or equal to the number of CP odd: $N_{\mathrm{CPall}} - f_L \cdot C_{\mathrm{CPall}} \geq N_{\mathrm{CPodd}} - f_L \cdot C_{\mathrm{CPodd}}$, where N is the number of events in the CP all or CP odd on peak data sample, and C the number in the corresponding continuum sample. The value in Table 13 corresponds to setting the number equal in CP odd and CP all.

11.1.4 Summary of continuum normalization

The values for f_L found by the different methods are summarized in Table 13. Note that these are not independent values that be simply averaged. For example, as noted in the section above, the CP odd data is a subset of the CP all. Instead, they should be considered different plausible ways to calculate the same quantity.

We take the mid point of the resulting spread of values as the value for f_L in the alternative fits in which it is fixed. It is 2.7% larger than the nominal value for CP odd, and 4.5% larger for CP all.

11.2 Background systematic errors for Run 7 on peak data

Figure 92 compares the systematic and statistical errors for the Run 7 on-peak data set. The systematic errors are smaller than the statistical errors on the background except near resonances. The most significant Higgs signals including the background systematic errors are 2.9σ at $1.295\ \mathrm{GeV}/c^2$ for CP-all and 3.1σ at $4.727\ \mathrm{GeV}/c^2$ for CP-odd.

A few of the fit variations are worth looking at in more detail. The nominal CP all fit has a large negative $f_0(980)$ signal, and one might wonder

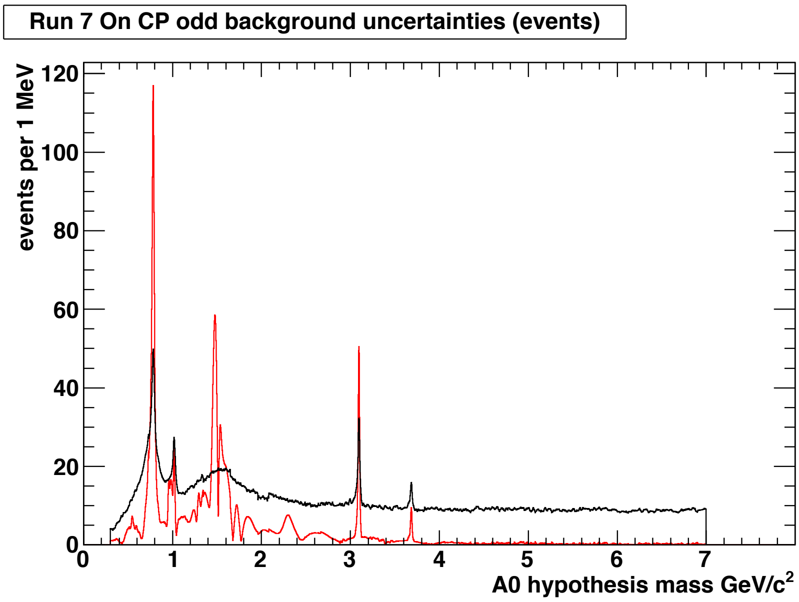

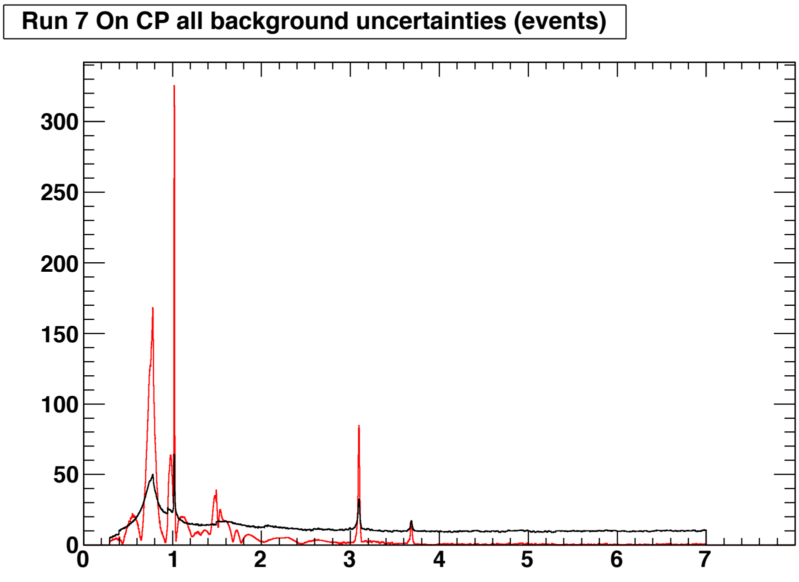

Figure 92: Statistical error (black) and systematic error (red) in the background estimate for (top) CP odd and (bottom) CP all Run 7 on peak data.

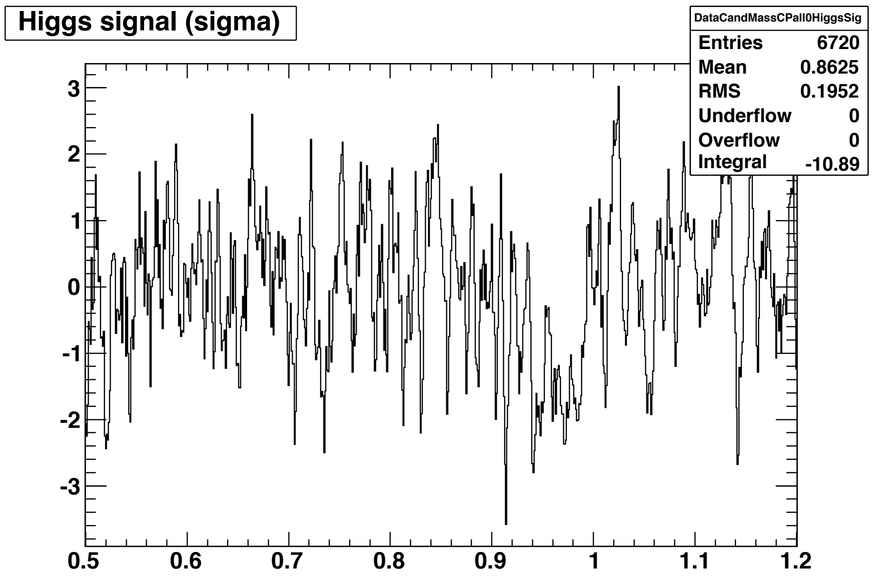

Figure 93: Statistical significance of the Higgs signal in the Run 7 on peak CP all analysis in the region of the $f_0(980)$ when that resonance is not included in the fit.

if removing that component from the fit would create a large negative Higgs signal at that mass. Figure 93 shows the statistical significance of the Higgs signal as a function of mass when the $f_0(980)$ is removed from the fit. The significances are on the order of -2σ or less.

The most significant additional resonance for the the CP all and CP odd fits is the $f_0(1500)$, for which the alternative fits find 1805 ± 443 events in CP all and 1676 ± 435 in CP odd. The CP odd fit including the $f_0(1500)$, is shown after continuum subtraction in Fig. 94. Recall, however, that the uncertainties on the resonances are not reliable.

12 Calculation of upper limits

The upper limit is calculated in terms of the product branching fractions $\mathcal{B}_{3S} \equiv \mathcal{B}(\Upsilon(3S) \to \gamma A^0) \cdot \mathcal{B}(A^0 \to \text{hadrons})$ and $\mathcal{B}_{2S} \equiv \mathcal{B}(\Upsilon(2S) \to \gamma A^0) \cdot \mathcal{B}(A^0 \to \text{hadrons})$, under the assumption that the decays are described by the same Lorentz-invariant matrix element $\mathcal{M}$. Because the phase space

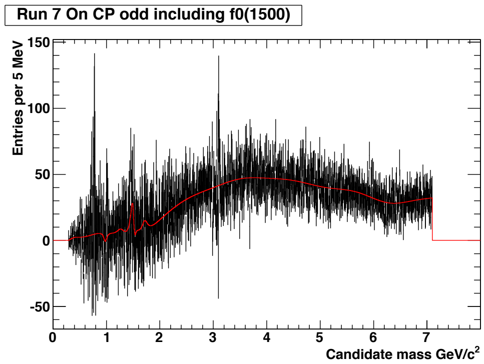

Figure 94: Fit to the Run 7 on peak CP odd candidate spectrum, after continuum subtraction, including as an extra resonance the $f_0(1500)$.

for the $\Upsilon(2S)$ and $\Upsilon(3S)$ decays are slightly different, the partial widths will also differ slightly. The two-body decay partial width is given by [14] Eq. 39.17:

$$d\Gamma = \frac{1}{32\pi}|\mathcal{M}|^2 \frac{p_{A^0}}{M^2_{\Upsilon(nS)}} d\Omega,$$

where the A^0 momentum p_{A^0} is

$$p_{A^0} = (M^2_{\Upsilon(nS)} - M^2_{A^0})/2 \cdot M_{\Upsilon(nS)}.$$

In terms of the decay branching fraction,

$$\mathcal{B}(\Upsilon(nS) \to \gamma A^0) \propto \frac{|\mathcal{M}|^2 \cdot p_{A^0}}{\Gamma_{nS} \cdot M^2_{\Upsilon(nS)}} = \frac{|\mathcal{M}|^2 \cdot (M^2_{\Upsilon(nS)} - M^2_{A^0})}{\Gamma_{nS} \cdot M^3_{\Upsilon(nS)}},$$

where Γ_{nS} is the full width of the $\Upsilon(2S)$ or $\Upsilon(3S)$.

We can use these formulas to relate the $\Upsilon(2S)$ and $\Upsilon(3S)$ product branching fractions:

$$\mathcal{B}_{2S} = \mathcal{B}_{3S} \cdot \frac{\Gamma_{3S}}{\Gamma_{2S}} \cdot \frac{M^3_{\Upsilon(3S)}}{M^3_{\Upsilon(2S)}} \cdot \frac{(M^2_{\Upsilon(2S)} - M^2_{A^0})}{(M^2_{\Upsilon(3S)} - M^2_{A^0})}.$$

where the phase space factor

$$R(M_{A^0}) \equiv \frac{M^3_{\Upsilon(3S)}}{M^3_{\Upsilon(2S)}} \cdot \frac{(M^2_{\Upsilon(2S)} - M^2_{A^0})}{(M^2_{\Upsilon(3S)} - M^2_{A^0})}$$

ranges from 1.033 to 0.975 depending on mass.

The limits are calculated using the combined $\Upsilon(2S)$ and $\Upsilon(3S)$ data set for each Higgs mass hypothesis m_i. The minimum mass hypothesis is the lower edge of the fit range, 0.290 GeV/c^2 plus one-half the width of the Higgs window, 0.291 GeV/c^2 for CP all and 0.300 GeV/c^2 for CP odd. The hypotheses extend in 1 MeV/c^2 steps to a maximum of 7 GeV/c^2.

The 90% CL upper limit is defined as the value of $\mathcal{B}_{3S}$ that contains 90% of the area of the likelihood function above zero, where $L(\mathcal{B}_{3S})$ is defined as the probability of observed $\leq N$ events in the mass window, given an expected background of $\hat{B} \pm \delta_B$, an efficiency $\epsilon \pm \delta_\epsilon$, and the number of $\Upsilon(2S)$ and $\Upsilon(3S)$ in the data set, $N_{2S} \pm \delta_{2S}$ and $N_{3S} \pm \delta_{3S}$. The expected number of events $\hat{N}$ is

$$\begin{aligned} \hat{N} &= \hat{B} + N_{3S} \cdot \mathcal{B}_{3S} \cdot \epsilon + N_{2S} \cdot \mathcal{B}_{2S} \cdot \epsilon \\ &= \hat{B} + N'_{3S} \cdot \mathcal{B}_{3S} \cdot \epsilon, \end{aligned} \tag{3}$$

where $N'_{3S} \equiv N_{3S} + N_{2S} \cdot R(M_{A^0}) \cdot \Gamma_{3S}/\Gamma_{2S}$. The likelihood curve is generated using a Monte Carlo method that integrates over the uncertainties.

The expected background is equal to the integral of the fit over the window, including continuum and Υ components. The uncertainty on the background has both a statistical component, from the continuum statistics, and a systematic component, due to uncertainty in the continuum scaling and in the inclusion or exclusion of resonances in the fit (Sec. 11). The efficiency and its uncertainty are discussed in Sec. 10. The numbers of Υ mesons are $N_{2S} = 98.3 \pm 0.9$M and $N_{3S} = 121.3 \pm 1.2$M.

If desired, the upper limits could be calculated for the $\Upsilon(2S)$ and $\Upsilon(3S)$ samples independently, presumably without the assumption that the partial decay widths are equal.

12.1 Expected upper limits

The expected upper limits are calculated using the average quantities found in the MC experiments described in Sec. 8. For each Higgs mass hypothesis, the average number of observed events N and the average background B and average uncertainty δ_B are used to find the upper limit for that bin. (On average, $B = N$, since no signal is included in these simulated experiments). Figures 95–97 show the results for the $\Upsilon(3S)$ and $\Upsilon(2S)$ data sets treated independently, and for the combined data set. The $\Upsilon(2S)$ and $\Upsilon(3S)$ results have not been updated to reflect the small changes in the analysis (the elimination of the cut on the highest momentum track) introduced in version 3 of this note, and they do not include the systematic error on the background. The background systematic has been included in the expected Run 7 on peak upper limits by using the errors calculated for actual Run 7 data.

The impact of the systematic errors is illustrated by the blue line in Fig. 97, which shows the expected CP all upper limits without systematic errors. The dominant systematic error at high mass is the 21% uncertainty on efficiency. The impact of the uncertainty on f_L can be seen near resonances. Note that the uncertainty on the background estimate is partially a statistical error, not systematic.

12.2 Run 7 on peak upper limits

Figure 98 shows the upper limits calculated for the Run 7 on peak data. The values are consistent with those predicted by the Toy studies. The systematic errors are noticeable at high masses, and at some of the resonances at low masses. The upper limits are calculated in terms of the $\Upsilon(3S)$ product branching fraction; the right axis gives the corresponding limits on the $\Upsilon(2S)$ product branching fraction assuming the phase space factor $R(M_{A^0}) = 1$. The error resulting from this assumption is less than 3.5% for all masses, and would not be visible on the plot.

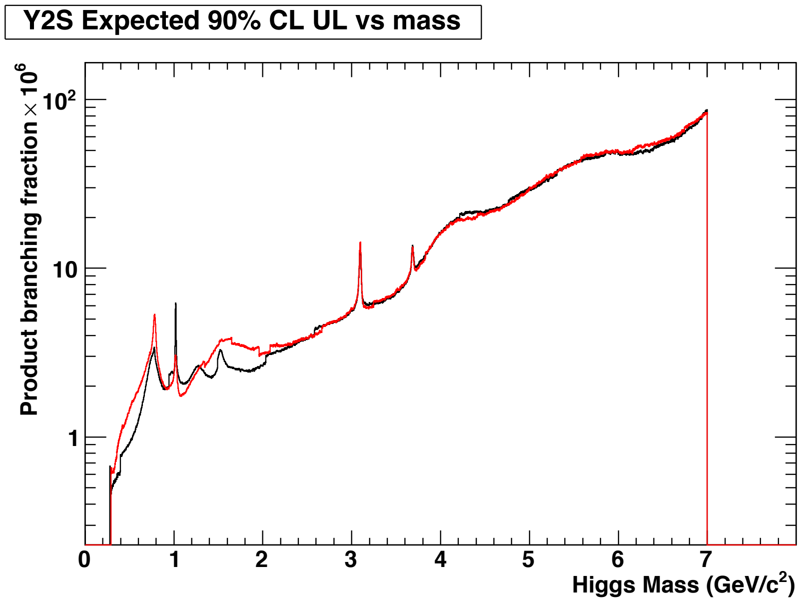

Figure 95: Expected 90% CL upper limit for the $\Upsilon(2S)$ data sample, CP odd hypothesis (red line) or CP not specified (black line).

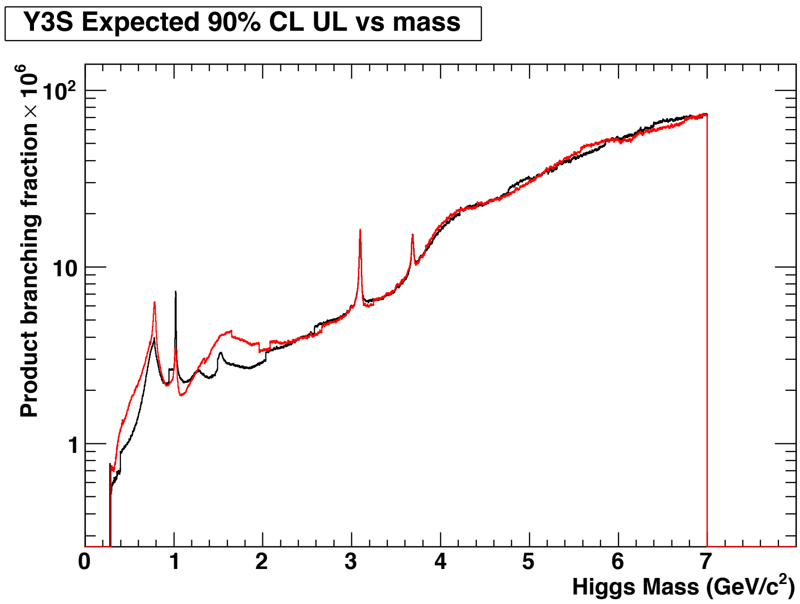

Figure 96: Expected 90% CL upper limit for the $\Upsilon(3S)$ data sample, CP odd hypothesis (red line) or CP not specified (black line).

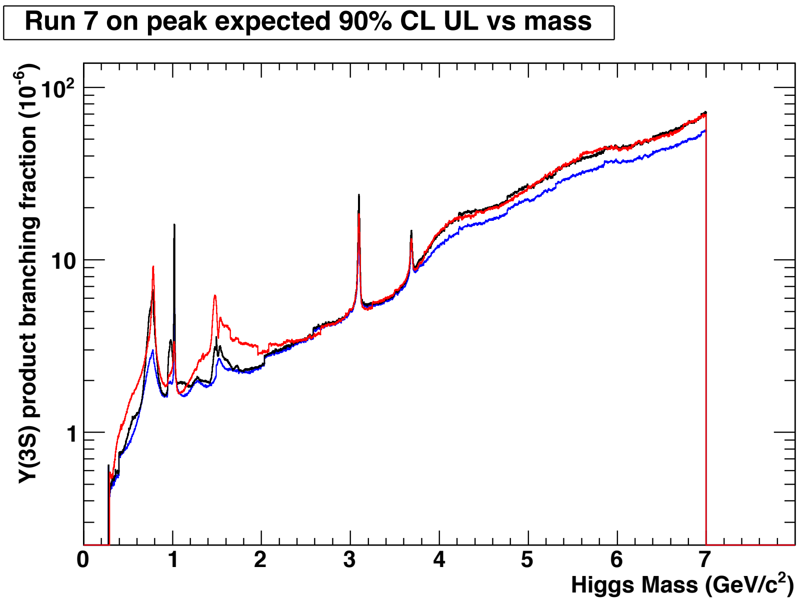

Figure 97: Expected 90% CL upper limit for the Run 7 on-peak data sample, CP odd hypothesis (red line) or CP not specified (black line). The blue curve shows the CP all case with systematic errors set to 0.

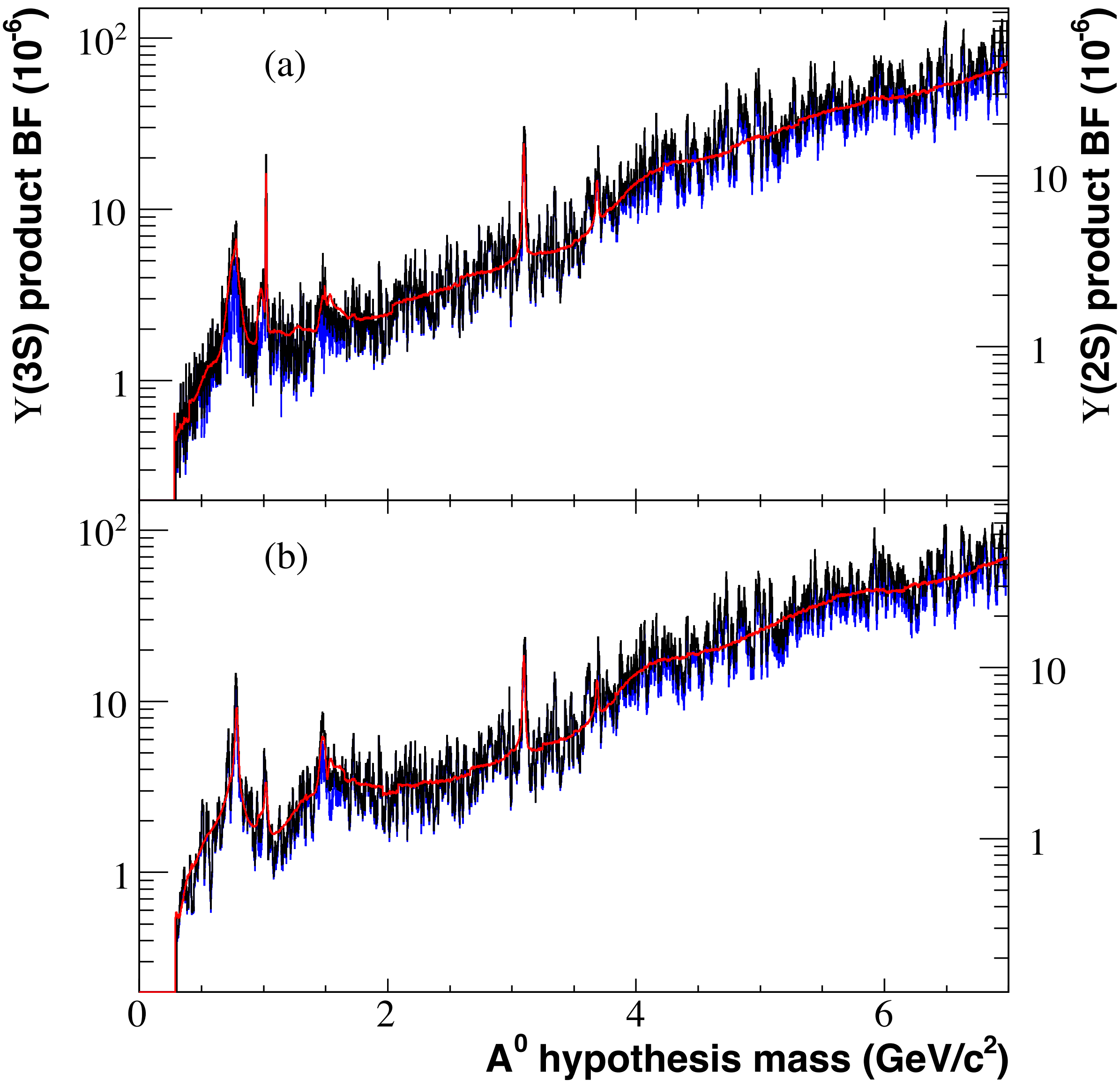

Figure 98: 90% CL upper limits on product branching fractions (BF) (left axis) $\mathcal{B}(\Upsilon(3S) \to \gamma A^0) \cdot \mathcal{B}(A^0 \to \text{hadrons})$ and (right axis) $\mathcal{B}(\Upsilon(2S) \to \gamma A^0) \cdot \mathcal{B}(A^0 \to \text{hadrons})$, for (a) CP-all analysis, and (b) CP-odd analysis. The overlaid curves in red are the limits expected from simulated experiments, while the blue curves are the limits from statistical errors only. The $\Upsilon(2S)$ limits do not include the phase space factor, which is at most a 3.5% correction.

References

[1] R. Dermisek and J. F. Gunion, "Escaping the Large Fine-Tuning and Little Hierarchy Problems in the Next to Minimal Supersymmetric Model and $h \to aa$ Decays", Phys. Rev. Lett. **95**, 041801 (2005).

[2] R. Dermisek, J. F. Gunion, and B. McElrath, "Probing next-to-minimal-supersymmetric models with minimal fine tuning by searching for decays of the Υ to a light $CP-$odd Higgs", Phys. Rev. D **76**, 051105(R) (2007).

[3] B. Aubert *et al.* (*BABAR* collaboration), "Search for dimuon decays of a light scalar boson in radiative transitions $\Upsilon \to \gamma A^0$", Phys. Rev. Lett. **103**, 081803 (2009).

[4] B. Aubert *et al.* (*BABAR* collaboration), "Search for a low-mass Higgs boson in $\Upsilon(3S) \to \gamma A^0$, $A^0 \to \tau^+\tau^-$ at *BABAR*", Phys. Rev. Lett. **103**, 181801 (2009).

[5] B. Aubert *et al.* (*BABAR* collaboration), "Search for Invisible Decays of a Light Scalar in Radiative Transitions $\Upsilon(3S) \to \gamma A^0$", SLAC-PUB-13328, arXiv:0808.0017 [hep-ex] (2008).

[6] B. Aubert *et al.* (*BABAR* collaboration), "Search for Production of Invisible Final States in Single-Photon Decays of $\Upsilon(1S)$", Phys. Rev. Lett. **107**, 021804 (2011).

[7] W. Love *et al.* (CLEO collaboration), "Search for Very Light CP-Odd Higgs Boson in Radiative Decays of $\Upsilon(1S)$", Phys. Rev. Lett. **101**, 151802 (2008).

[8] F. Domingo, U. Ellwanger, E. Fullana, C. Hugoniec and M.-A. Sanchis-Lozano, "Radiative Υ decays and a light pseudoscalar Higgs in the NMSSM", JHEP01, 061 (2009).

[9] B. Aubert *et al.* (*BABAR* collaboration), "Test of lepton universality in $\Upsilon(1S)$ decays at *BABAR*", Phys. Rev. Lett. **104**, 191801 (2010).

[10] R. Dermisek and J. F. Gunion, "New constraints on a light $CP-$odd Higgs boson and related NMSSM ideal Higgs scenarios", Phys. Rev. D **81**, 075003 (2010).

[11] F. Domingo, "Updated constraints from radiative Υ decays on a light CP-odd Higgs", 1010.4701 [hep-ph] (2010).

[12] J. P. Burke *et al.*, "Offline measurement of recorded BABAR luminosity in R24", BAD-2186v4 (2011).

[13] S. B. Athar *et al.* (CLEO collaboration), "Radiative decays of the $\Upsilon(1S)$ to a pair of charged hadrons", Phys. Rev. D **73**, 032001 (2006).

[14] K. Nakamura *et al.* (Particle Data Group), Journal of Physics G **37**, 075021 (2010).

[15] C. P. Shen *et al.* (Belle collaboration), "Search for charmonium and charmonium-like states in $\Upsilon(1S)$ radiative decays", Phys. Rev. D **82**, 051504(R) (2010).

[16] M. Benayoun, S. I. Eidelman, V. N. Ivanchenko and Z. K. Silagadze, "Spectroscopy at B factories using hard photon emission", Mod. Phys. Lett. A **14**, 2605 (1999).

[17] Y. Kolomensky, private communication (Dec. 2010); B. Fulsom, private communication (May 2011).